9613400.0897
START
0042883

PNL-8846
UC-602

Underground Tank Vitrification: A Pilot-Scale In Situ Vitrification Test of a Tank Containing a Simulated Mixed Waste Sludge

L. E. Thompson
P. C. Owczarski
M. C. Miller
T. D. Powell
J. S. Tixier

September 1993

Prepared for the U.S. Department of Energy
under Contract DE-AC06-76RLO 1830

Pacific Northwest Laboratory
Operated for the U.S. Department of Energy
by Battelle Memorial Institute

Battelle

FEB 1996
RECEIVED
EDMC

PNL-8846

START

DISCLAIMER

This report was prepared as an account of work sponsored by an agency of the United States Government. Neither the United States Government nor any agency thereof, nor Battelle Memorial Institute, nor any of their employees, makes any **warranty, expressed or implied, or assumes any legal liability or responsibility for the accuracy, completeness, or usefulness of any information, apparatus, product, or process disclosed, or represents that its use would not infringe privately owned rights.** Reference herein to any specific commercial product, process, or service by trade name, trademark, manufacturer, or otherwise does not necessarily constitute or imply its endorsement, recommendation, or favoring by the United States Government or any agency thereof, or Battelle Memorial Institute. The views and opinions of authors expressed herein do not necessarily state or reflect those of the United States Government or any agency thereof.

PACIFIC NORTHWEST LABORATORY
operated by
BATTELLE MEMORIAL INSTITUTE
for the
UNITED STATES DEPARTMENT OF ENERGY
under Contract DE-AC06-76RLO 1830

Printed in the United States of America

Available to DOE and DOE contractors from the Office of Scientific and Technical Information, P.O. Box 62, Oak Ridge, TN 37831; prices available from (615) 576-8401. FTS 626-8401.

Available to the public from the National Technical Information Service, U.S. Department of Commerce, 5285 Port Royal Rd., Springfield, VA 22161.

The contents of this report were printed on recycled paper

9613100.0898

PNL-8846
UC-602

UNDERGROUND TANK VITRIFICATION: A PILOT-SCALE IN SITU VITRIFICATION TEST OF A TANK CONTAINING A SIMULATED MIXED WASTE SLUDGE

L. E. Thompson
T. D. Powell
P. C. Owczarski[a]
J. S. Tixier
M. C. Miller

September 1993

Prepared for
the U.S. Department of Energy
under Contract DE-AC06-76RLO 1830

Pacific Northwest Laboratory
Richland, Washington 99352

(a) Science Applications International Corporation, Richland, Washington.

9613400.0899

SUMMARY

The first pilot-scale in situ vitrification (ISV) test of a simulated underground tank was successfully completed by researchers at Pacific Northwest Laboratory (PNL) in September 1990. This tank contained a simulated refractory sludge and was buried in soil from Oak Ridge National Laboratory. Pending further development and verification at large scale, analyses of posttest samples and operation data indicate the ISV process is a viable treatment technology for many underground tanks and structures.

The test was initiated on September 11, 1990, but was temporarily halted 19 h into the test due to a pressurization of the off-gas containment hood. Melt depth at the time of the event was ~1 m (3.28 ft). Once the pressurization was fully evaluated and measures were implemented to prevent reoccurrence of a similar event, the test was restarted from grade on September 25, 1990, and conducted without further interruption until the target melt depth of 2.4 m (8 ft) was reached.

The primary objectives of the pilot-scale test, which was performed by PNL for the U.S. Department of Energy (DOE), were to verify the applicability of the ISV process for tank remediation and to provide additional data to better determine near full-scale process behavior when vitrifying tanks; both objectives were met. Key observations and conclusions regarding the pilot-scale ISV test are summarized below.

- The ISV process completely destroyed the 723-L (190-gal) tank and the tank's supporting structures and vitrified the tank contents and the soil below the tank to the target depth of 2.4 m (8 ft). Vitrification produced a uniform glass and crystalline monolith with a mass estimated to be ~24 metric tons.

- The ISV process effectively immobilized the vast majority of radionuclide simulants. Greater than 99.96% of the nonradioactive strontium and the vast majority of toxic metals were retained in the melt and uniformly distributed throughout the monolith. Eighty-nine percent of the lead was retained in the glass, and other volatile species such as cadmium and mercury were effectively captured by the off-gas treatment system.

- The resulting glass and crystalline waste form easily passed Toxicity Characteristics Leach Procedure (TCLP) criteria for all regulated metal.

- Surrounding soils were free of contamination by all simulated sludge species.

- A previously unknown phenomenon that generates significant pressurizations of the off-gas containment hood was observed and characterized. This event occurred during the test and necessitated a temporary suspension of the process to evaluate the cause and determine appropriate means to prevent its recurrence. The mechanism that creates the pressurization is the instantaneous radiant shine to suspended particulate in the containment hood upon the sudden disruption of the frozen layer of glass on the top surface of the melt. After the mechanism was identified, a relatively simple engineered system, consisting of a graphite

vent pipe and a radiant heat shield designed to prevent, or at least dramatically reduce the magnitude of the pressurizations, was installed and successfully used during the remainder of the test. In addition to gaining an understanding of the pressurization mechanism, significant process data regarding the behavior of ISV tank processing (including off-gas characteristics, melt behavior, and electrical system response) were obtained from the test.

- Steel tanks create a metal waste form that sinks to the bottom of the molten pool of soil as the steel is melted. The metallic waste form was highly crystallized and successfully passed TCLP criteria, even though the waste contained high concentrations of lead and other heavy metals (representative of the near worst-case concentration of any single inactive tank at ORNL).

- Electrode feeding technology (movable electrodes that can be inserted or retracted) proved invaluable in recovering from electrical short circuits when the electrodes approached or contacted molten pools of metal in the bottom of the melt. By simply raising one or more electrodes a few centimeters from the bottom of the molten glass pool, recovery from electrical short circuits was achieved. In addition, adjustment of the electrode insertion depth was an effective means to assist in the control of the electrical system. Inexpensive graphite electrodes proved capable of withstanding the extreme oxidizing environment at the melt surface. Due to an off-normal event during the test, all four electrodes had to be held in position for an extended period. One electrode failed due to oxidation; however, recovery was effected simply by inserting an additional electrode into the melt.

- A barrier wall made of castable refractory was designed to deflect the melt shape. The wall directly contacted the molten soil for the duration of the test and survived the test with essentially no degradation. For actual remedial operations, it may be necessary to protect nearby tanks and active pipelines from the destructive forces of the vitrification process. The wall was designed to test a candidate material under actual conditions.

Additional testing will be necessary to increase the scale of the process for applications to larger tanks. In addition to testing the process on refractory sludges, additional work will be required to evaluate the processing behavior and resulting waste form associated with tanks containing high concentrations of salts. The salt cake contained in many tanks poses unique concerns such as the influence of salt on the electrical conductivity of the melt as well as on the resulting waste form.

Current ISV development activities are being directed to contaminated soils applications. Development of ISV for advanced applications is not being pursued at this time pending deployment of ISV within the DOE complex on contaminated soils sites.

9613400.0900

ACKNOWLEDGMENTS

This work was funded by the Office of Technology Development under the InSitu Vitrification Integrated Program.

The authors gratefully acknowledge the support received from several fellow researchers, technical specialists, technicians, and personnel from support organizations within PNL who helped make this test a success. Listed below are the contributors and their areas of expertise.

G. L. Andrews, project administrative and meteorological support

C. E. Bigelow, off-gas hood containment shell design and test operations

R. L. Bogart, off-gas hood containment shell design

W. F. Bonner, project control and technical support

R. M. Burnside, tank design and analyses

B. E. Campbell, test operations

R. M. Douglass, off-gas hood containment shell fabrication

N. W. Dunbar, igneous petrologist

R. E. Garcia, test operations

R. D. Gibby, test operations and data analysis

A. B. Helgerson, secretarial support

C. R. Hymas, test operations

J. T. Jeffs, test operations and recovery

G. L. Ketner, off-gas hood containment shell design analyses

S. S. Koegler, project control and technical support

K. M. Olson, analytical support

M. E. Peterson, test operations

R. L. Richardson, electrical engineering

R. M. Sanders, analytical support

R. D. Sharp, test operations, posttest operations, and sampling

E. J. Wyse, analytical support

9615900.0901

CONTENTS

SUMMARY iii

ACKNOWLEDGMENTS v

1.0 INTRODUCTION 1.1

2.0 PROCESS DESCRIPTION AND STATUS OF DEVELOPMENT 2.1

3.0 PILOT-SCALE ISV TEST SYSTEM 3.1

3.1 POWER SYSTEM DESIGN 3.1

3.2 ELECTRODES AND ELECTRODE FEED SYSTEM 3.1

3.3 STARTER PATH 3.4

3.4 OFF-GAS CONTAINMENT HOOD 3.5

3.5 OFF-GAS TREATMENT SYSTEM 3.7

3.6 DATA ACQUISITION SYSTEMS 3.10

4.0 TEST CONFIGURATION 4.1

4.1 TANK DESIGN 4.1

4.2 SITE LAYOUT 4.1

4.3 SLUDGE COMPOSITION 4.5

4.4 OFF-GAS SAMPLING 4.8

5.0 OPERATIONAL RESULTS 5.1

5.1 TEST OVERVIEW 5.2

5.2 ELECTRICAL POWER SYSTEM PERFORMANCE 5.4

5.3 ELECTRODE AND ELECTRODE FEED SYSTEM PERFORMANCE 5.10

5.4 OFF-GAS TREATMENT SYSTEM PERFORMANCE 5.11

5.5 OFF-GAS CONTAINMENT SYSTEM PERFORMANCE 5.15

6.0 MAJOR PRESSURE EVENT 6.1

6.1 EVENT DESCRIPTION 6.1

6.2 ANALYSES OF MECHANISM 6.2

6.3 RADIANT HEAT TRANSFER MODELLING 6.5

6.4 EVENT RECOVERY AND CORRECTIVE ACTIONS 6.5

7.0 POSTTEST MONITORING EXCAVATION AND SAMPLING 7.1

7.1 MONITORING OF THERMAL GRADIENTS 7.1

7.2 EVALUATION OF CASTABLE WALL 7.2

7.3 POSTTEST SAMPLING 7.4

7.3.1 Internal Hood Samples 7.4

7.3.2 Near-Surface Soil Samples 7.4

7.3.3 Surrounding Soil Samples 7.4

7.4 VITRIFIED PRODUCT 7.7

7.4.1 Vitrified Product Sampling 7.7

7.4.2 Geologic Description of the Block 7.8

8.0 ANALYTICAL RESULTS AND INTERPRETATION 8.1

8.1 GLASS WASTE FORM CHARACTERISTICS 8.1

8.2 METAL PHASE 8.4

8.3 SURROUNDING SOIL ANALYSES 8.7

8.3.1 Strontium 8.7

8.3.2 Cesium 8.8

8.3.3 Mercury 8.8

8.3.4 Cadmium 8.8

8.4 OFF GAS 8.8

9615408.0902

8.5 WATER BALANCE 8.11

8.6 TOTAL MASS BALANCE 8.12

9.0 REFERENCES 9.1

APPENDIX A - MODELING PRESSURE PULSES DURING IN SITU VITRIFICATION A.1

APPENDIX B - OFF-GAS DATA FROM METHOD 5 SAMPLERS B.1

FIGURES

2.1 The ISV Process 2.1

3.1 Cutaway View of the Pilot-Scale ISV Process Trailer and Off-Gas Hood 3.2

3.2 Scott Electrical Connection for the Pilot-Scale ISV System 3.3

3.3 Off-Gas Containment Hood 3.6

3.4 Schematic Diagram of the Off-Gas System for the Pilot-Scale ISV Process 3.8

3.5 Tandem Nozzle Hydro-Sonic Scrubber 3.9

4.1 Tank Undergoing Leak Test Prior to the Concrete Shell Application 4.2

4.2 Side View of Test Site Illustrating the Instrumentation and Tank Layout 4.3

4.3 Top View of Pilot-Scale Underground Tank Test Site 4.4

4.4 Tank and Wall Positioning as Shown During Site Construction Activities 4.7

4.5 Method 5 Off-Gas Sampling System Configuration 4.9

5.1 Average Electrode Depth During Phase Two of Test 5.3

5.2 Average Tank Pressure Versus Time 5.4

5.3 Total Power to Electrodes 5.7

5.4 Resistance for the Initial Hours of the Restart 5.8

5.5 Hood Vacuum at 17.6 to 17.7 Test Hours 5.9

5.6 Plenum Temperature at 17.5 to 18.2 Test Hours 5.9

5.7 Total Power at 17.5 to 18.2 Test Hours 5.10

5.8 Average Venturi-Ejector Inlet and Outlet Temperatures 5.12

5.9 Average Differential Pressures for the Venturi-Ejector and the Hydro-Sonic Scrubbers 5.12

5.10 Hydro-Sonic Scrubber and Primary HEPA Filter Differential Pressure 5.13

5.11 Average Stack Off-Gas Flow 5.14

5.12 Stack Oxygen Concentrations During the Later Stages of Test Phase 1 ..... 5.14

9615400.0905

5.13 Average Carbon Monoxide Concentration During Test Phase 2 ..... 5.15

5.14 Hood Vacuum for Test Phase 2 and Average Plenum Temperature 5.16

5.15 Plenum, Roof, and Wall Interior Temperature 5.16

6.1 Hood Pressurization Event at 19:28 Test Hours on 9/12/90 ..... 6.1

6.2 Tank Pressure During Test Phase 1 ..... 6.2

6.3 Response of a 1-1/8-in. Sheathed Type K Thermocouple Exposed to a 950°C Flame at T = 0 ..... 6.4

7.1 Surrounding Soil Temperatures During Late Stages of Powered Operations 7.2

7.2 Posttest Location of the 100°C Isotherm Versus Time 7.3

7.3 Castable Barrier Wall Abutted Against the Vitrified Block 7.5

7.4 Soil Sampling Locations 7.6

7.5 Vitrified Block Shape 7.8

7.6 Vitrified Block Demolition by Use of a Back Hoe 7.9

TABLES

4.1 Elemental Composition of Pretest Hanford Soil and ORNL Soil via X-Ray Fluorescence Analysis 4.5

4.2 Oxide Composition of ORNL Limestone Gravel via Fusion/ICP Analysis 4.6

4.3 Composition of Simulated Sludge in Pilot-Scale Tank Test 4.8

5.1 Chronology of Events of Pilot-Scale Test 5.5

8.1 Vitrified Product Composition for Target Simulated-Waste Components 8.2

8.2 TCLP Results for the Vitrified Product 8.3

8.3 Bulk Elemental Composition of the Vitrified Product 8.3

8.4 Composition of Metallic Phase via SW-846 Methods 8.5

8.5 Metal Phase Composition via X-Ray Fluorescence 8.6

8.6 TCLP Results of Metal Phase Samples 8.7

8.7 Surrounding Soil Analytical Results for Target Simulated-Waste Components 8.9

8.8 Hood and Off-Gas Sample Composition Summary for Target Simulated-Waste Components 8.10

8.9 Elemental Distribution of Target Simulated-Sludge Components in the Off Gas 8.10

8.10 Stack Off-Gas Composition for Target Simulated-Sludge Components 8.11

8.11 Mass Balance Distribution of Elemental Target Simulated-Sludge Components 8.13

8.12 Summary Distribution of Target Sludge Species Based on Off Gas and Surrounding Soil Data 8.14

9413301.0904

1.0 INTRODUCTION

Underground storage tanks containing sludges and salt cakes of radioactive and/or hazardous chemicals represent a significant environmental concern and a major cleanup challenge in terms of technology. Numerous inactive tanks at Oak Ridge National Laboratory (ORNL), the Hanford Site, and other U.S. Department of Energy (DOE) sites require timely remediation to comply with state or federal environmental regulations. Thirty-three inactive tanks at ORNL no longer comply with U.S. Environmental Protection Agency (EPA) regulations and require closure (Autrey et al. 1990). Single-shell tanks at Hanford require remediation in accordance with schedules set forth in the Tri-Party Agreement. Several of the inactive tanks at ORNL and numerous single-shell tanks and other subsurface structures at Hanford are known to leak and have resulted in soil contamination below the tanks (DeFigh-Price 1990). Sixty-six single-shell tanks at Hanford are assumed to have leaked at least 2.8×10^6 L (750,000 gal) of liquid waste into the underlying soil column exclusive of intentional discharges (Waite 1991). Highly contaminated tanks remaining after waste retrieval operations, tanks that contain materials that cannot be economically or safely removed, and tanks that have outlying contaminated soil are likely candidates for permanent remediation using the in situ vitrification (ISV) technology.

In situ vitrification is a process that converts contaminated soils, sludges, and buried objects such as tanks or wastes into a durable glass and crystalline product similar to naturally occurring obsidian. The resulting product is stable for geologic periods and is highly resistant to leaching. The ISV process is based on the joule heating principle of glass melter technology developed at Pacific Northwest Laboratory[a] (PNL) for immobilizing high-level nuclear waste. In situ vitrification was originally tested by PNL researchers in August 1980 (Brouns, Buelt, and Bonner 1983). Since then, numerous developmental tests and demonstrations ranging from small bench- and engineering-scale tests to larger field-sized pilot- and large-scale tests have been conducted, with resulting monoliths as large as 816 metric tons (900 tons) and 10.7 m (35 ft) in diameter. In situ vitrification has emerged in recent years as an effective and efficient technology for the remediation of contaminated soil sites, and the technology has recently been transferred to the Geosafe Corporation for commercial applications to soils contaminated with hazardous wastes.

Application of ISV to underground tanks appears to be a cost-effective, safe, and environmentally sound remedial technology for a majority of tanks at DOE facilities. Using conservative assumptions, tank

---

(a) Pacific Northwest Laboratory is operated by Battelle Memorial Institute for the U.S. Department of Energy under Contract DE-AC06-76RLO 1830.

vitrification cost estimates indicate the possibility of greater than an order-of-magnitude savings over alternative remedial technologies or waste retrieval. By vitrifying the tank, its contents, and any contaminated surrounding soil, the tank is destroyed and essentially all radioactive and nonvolatile hazardous constituents are immobilized in the glass. Volatile radioactive and hazardous species released from the melt are captured by an off-gas treatment system.

This report details the first pilot-scale ISV test on a simulated underground tank and builds upon an engineering-scale test conducted by PNL in 1989. The primary objectives of the pilot-scale test, which was performed by PNL for DOE, were to verify the applicability of the ISV process for tank remediation and to provide additional data to better determine near full-scale process behavior when vitrifying tanks. The 723-L (190-gal) tank contained a simulated, nonradioactive sludge recipe that was designed to represent a near worst-case refractory sludge composition based on characterization data of the 33 inactive tanks at the ORNL. The sludge accounted for one-third of the total tank volume. The tank was scaled in size, and its construction characteristics were typical of tanks at ORNL; however, the tank also included construction features representative of tanks at other DOE sites.

Results of operational data and posttest sampling and analyses reveal that the test completely destroyed the tank and its supporting structures and immobilized nonradioactive simulants uniformly throughout the resulting monolith. Significant operational data relating to understanding the behavior of the ISV process during tank processing were obtained from this test.

9613400.0905

2.0 PROCESS DESCRIPTION AND STATUS OF DEVELOPMENT

In situ vitrification has been developed as a remedial action process for soils contaminated with hazardous chemical wastes and/or radionuclides. Figure 2.1 illustrates the ISV process as applied to contaminated soil. A square array of four graphite electrodes is inserted a few inches into the ground. Because soil is not electrically conductive after its moisture has been driven off, a conductive mixture of flaked graphite and glass frit is placed between the electrodes to serve as a starter path. An electrical potential is applied to the electrodes to establish an electrical current in the starter path. The current flow heats the starter path and surrounding soil to well above the initial soil-melting temperatures of 1100° to 1400°C. The graphite starter path is eventually consumed by oxidation, and the current is transferred to the molten soil, which is processed at temperatures between 1450° and 2000°C. As the molten or vitrified zone grows, it incorporates or encapsulates any radionuclides and nonvolatile hazardous elements, such as heavy metals, into the glass structure. The high temperature of the process destroys organic components by pyrolysis. The pyrolyzed byproducts migrate to the surface of the vitrified zone, where they combust in the presence of air. A hood placed over the area being vitrified directs the gaseous effluents to an off-gas treatment system.

Pacific Northwest Laboratory began developing ISV technology in 1980. Since that time, numerous developmental tests under a variety of site conditions and with a variety of waste types have been

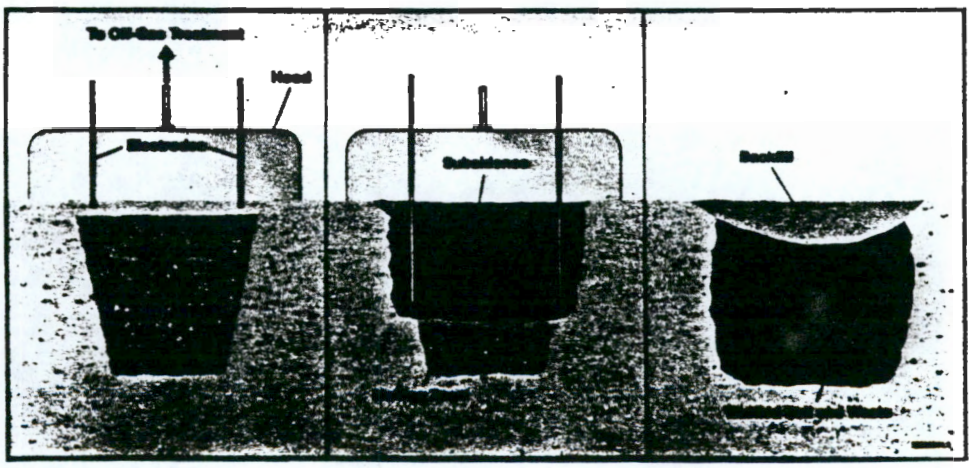

FIGURE 2.1. The ISV Process

conducted (Buelt et al. 1987). The successful results of numerous bench-, engineering-, intermediate-(pilot-), and large-scale tests have proven the general feasibility and widespread applications of the process. The ISV technology has been refined to the point that it has been commercialized for specific types of contaminated soil sites. The ISV process has been broadly patented within the United States, Canada, Japan, Great Britain, and France. Battelle Memorial Institute (BMI) holds an exclusive license to those patents. Except for U.S. governmental applications of ISV, BMI has exclusive worldwide rights to all ISV technology. Current emphasis is to develop the technology for application to contaminated soils.

1014900.090b

3.0 PILOT-SCALE ISV TEST SYSTEM

The pilot-scale test equipment consists of a power supply and control system, a high-efficiency particulate air (HEPA) prefilter, and an off-gas treatment system housed in a portable semi-trailer and an off-gas containment hood over the test site (see Figure 3.1).

3.1 POWER SYSTEM DESIGN

The pilot-scale system requires 750 kW of power at 480 VAC, 800 A, three-phase, 60 Hz. A backup diesel generator automatically provides energy in the event utility line power is interrupted. The diesel generator provides 93 kVA of power at 480 VAC, three-phase, and 60 Hz to equipment essential to personnel and environmental safety. Essential equipment includes the off-gas system, data acquisition system, environmental and system monitoring equipment, HVAC, and system lighting.

The pilot-scale electrode power system uses a 500 kVA Scott connected transformer that produces a variable voltage output through a range of four operator-selectable voltage taps. Power output is controlled at the primary side of the transformer with SCR (silicon control rectifier) technology using a single potentiometer for either voltage or current control. The Scott connected transformer is a phase conversion system converting three-phase power (three-wire primary) to four-phase power (four-wire secondary). To effect this conversion, the tapped winding must resonate between its halves and operate one winding at a leading power factor of 30° and the other winding at a lagging power factor of 30°. These balanced phase shifts are accomplished using a portable power generator that has three voltages of equal magnitude, separated by phase angles of 120°. The two secondary windings yield quadradture voltages that when ungrounded, provide four phases that are of equal magnitude and separated by 90° only if the secondary loads are equal and of unity power factor. This unique balance of voltages and currents is valid for one frequency. The transformer has four separate voltage tap settings--1000 V, 650 V, 430 V, and 250 V. The voltage taps have corresponding amperage rating of 250 A, 385 A, 580 A, and 1000 A per phase, respectively. A schematic of the Scott connection transformer is shown in Figure 3.2.

3.2 ELECTRODES AND ELECTRODE FEED SYSTEM

The electrodes used to conduct current to the molten soil consist of graphite sections measuring ~15 cm diameter by 2 m long (~6 in. by 6 ft). Each graphite section is machined at both ends with female threads to allow connection of successive lengths via male-threaded graphite connecting pins. After assembly, the electrodes are initially buried to depths of 15.24 cm to 63.5 cm (6 to 24 in.), and the starter

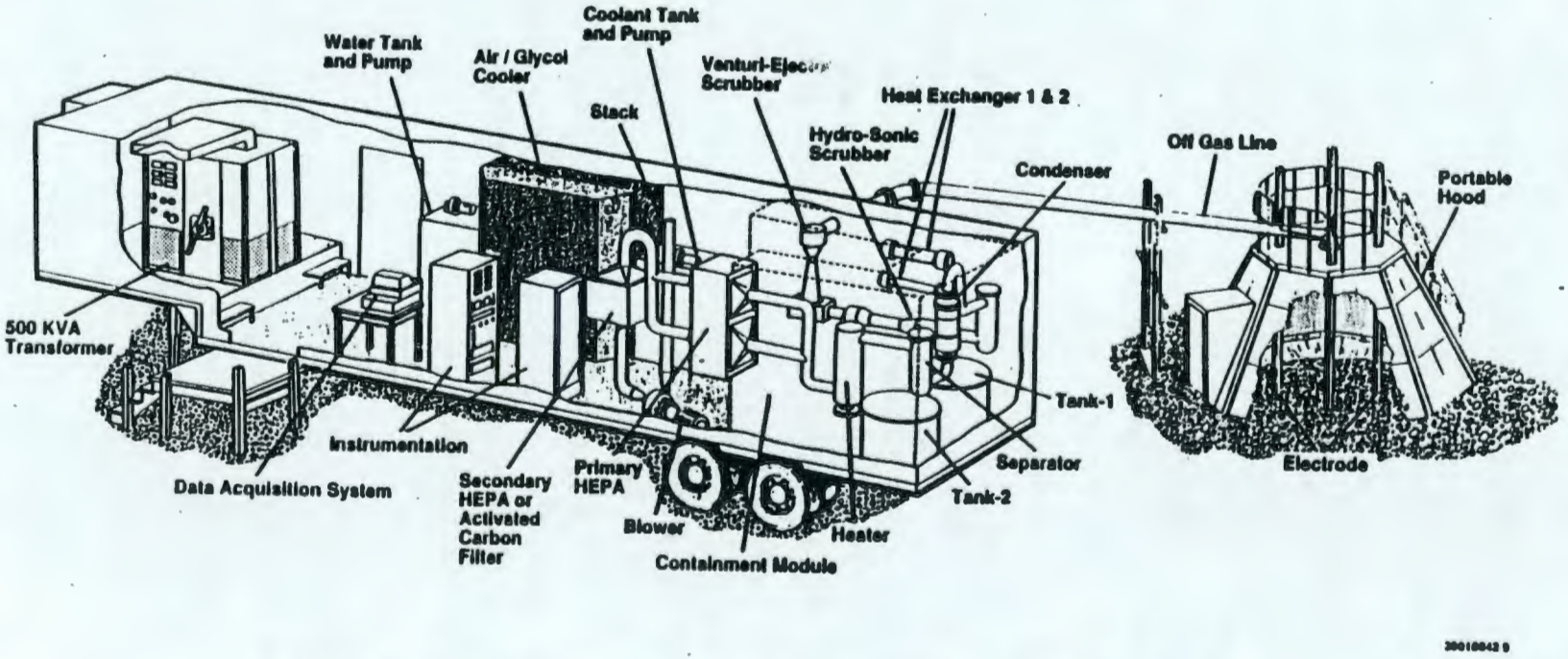

FIGURE 3.1. Cutaway View of the Pilot-Scale ISV Process Trailer and Off-Gas Hood

4613400.0997

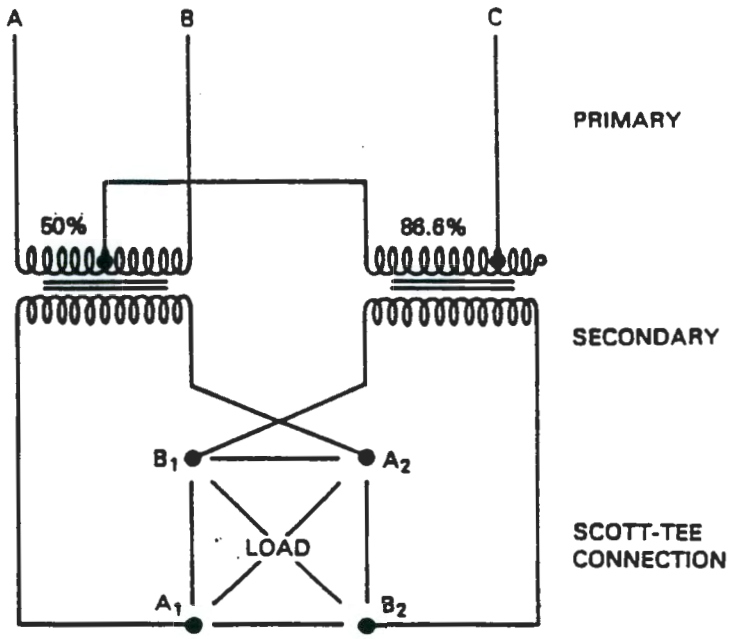

FIGURE 3.2. Scott Electrical Connection for the Pilot-Scale ISV System

path consisting of graphite and glass frit is laid around and between the electrodes. For this test the electrodes were arranged in a square array. Along the sides of the array, the electrodes are separated by a distance of 1.22 m (4.0 ft).

The electrode feed system consists of four independently controlled, pneumatically powered feed units (one for each electrode), and a control unit with manually operated valves for each feed unit. Each feed unit is equipped with a pneumatic motor that provides the means to vertically move a compressed-air actuated clamp, allowing for the retraction or insertion of a given electrode. In addition, a stationary clamp holds each electrode while the mobile clamp is repositioned to prepare for additional electrode movement.

Electrical contact from the power cables to each electrode is provided by a copper contact ring (brushes). Contact with the electrode is optimized by using a set of adjustable tension springs on the contractor ring. Normally, operations are conducted with the electrodes in a gravity fed, nongripped mode (electrode feed system clamps not engaged), allowing the electrodes to rest on the bottom of the advancing melt front. As metallic objects, molten metal pools, or other electrically disruptive situations are encountered, the feed system retracts the affected electrode(s) until a stable electrical balance is achieved. Typically, retraction of 2 to 3 cm (0.79 to 1.2 in.) is sufficient to restore balance.

The addition of the electrode feed system has realized cost savings for ISV operations. For example, the feed system has allowed replacement of the earlier molybdenum core, graphite collar design electrodes with less expensive solid graphite electrodes. Also, the predrilling of holes into the ground and the handling of drilling spoils for insertion of stationary electrodes have been eliminated, and the electrode setup and recovery procedures have been simplified.

3.3 STARTER PATH

The starter path consists of a mixture of 35% glass frit and 65% graphite flake. The starter path configuration is a rectangle with an electrode at each of the four corners and an "X" connecting the diagonally opposed electrodes. In preparation for laying the starter path, any coarse rock and other nonhomogeneous inclusions are removed from the top soil of the area to be vitrified. The area is then typically covered with a 15.24 cm (6 in.) layer of sand. Next, a form is constructed from wooden boards measuring 3.8 cm by 8.9 cm (1.5 by 3.5 in.). The boards are cut to fit the corresponding lengths of the electrode separation distances and buried horizontally in sand to grade level. The sand in which the form is buried is moistened with a small amount of water. When the water has permeated the sand to the depth of the bottom of the form, the boards are carefully removed, leaving a molded trench with the approximate dimensions of 3.8 cm (1.5 in.) wide by 8.9 cm (3.5 in.) deep. Trenches of these same dimensions are formed by hand around each of the four electrodes. At this point, a 2.5-cm (1-in.)-deep layer of pure graphite flake is placed around the circumference of each electrode. Next, a 2.5-cm (1-in.) layer of the graphite/frit mixture is placed above the layer of pure graphite. Finally, a 3.8- to 5.0-cm (1.5- to 2-in.) layer of the graphite/frit mixture is placed in the rectangular trench and in the trenches of the diagonally opposing electrode pairs.

After the starter path is complete, it is covered with a 2.5- to 5.0-cm (1- to 2-in.)-thick layer of fine soil or sand that is carefully compacted into place. This layer of soil helps reduce the graphite particulate generation and carryover to the off-gas treatment system when powered operations are initiated.

Finally, two layers of a 2.5-cm (1-in.)-thick, alumina-silica content insulating blanket are placed over the area to be vitrified. This insulating blanket minimizes heat loss from the molten soil during start-up and promotes subsidence of the melt. During the later stages of operations, after the melt has achieved greater depths, heat loss is limited by the formation of the naturally occurring cold cap, which is a frozen layer of glass on top of the molten zone.

9611190C.0909

3.4 OFF-GAS CONTAINMENT HOOD

The stainless steel off-gas containment hood is designed to collect off gases emanating from the melt and to direct them to an off-gas treatment system. A 1- to 2-in. water column (W.C.) vacuum and temperatures ranging from 200° to 400°C are typical operating conditions in the hood. The hood is operated at a slight vacuum created by an induced draft blower. The hood, with a volume of ~27.6 m^3 (975 ft^3), provides a surge capacity that minimizes vacuum loss during periods of sudden gas release. With a typical flow between 10 and 20 m^3/min (350 and 700 cfm), gases in the hood have a residence time of up to ~2 min.

The hood is configured as an octagonal pyramid as shown in Figure 3.3. A superstructure positioned above the containment hood provides a working platform for the electrode feed system, personnel access for maintenance during nonpowered periods of operation, and support for the containment shell. Off gases collected in the hood are directed to the off-gas treatment system via a 20.3-cm (8-in.)-diameter off-gas pipe. The complete off-gas hood assembly is portable and can be assembled for operation in less than one day.

The containment hood is constructed from 304L stainless steel sheet metal. The side panels are constructed from 18-gauge sheet metal, and the top is constructed of 14-gauge sheet metal. The containment hood is fitted with a removable door allowing access before and after the test. A viewing window from which to observe the melt during processing is an integral part of the door design. The electrodes penetrate the roof of the hood and extend down to the zone to be vitrified. The seals around each electrode are composed of three independent layers of a tightly woven high-silica fabric suitable for use in high-temperature applications. The electrode seals are created by an interference fit of the 15.25-cm (6-in.)-diameter electrodes through 14-cm (5.5-in.)-diameter holes in each of the fabric layers to provide a relatively tight seal around each electrode. The base of the containment shell is sealed to the ground by soil piled around the base.

Attached to the hood via a 15.2 cm (6 in.) stainless steel pipe is a seal pot assembly with a HEPA filter assembly and a blower. The seal pot assembly allows combustion air into the hood via a regulating valve. The regulating valve is used to maintain a specific vacuum in the hood as conditions change during operation. The seal pot also acts as a pressure relief system if the hood pressurizes from sudden gas releases. Over pressures of ~1-in. W.C. cause a water seal to be relieved, which allows off gases to exit through the seal pot and the HEPA filter. Filtered gases exiting the filter are then released to the environment. The seal pot blower provides assistance to the main blower to keep the hood under a slight

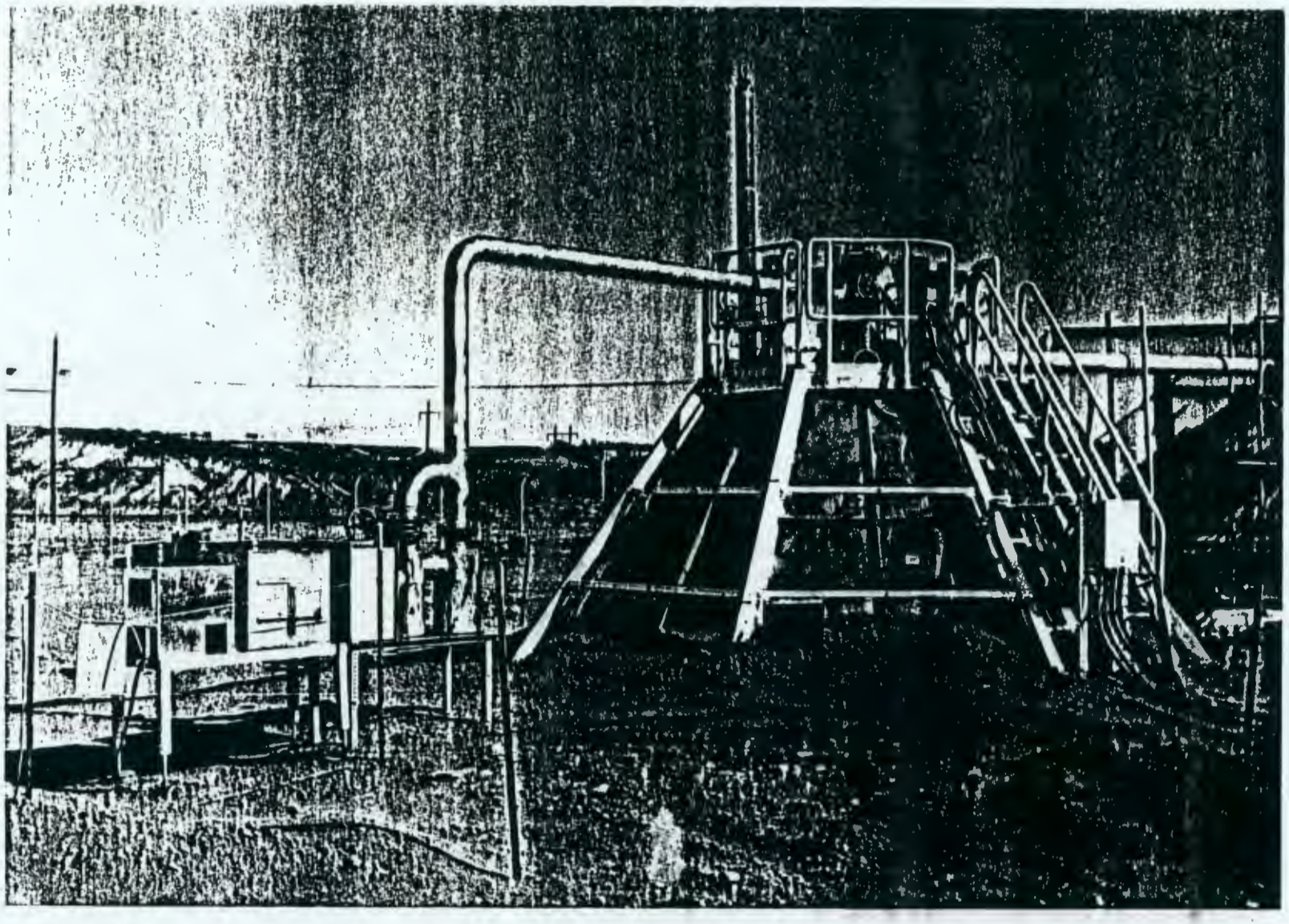

FIGURE 3.3. Off-Gas Containment Hood

vacuum. Under normal operating conditions, the seal pot blower is not energized. Control of the seal pot blower is linked to a pressure transducer mounted on the hood; the blower is activated automatically when the hood vacuum falls below 1-in. W.C.

3.5 OFF-GAS TREATMENT SYSTEM

The off-gas treatment system is shown schematically in Figure 3.4. The off gas passes through a Venturi-Ejector scrubber and separator, a Hydro-Sonic scrubber, a separator, a condenser, another separator, a heater, two stages of HEPA filtration, and a blower. Liquid to the two wet scrubbers is supplied by two independent scrub recirculation tanks, each equipped with a pump and heat exchanger. The entire off-gas system has been installed in a 13.7-m (45-ft)-long semi-trailer to facilitate transport to waste sites. Equipment layout within the trailer is illustrated in Figure 3.1. All off-gas components, except the final-stage HEPA filter and blower, are housed within a removable containment module. The containment module, designed for processing radioactive-contaminated soils, has gloved access for remote operations and is maintained under a slight vacuum. This system was originally designed for radioactive-contaminated soil testing at DOE's Hanford Site.

Heat is removed from the off gas primarily in the Venturi-Ejector scrubber where aqueous scrubbing solution is sprayed into the off-gas stream. A closed loop cooling system removes heat from the scrub solution. The cooling system consists of an air/liquid heat exchanger, a coolant storage tank, and a pump. A 50% water/ethylene glycol mix is pumped from the storage tank through the shell side of the condenser and the two scrub solution heat exchangers and then through the air/liquid exchanger, where heat is removed from the coolant and discharged to the environment. In addition to its role as a quencher, the Venturi-Ejector scrubber serves as a high-energy scrubber.

The second scrubber is a two-stage Hydro-Sonic scrubber (tandem nozzle scrubber), as illustrated in Figure 3.5. The first stage condenses vapors, removes larger particles, and initiates growth of the finer particles so that they are more easily captured in the second stage. Particulate is captured when the gas is mixed with fine water droplets produced by spraying water into the exhaust of the subsonic nozzle. Mixing and droplet growth continue down the length of the mixing tube. Large droplets containing the particulate are then removed by a vane separator and drained back into the scrub tank. The Hydro-Sonic scrubber is designed to remove over 90% of all particulates greater than 0.5 μm in diameter when operated at a differential pressure of 50-in. W.C. Removal efficiency improves with an increase in pressure differential. Additional water is removed from the off gas by a condenser that has a heat exchange area of 8.9 m^2 (96 ft^2) and a final separator. The gases are then reheated to ~25°C above the dew point in a 30-kW heater to prevent condensation in the HEPA filters.

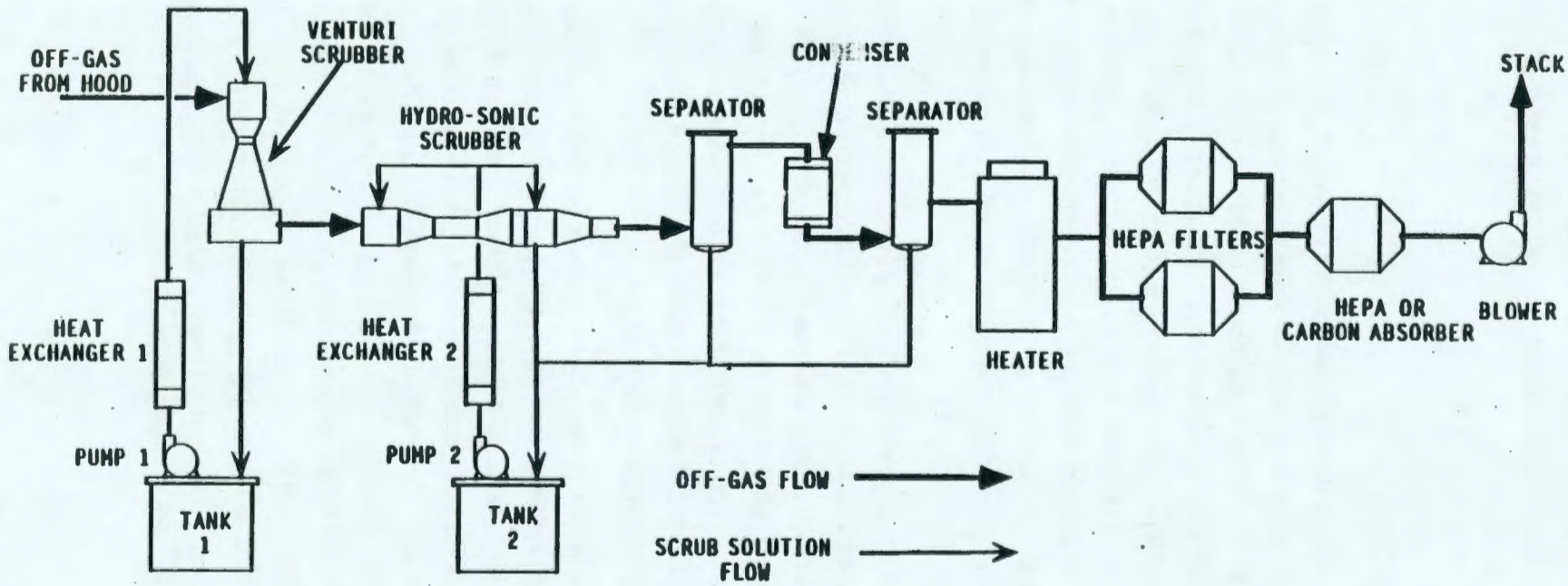

FIGURE 3.4. Schematic Diagram of the Off-Gas System for the Pilot-Scale ISV Process

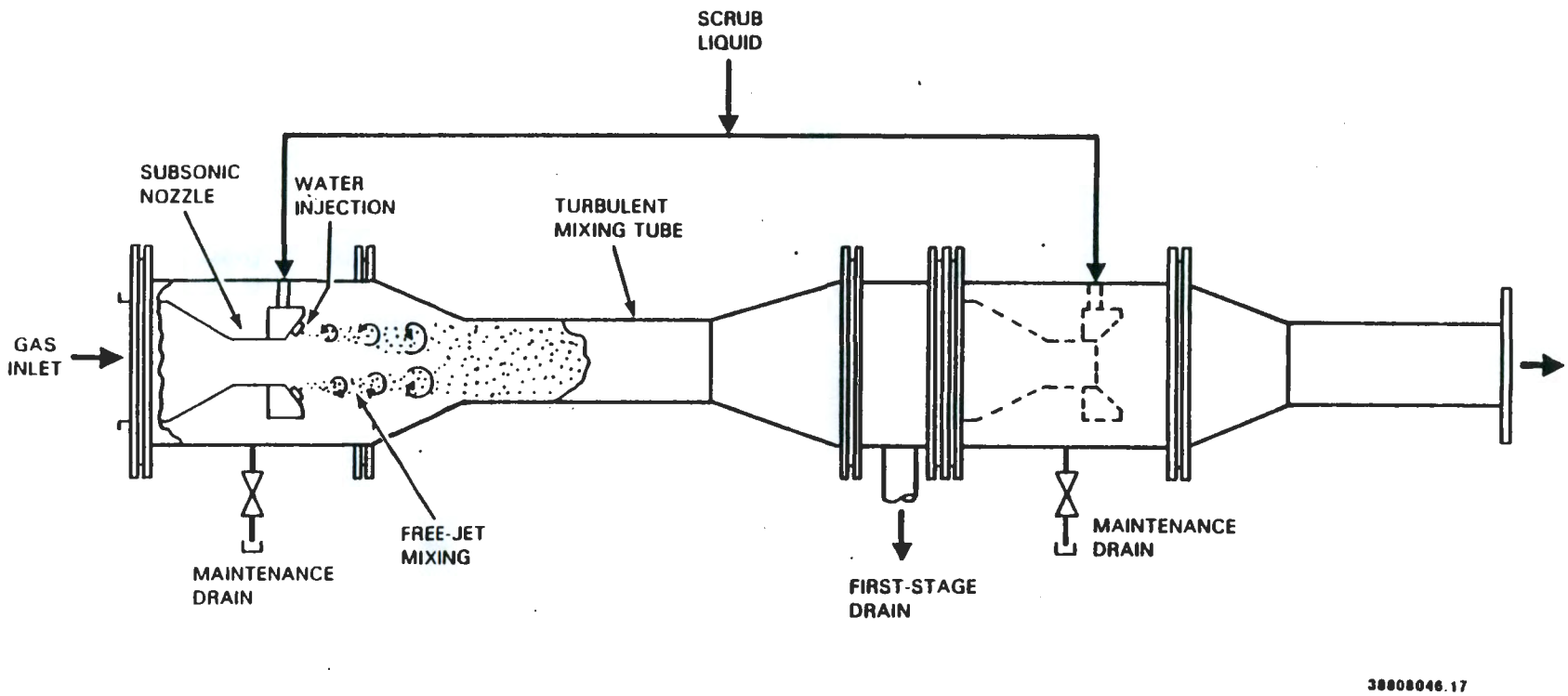

FIGURE 3.5. Tandem Nozzle Hydro-Sonic Scrubber

The first stage of filtration consists of two 61 cm by 61 cm by 29 cm (24 in. by 24 in. by 11.5 in.) HEPA filters in parallel. During operation, one filter is used, and the other remains as a backup in case the primary filter becomes loaded. The primary filter can be changed during operation without process shutdown. The second-stage filter acts as a backup particulate filter in case a first-stage filter fails. This second-stage filter is identical to the initial-stage filters in construction and filtering efficiency. The final component in the off-gas treatment system is an induced draft blower that creates a vacuum of ~100-in. W.C. The blower provides a total off-gas flow between 10 to 20 m^3/min (350 to 700 cfm).

3.6 DATA ACQUISITION SYSTEMS

The data acquisition system (DAS) and associated instrumentation provide extensive process monitoring capabilities for ISV testing. For process monitoring, inputs from process instruments are routed through a Hewlett Packard model 3497A data acquisition and control unit linked to a Macintosh IIcx computer operating LabView 2.0 software. The DAS scans, records, displays, and files process-control informational data at the rate of two samples per minute. The LabView software allows essentially simultaneous manipulation of recorded data (for producing trend plots, etc.) while acquiring and storing data.

A second system, the priority data (PD) system, independently scans, records, displays, and files critical process data at the rate of one sample per second. The PD system also features a visual alarm function to notify operators that operational limits have been reached. This system uses a second Macintosh IIcx computer operating LabView 2.0 software to monitor the following eight data points associated with the off-gas containment hood:

- 2 redundant hood vacuum measurements
- 1 plenum temperature
- 1 off-gas exit temperature
- 2 wall temperatures (external and internal)
- 2 roof temperatures (external and internal).

The pressure transducers are Validyne variable reluctance differential pressure transducers with a response time significantly better than 1 s. The transducers measure hood vacuum within a range of 5-in. W.C. vacuum to 5-in. W.C. pressure. The hood temperatures monitored by the PD system are acquired via 1/8-in. ungrounded stainless steel-sheathed Type K thermocouples. The response time (time constant) for the Type K thermocouples in air is ~10 s to reach 63.2% of the instantaneous

temperature change. Instrumentation and signal conditioners associated with the PD system that measure hood temperatures have an upper limit of 600°C. Consequently, any temperature spikes in the hood in excess of 600°C are plotted at the 600°C ceiling.

Note that most of the data plots presented in Section 5.0 are taken from the DAS using the data collected at 30-s intervals. Consequently, some peak values or other transient events that occur between measurement intervals may not be collected by the DAS. For the key data plots from the PD system, the 1-s collection interval effectively captures the rapid transient conditions.

9613906.0912

4.0 TEST CONFIGURATION

4.1 TANK DESIGN

The tank design was based on a study of the 33 inactive ORNL tanks and was identified as 1) representing a majority of tank construction styles and 2) including a range of features that would pose a processing challenge. This design simulates tanks made from either stainless steel or gunite. Other features that represent tank construction typical at other DOE sites were added to generate the most useful information possible from a single test.

The tank used for this test consisted of a stainless steel shell 91.4-cm-diameter by 111.7-cm-height (36-in.-diameter by 44-in.-height) encased in a 10.2-cm (4-in.) layer of reinforced concrete. The tank (shown in Figure 4.1) includes a 7.6-cm (3-in.) and a 15.2-cm (6-in.) flange on top and was situated on four concrete building blocks set on a 7.6-cm (3-in.)-thick concrete pad. To more accurately reflect a large-scale test, the tank was scaled down in size using a scaling factor based on electrical density per unit area. A 20.3-cm (8-in.) flange on the bottom of the tank provided a portal for instrumentation. A 10-psi rupture disk fitted to the bottom of the tank prevented build-up of excessive overpressures during ISV processing. Although the presence of a rupture disk is not representative of actual tanks, the disk was included in the event vitrification generated unexpected pressure.

Instrumentation used to monitor conditions inside the tank during processing includes six Type K thermocouples and three pressure taps as shown in Figure 4.2. The pressure taps consist of 1/8-in. ID stainless steel tubing from the tank to strain gauge pressure transducers with a range from 0 to 5 psig. Noncombustible silica-based fabric was laid inside the containment hood to surround the area to be vitrified and prevent airborne contaminants from settling onto the uncontaminated surface soil.

4.2 SITE LAYOUT

Approximately 19 m^3 (25 yd^3) of ORNL soil was shipped to the Hanford test site to provide sufficient soil for vitrification and posttest soil sampling. A 2.1-m by 3-m by 3-m (7-ft by 10-ft by 10-ft)-deep rectangular zone of ORNL soil was prepared (Figure 4.3). The tank was buried in the ORNL soil; it was installed to a depth of 2.36 m (7 ft 9 in.), allowing for 0.6 m (2 ft) of soil overburden above the tank. The tank was surrounded by a 10.2-cm (4-in.) cocoon of limestone gravel representative of ORNL conditions. The composition of ORNL and Hanford soil as determined by x-ray fluorescence is provided in Table 4.1. The oxide composition of the limestone gravel is presented in Table 4.2.

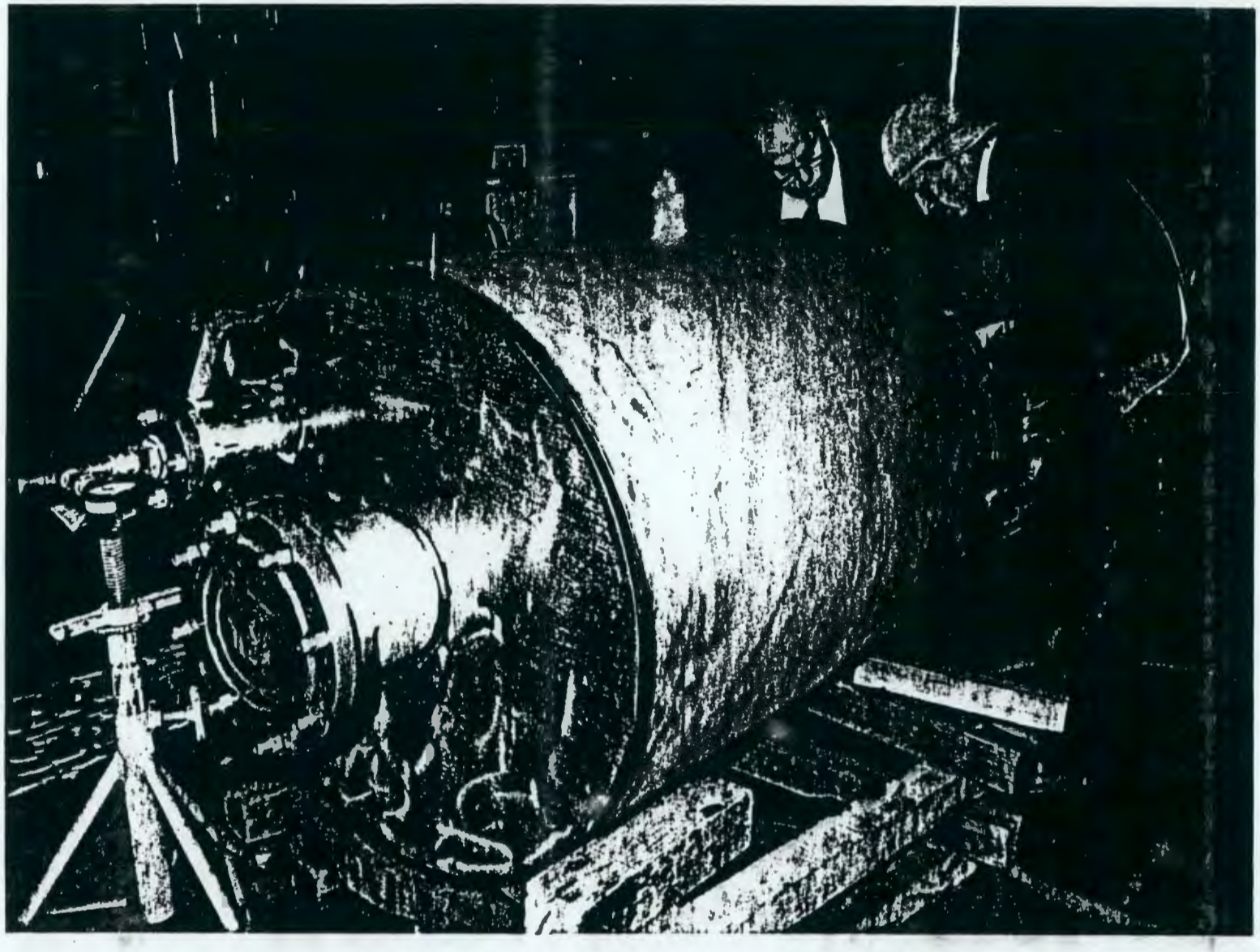

FIGURE 4.1. Tank Undergoing Leak Test Prior to the Concrete Shell Application

9613400.0913

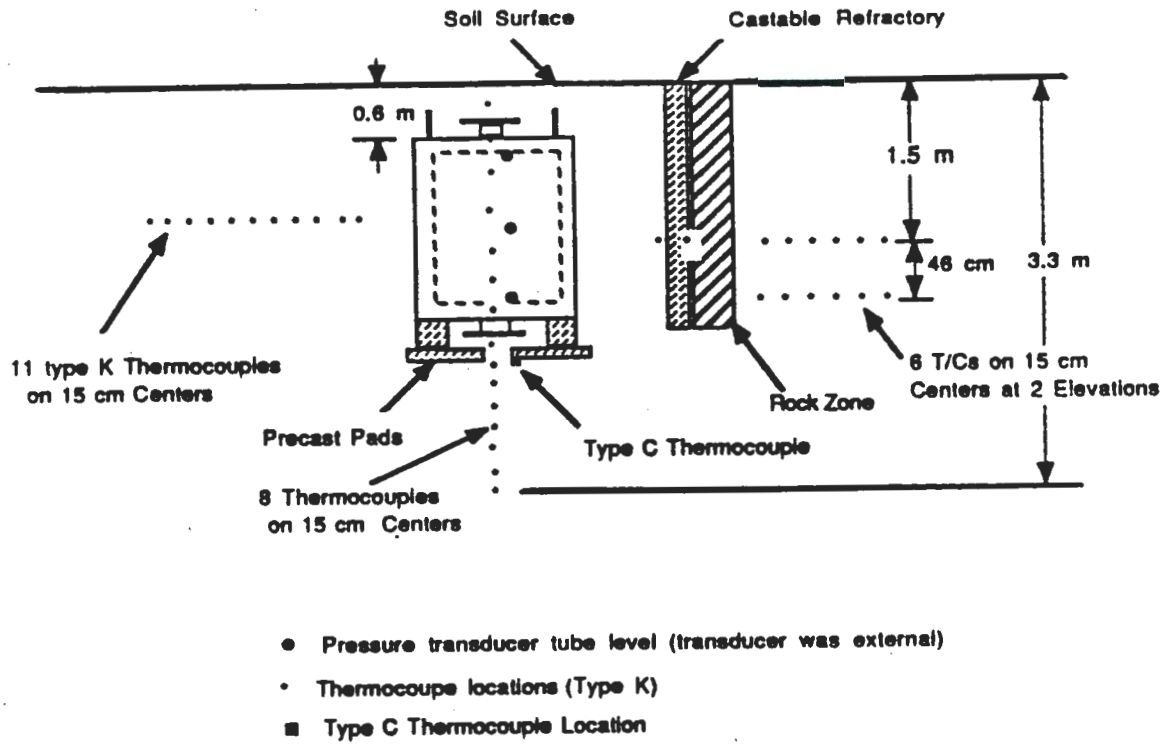

FIGURE 4.2. Side View of Test Site Illustrating the Instrumentation and Tank Layout

Instrumentation in the surrounding soil included two arrays of Type K thermocouples, one array oriented vertically directly below the tank and one oriented horizontally to one side of the tank at a 1.5-m (5-ft) depth, as shown in Figure 4.2. The thermocouples monitored the progression of melt growth and tracked the movement of the thermal gradients after the test. A single Type C thermocouple located in the center of the cement pad directly below the tank provided a positive indication of melt depth and melt temperature.

A wall of castable refractory (Koacrete 32CM) with a melting temperature of greater than 1650°C and measuring 2.4-m by 1.8-cm by 15-cm (8-ft by 6-ft by 6-in.) thick was located adjacent to the tank as shown in Figure 4.2. The purpose of the wall was to demonstrate that the shape and growth of the melt could be controlled in order to protect nearby pipes or tanks. A zone of large rocks was placed behind the wall to act as a passive cooling system, and two horizontal arrays of Type K thermocouples were located behind the wall. During actual remedial operations, a blower could be used to force air through air distribution pipes located in the rock zone behind the wall. This active cooling system would remove heat from the area behind the wall and would sufficiently protect nearby tanks or pipes, although it is possible that an

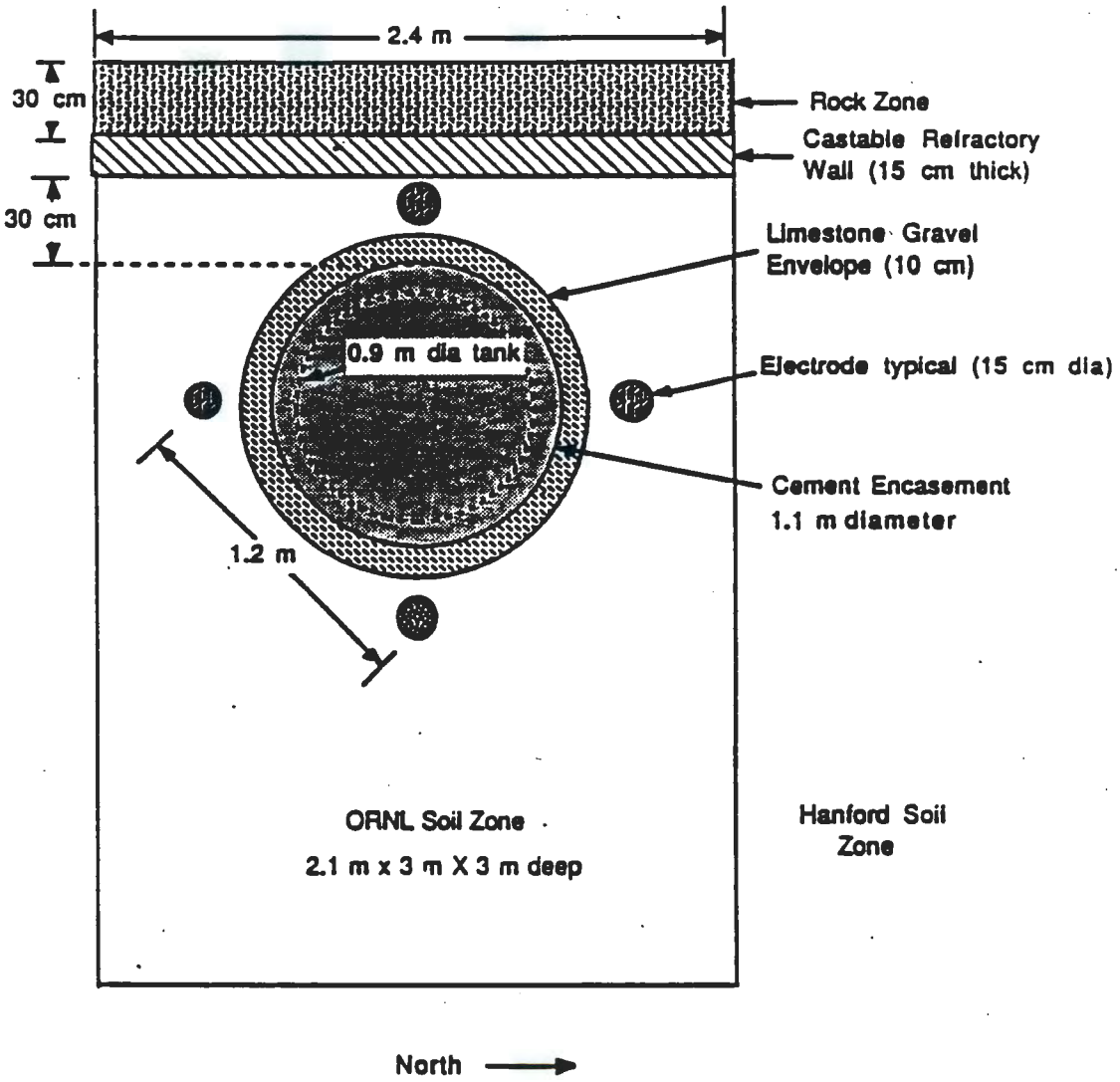

FIGURE 4.3. Top View of Pilot-Scale Underground Tank Test Site

improved passive system may suffice. A blower and distribution pipes were not included in this test since the off-gas capacity of the pilot-scale system was insufficient to accommodate the additional volume of air needed to cool the zone. The tank and castable wall are shown during site construction activities in Figure 4.4. The metal culvert surrounding the tank was used to form the limestone gravel cocoon and was removed prior to the test.

TABLE 4.1. Elemental Composition of Pretest Hanford Soil and ORNL Soil via X-Ray Fluorescence Analysis

Element	Concentration [a] Hanford Soil	ORNL Soil
Ag	<5.8	<6.4
Al	7.2 wt%	10.27 wt%
As	<2.2	4.2
Ba	799	660
Br	16.3	26.6
Ca	2.7 wt%	1.2 wt%
Cd	<6.2	<6.9
Ce	73	92
Cr	34	107
Cs	<13	<13
Cu	21	13.8
Fe	4.77 wt%	4.39 wt%
Ga	15.2	23.1
Hg	<3.1	<3
In	<6.8	10.7
K	1.7 wt%	3.6 wt%
La	25	31.4
Mn	818	568
Nb	7	11.4
Ni	22.1	44.2
Pb	60.6	39.7
Rb	64.6	145.6
Se	<0.9	<0.9
Si	29.7 wt%	26.1 wt%
Sn	107.3	27.7
Sr	431	134
Ti	0.8 wt%	0.6 wt%
V	162	106
Y	40.9	34.2
Zn	85	104.7
Zr	242	290

(a) Values in ppm unless otherwise noted.

4.3 SLUDGE COMPOSITION

The simulated sludge was composed of chemicals that were selected on the basis of an ORNL inactive tank characterization effort (Autrey et al. 1990). The simulant was designed to represent a refractory-type sludge as opposed to a salt cake. The maximum simulated sludge composition, shown in Table 4.3, was established by selecting the representative maximum concentrations of the various tank

TABLE 4.2. Oxide Composition of ORNL Limestone Gravel via Fusion/ICP Analysis

Na Fusion		K Fusion	
Oxide	Concentration (wt%)	Oxide	Concentration (wt%)
Al_2O_3	0.707	BaO	0.00657
BaO	0.00686	CaO	50.440
CaO	49.810	Fe_2O_3	0.512
Fe_2O_3	0.450	La_2O_3	0.0165
K_2O	0.640	MgO	2.442
La_2O_3	0.0187	MnO_2	0.0349
MgO	2.453	Na_2O	0.276
MnO_2	0.0128	SiO_2	2.670
NiO	0.0511	SrO	0.0309
SiO_2	2.541	TiO_2	0.0445
SrO	0.0359	ZrO_2	0.0385
TiO_2	0.0312		

sludge components measured in any single tank. The chemicals were mixed with approximately 220 L (58 gal) of soil to provide a simulated sludge equaling 30% of the tank's volume. Soil was used as a base material for the sludge and represented an alumina-silica base. Actual data for the bulk composition of the sludge were unavailable. The alumina-silica base material is considered to be a suitably conservative surrogate since the sludge layer in most tanks accounts for only a few percent of the volume, and the tanks would be backfilled with soil before processing. In addition, it is anticipated that the sludge will actually constitute a minor portion of the overall vitrified waste form once the backfill and surrounding soil are intermixed with the waste by the melting process.

The water content of the sludge was limited to 8.5%. A typical sludge may have greater than 50% water; however, the 8% water content was adequate to characterize gas releases from the melt. Water has no impact on the quality of the resulting waste form and is primarily an economic factor of processing because the downward melt rate slows as water evaporates.

Once the sludge was placed in the tank, the tank was backfilled with finely ground ORNL soil with an estimated consistency of 100 mesh (150 μm). Finely ground soil was required for backfill since the small

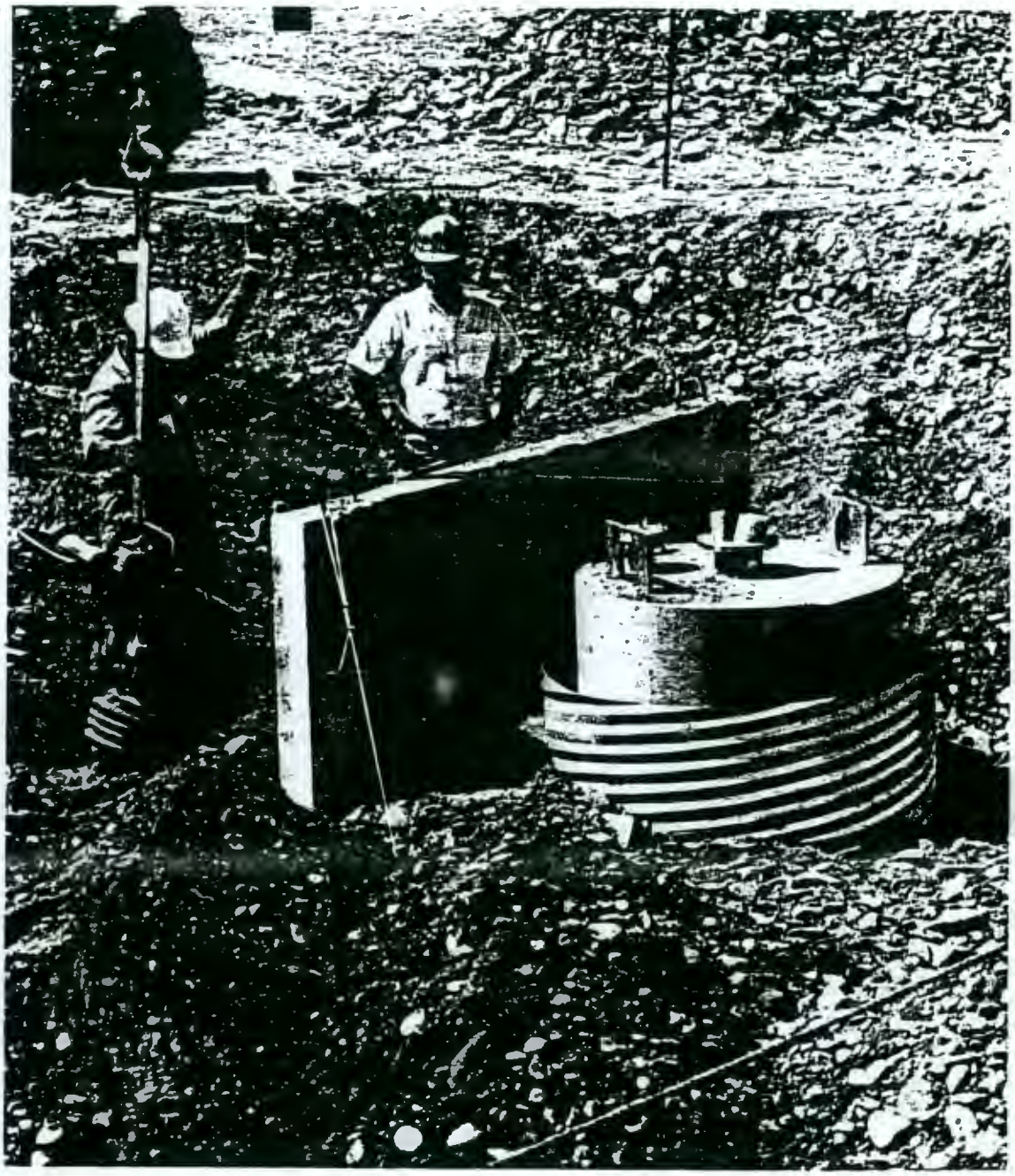

FIGURE 4.4. Tank and Wall Positioning as Shown During Site Construction Activities

TABLE 4.3. Composition of Simulated Sludge in Pilot-Scale Tank Test

Species	Quantity (g)	Concentration (wt%)
Cr_2O_3	2,315	0.58
CoO	420	0.10
Tri-butyl phosphate	990	0.25
HgO	270	0.067
$CsNO_3$	270	0.067
$Sr(NO_3)_2$	675	0.17
Pb (30 mesh)	4,620	1.16
Ni (powder)	1,000	0.25
BaO	3,012	0.76
CdO	62	0.016
Hydraulic oil (source of TOC)	9,900	2.48
Total	23,534	~5.9%
Balance ORNL soil (alumina-silica base)	375 kg	

ports in the top of the tank would not accept the large shale-like slabs of ORNL soil. Tanks in the field with larger ports could be backfilled directly with local soil without the need to grind or otherwise prepare the soil.

4.4 OFF-GAS SAMPLING

The off gases generated during the test were sampled at two locations in the off-gas system: 1) from the off-gas line before off-gas treatment, and 2) from the stack exiting the off-gas system after treatment. At both locations samples were collected using a commercial stack sampler in accordance with EPA standards as outlined in the Federal Register Vol. 42, No. 160, dated August 18, 1977. This sampling method is described in 40 CFR, Part 60, App. A as Method 5, "Determination of Particulate Emissions

from Stationary Sources." A schematic of the sample system used on the off-gas line is shown in Figure 4.5. Besides collecting samples, the system measures off-gas flow rate and temperature. In addition, the percent moisture in the off-gas stream is calculated based on the amount of water condensed in the impingers. Off gases are isokinetically extracted through a nozzle and a heated probe into a heated filter where the particulates are removed. The hot gases are then passed through a series of five cooled impingers where the condensibles are removed and the gases are cooled before passing through the pump, dry gas meter, and flow orifice. The filter media used to capture particulates is composed of borosilicate glass fibers and has a collection efficiency of 99.97% on 0.3-µm DOP particles [standard DOP (dioctylphthalate) penetration test]. For this test, the samplers were operated continuously except for brief periods during filter and solution change-out. The impinger solutions were selected to maximize collection of the specific metals that were placed into the tank. The samples collected from the two samplers (filter media, impinger solutions, and any condensed water) were analyzed to determine the composition of the off gas prior to treatment and the effectiveness of the off-gas treatment system.

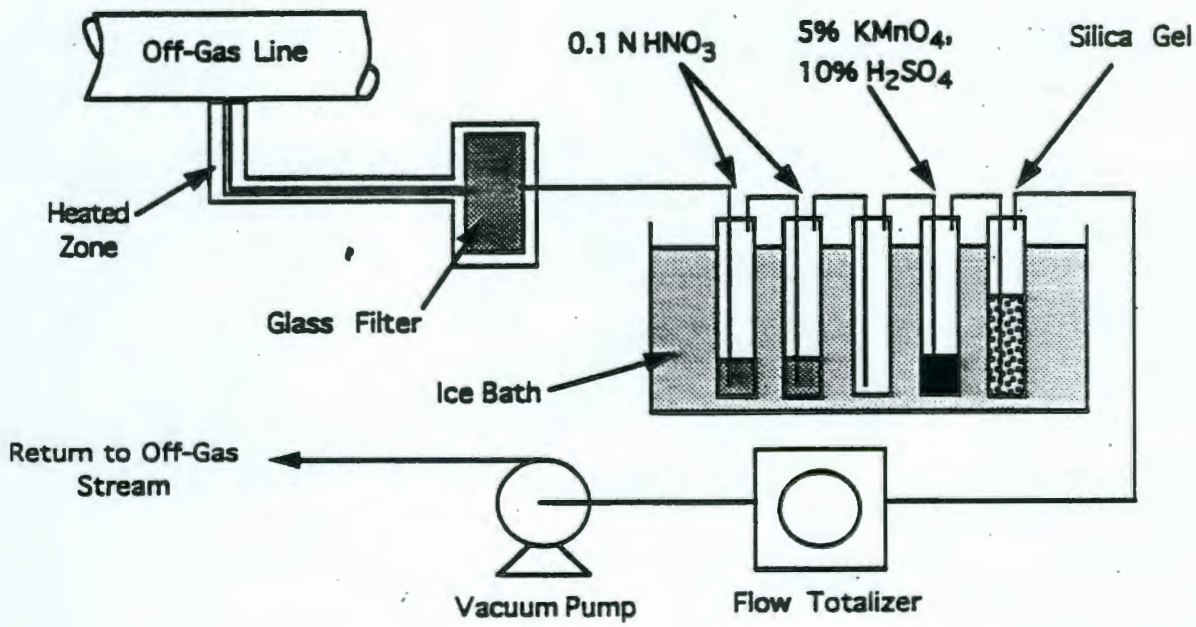

FIGURE 4.5. Method 5 Off-Gas Sampling System Configuration

The sampler placed "before off-gas treatment" used a 0.1 N nitric acid solution in the first and second impinger; this solution is preferred for use as a multiple metal screen. The third impinger began the sampling period empty and was used to collect condensation from the off-gas stream. The fourth impinger contained a 10% sulfuric acid and 4% potassium permanganate solution specifically designed to capture mercury. The fifth and last impinger in the sampling train contained 300 g of color-indicating silica gel to capture any remaining moisture in the sample stream. The sample system used on the stack after off-gas treatment was identical to the sampler on the off-gas line with the exception of the impingers. The first and second impingers used a 0.1 N nitric acid solution, the third impinger was empty, and the fourth impinger contained color-indicating silica gel.

5.0 OPERATIONAL RESULTS

The primary objectives of the pilot-scale, underground tank ISV test were to verify the applicability of the ISV process for tank remediation and to determine near full-scale process behavior when vitrifying tanks. In specific terms relative to equipment and process operations, this research sought to:

- Demonstrate that the ISV process could completely melt a tank and supporting structures.
- Obtain performance data concerning electrode feeding and the use of graphite electrodes.
- Collect process performance data relative to future full-scale applications.
- Evaluate the performance of the castable refractory wall, which was designed to deflect the shape of the melt for future large-scale applications, to thermally protect nearby tanks and pipelines.

The test successfully met each of these objectives. Consider the following observations:

- The target vitrification depth of 2.4 m (8.ft) was achieved. The test was terminated at the 2.4-m (8-ft) target depth to allow posttest soil sampling of the ORNL soil remaining below the tank.
- The ISV process completely destroyed the tank and the tank's supporting structures, and vitrified the tank contents and the soil below the tank. A uniform glass and crystalline monolith was produced with a mass estimated at 24 metric tons.
- A previously unknown phenomenon that generates significant pressurizations of the off-gas containment hood was observed and characterized. In addition, a means to prevent or at least dramatically reduce the potential for pressurizations was developed and successfully implemented. The mechanism that creates the pressurization is the instantaneous radiant shine to particulate-laden gas in the containment hood upon the sudden disruption of the frozen layer of glass on the surface of the melt. This event occurred during the test and necessitated a temporary suspension of the test to evaluate the cause and determine appropriate means to prevent its recurrence. In addition to gaining an understanding of the pressurization mechanism, significant process data regarding the ISV behavior of tank processing (including off-gas characteristics, melt behavior, and electrical system response) were obtained from the test.
- During the test, the ability to restart the process and remelt a significant volume of frozen glass was easily demonstrated. As a result of the pressurization event that required a temporary suspension of the test, the process had to be restarted, and 106 cm (42 in.) of previously vitrified material was remelted. This indicates that for future large-scale operations, recovery from extended periods of down time is possible. Frozen glass requires less energy to melt than soil since nitrates, carbonates, water, and other organic-based components such as humus have already been destroyed or driven off.
- Electrode feeding technology (movable electrodes that can be inserted or retracted) proved to be invaluable in recovering from electrical short circuits when the electrodes approached or contacted molten pools of metal in the bottom of the melt. By simply raising one or more electrodes a few centimeters from the bottom of the molten glass pool, recovery from electrical

short circuits was achieved. In addition, adjustment of the electrode insertion depth was an effective means to assist in the control of the electrical system. Inexpensive graphite electrodes proved capable of withstanding the extreme oxidizing environment. Due to an off-normal event during the test, all four electrodes had to be held in position for an extended period. One electrode failed due to oxidation; however, recovery was effected in less than 20 min simply by inserting an additional electrode into the melt.

- A barrier wall made of castable refractory was designed to deflect the melt shape. The wall directly contacted the molten soil for the duration of the test and survived the test with essentially no degradation. For actual remedial operations, it may be necessary to protect nearby tanks and active pipelines from the destructive forces of the vitrification process. The wall was designed to test a candidate material under actual conditions. Active cooling with an air blower in the area immediately behind such a wall will result in acceptably cool temperatures to protect nearby tanks and pipelines.

Operational aspects of the test for both the initial portion of the test (including the significant hood pressurization event at 19 h) and the balance of the test are detailed below. The following aspects of the test are discussed in Section 5 to provide a comprehensive evaluation of the test phases:

- electrical power system performance
- electrode and electrode feed system performance
- off-gas treatment system performance
- off-gas containment system performance.

In all cases, it is the intent to evaluate the generic ISV process relative to future large-scale applications rather than to evaluate the specific performance of the smaller pilot-scale system. Considerable analysis regarding the pressurization of the containment hood is provided in Section 6.0 and Appendix A. Post-test activities such as block excavation, sampling, and analyses (including product analyses) are detailed in Section 7.0.

5.1 TEST OVERVIEW

The underground tank vitrification pilot-scale test was initiated at 19:27 h on September 11, 1990. The early hours of the test proceeded smoothly with relatively balanced electrode power and steady performance by the off-gas treatment system. The downward melt rate averaged 5.6 cm/h (2.2 in./h). The melt depth was approximately 106 cm (42 in.) (as indicated by thermocouple data) when the hood pressurization occurred at 19 h, which resulted in the temporary suspension of the test.

Following an evaluation of the pressurization event, it was determined that the pressurization was caused by a relatively small volume of steam and soil that was released from the melt to the hood. The steam and particulate erupted up through the molten glass and rapidly disrupted the layer of frozen glass

9613400.0910

(cold cap) covering the top of the molten pool. Once disrupted, the temperature and pressure in the plenum dramatically increased due to radiation heat transfer to the gases and suspended particulate in the plenum from the near instantaneous exposure of the melt. (The mechanisms for this event are discussed in detail in subsection 6.2.) To prevent the recurrence of this type of event during the remainder of the test, a radiant heat shield was installed inside the off-gas containment hood. The shield was made of a carbon steel frame covered with a high-temperature fabric that spanned the area being vitrified and blocked the radiant heat from the melt. In addition to the heat shield, a graphite pipe was installed in the bottom of the tank to act as a passive vent to release gases from the tank as they were produced.

The test was restarted from grade level on September 25, 1990, at 19:16 h. The melt proceeded rapidly through the glass that had been formed during the initial startup (phase 1) of the test at a rate greater than 8.9 cm/h (3.5 in./h) and then slowed to 2.8 cm/h (1.1 in./h) after the melt front reached the unmelted regions of the tank, as shown in Figure 5.1. The second phase of the test progressed smoothly with no transient gas releases from the melt, indicating that the heat shield/vent combination performed as designed. Significant gas generation did occur as the tank was being vitrified, as evidenced by visible gas flame at the vent pipe exit. With the exception of one electrode failure, the remainder of the test was relatively uneventful. A plot of the pressure in the tank for the second test phase is provided as Figure 5.2. The minimal tank pressure is due to the resistance of the gas moving through the soil backfill

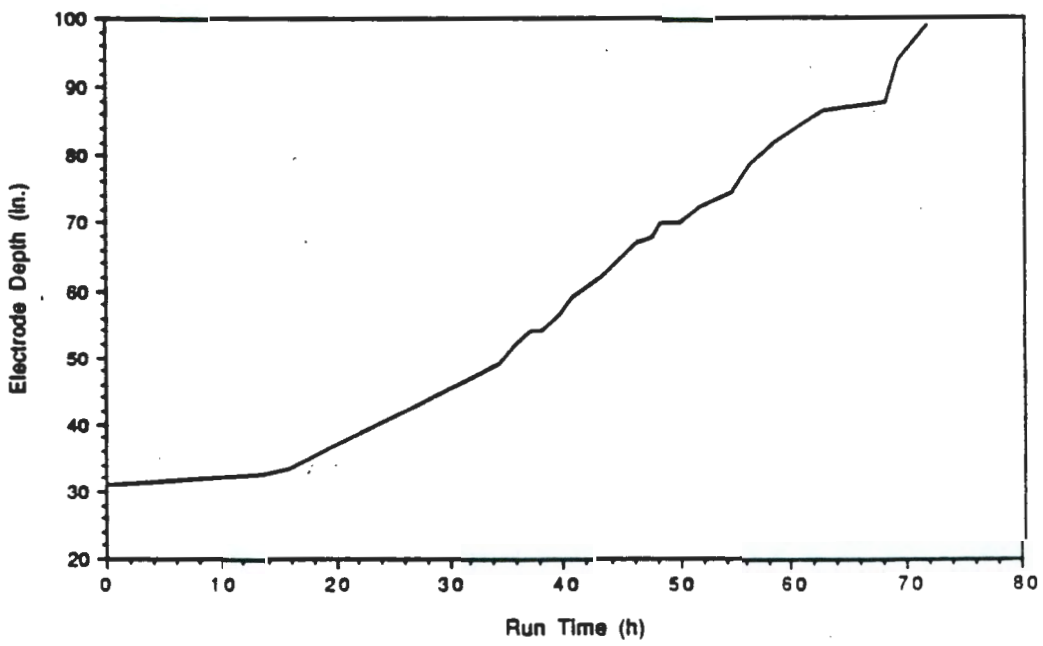

FIGURE 5.1. Average Electrode Depth During Phase Two of Test

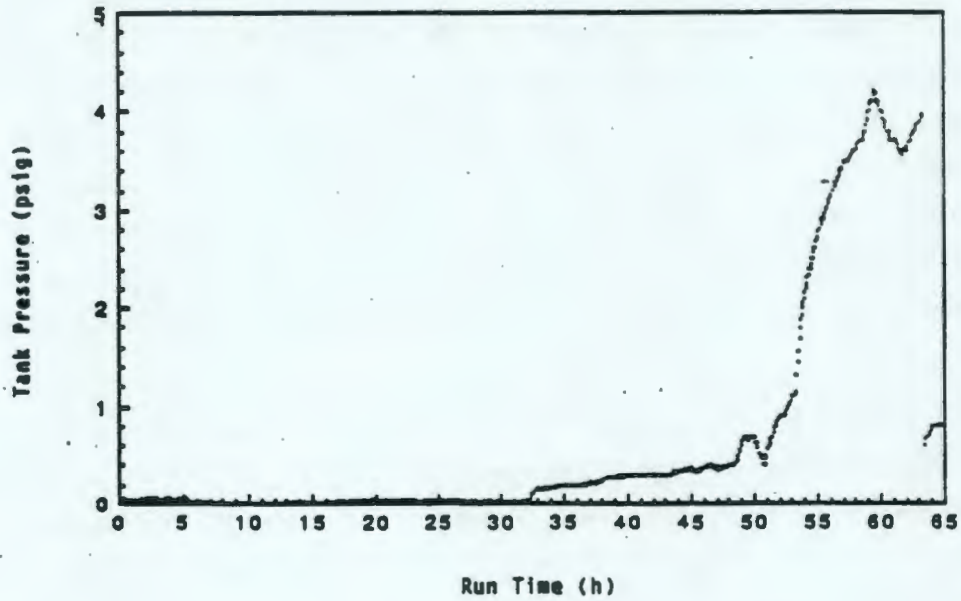

FIGURE 5.2. Average Tank Pressure Versus Time

before releasing through the vent. Once the melt reached the bottom of the tank and the vent pipe filled with molten glass, the tank pressures increased to the head pressure of the melt. A chronological listing of events for the test is contained in Table 5.1.

5.2 ELECTRICAL POWER SYSTEM PERFORMANCE

The power system performed well throughout the test. The average power applied to the molten soil equaled 300 kW for the duration of the second test phase (Figure 5.3). Occasional periods of electrical instability and imbalance between electrical phases occurred late in the test, but did not hamper operations. The only notable imbalance for the initial phase of the test occurred when the melt progressed through the top of the tank. A high localized concentration of calcium existed in the melt after the advancing melt front dissolved the top layer of concrete that covered the top of the tank and the adjacent limestone gravel. Concrete is composed of high concentrations of CaO, typically ranging from 40 to 65 wt%. When concrete decomposes during vitrification, the resulting CaO can decrease electrical conductivity in the melt (Buelt et al. 1987). The contribution of the increased amount of calcium from the decomposition of the concrete shell combined with some small transient gas releases from the tank resulted in some minor electrical instabilities during the initial phases of the test. The voltage imbalances late in the test were due to both the increased calcium from the bottom of the tank shell and the disruptions created by molten metal pools. Electrical shorts occasionally occur when electrodes contact molten

96/9900,0919

TABLE 5.1. Chronology of Events of Pilot-Scale Test

Date	Run Time (h)	Event
9/11/90	0.00	Test start-up. Power applied to the soil.
9/11/90	3.36	Type K thermocouple (T/C) No. 1 at a depth of 20.3 cm (8 in.) reaches 100°C. Power increasing 1 kW/min.
9/11/90	4.13	Melt resistance peaks at 6.8 ohms.
9/12/90	5.45	Tap change to the 650-V tap.
9/12/90	6.14	Hood vacuum adjusted from ~1.7 to ~2.0-in. W.C.
9/12/90	6.35	Power to the melt terminated due to 100-A imbalance on the primary electrical phase. Electrode adjustment corrected imbalance.
9/12/90	7.00	Power to melt restored. Electrode depths at 32.4 cm (12.75 in.).
9/12/90	9.20	Electrodes show 1.3-cm (0.5-in.) loss of diameter due to air oxidation.
9/12/90	11.23	Tap change to the 430-V tap.
9/12/90	12.33	Hood vacuum spikes to ~0-in. W.C. for a few seconds, corresponding to the top of the tank melting.
9/12/90	16.13	Electrode depths at 68.6 cm (27 in.).
9/12/90	17.48	Power equals 409 kW.
9/12/90	17.73	Gas release from melt results in vacuum spikes. B/U blower automatically energized. Power loss of 75 kW as a result of increased resistance. Tank pressures unchanged at 2.5 psig. Hood air inlet adjusted to increase vacuum.
9/12/90	18.30	T/C No. 4 reaches 1250°C, indicating a melt depth of 106 cm (42 in.).
9/12/90	19.22	Major hood pressurization occurred to >5-in. W.C. Power to melt immediately terminated.
9/12/90	27.55	Off-gas system shut down. Test suspended.
9/25/90	0.00	Restart with vent and heat shield installed.
9/25/90	3.45	Restart going smoothly, temperature is 113°C at hood plenum and 307°C inside heat shield.

TABLE 5.1. (contd)

Date	Run Time(h)	Event
9/26/90	5.28	Tap change to the 650-V tap. Power at 284 kW.
9/26/90	6.98	Tap change to 430-V tap. Power at 287 kW with the system very balanced.
9/26/90	8.00	Total power now at 400 kW. Temperature inside heat shield is approximately 600°C, as no cold cap is present.
9/26/90	8.98	Strong flares 15 to 30.5 cm (6 to 12 in.) high around all four electrodes and the vent pipe. Cold cap is established.
9/26/90	11.58	Three of four electrodes are now free from the frozen glass created in the initial test phase. This indicates a melt depth of at least 106 cm (42 in.).
9/26/90	12.43	Flaring 15 cm (6 in.) high visible at top of vent, indicating gas release through vent.
9/26/90	20.63	Power to melt terminated for ~1 h for electrode gripper repairs.
9/26/90	23.32	Temperature inside heat shield is 707°C. Hood plenum is 321°C.
9/27/90	29.95	Electrical imbalances experienced over the last several hours. A maximum of 90 A (17%) imbalance on the primary and 90 A (16%) on the secondary was observed.
9/27/90	33.15	Tap change to the 250-V tap. Electrode depths average 127 cm (50 in.).
9/27/90	35.68	Hood plenum temperature at 205°C and inside heat shield, 423°C. Power at 304 kW.
9/27/90	41.42	Hood plenum at 220°C, inside heat shield 486°C, off-gas temperature at the inlet to the trailer is 198°C.
9/27/90	42.00	Power to the melt terminated to install additional section to each electrode.
9/27/90	49.63	Metal pool located under B2 since contact with bottom produces electrical short. A2 on bottom with no effect.
9/28/90	54.73	Electrode depth averages 185 cm (73 in.).
9/28/90	64.73	Melt depth 12.7 cm (5 in.) below bottom of tank. Type C T/C at pad level below tank is at 921°C.
9/28/90	67.90	Type C T/C at pad level is 1380°C.
9/28/90	72.07	Electrode depth averages 2.5 m (99 in.). Power to melt terminated, and shutdown activities commence.

9615400.0920

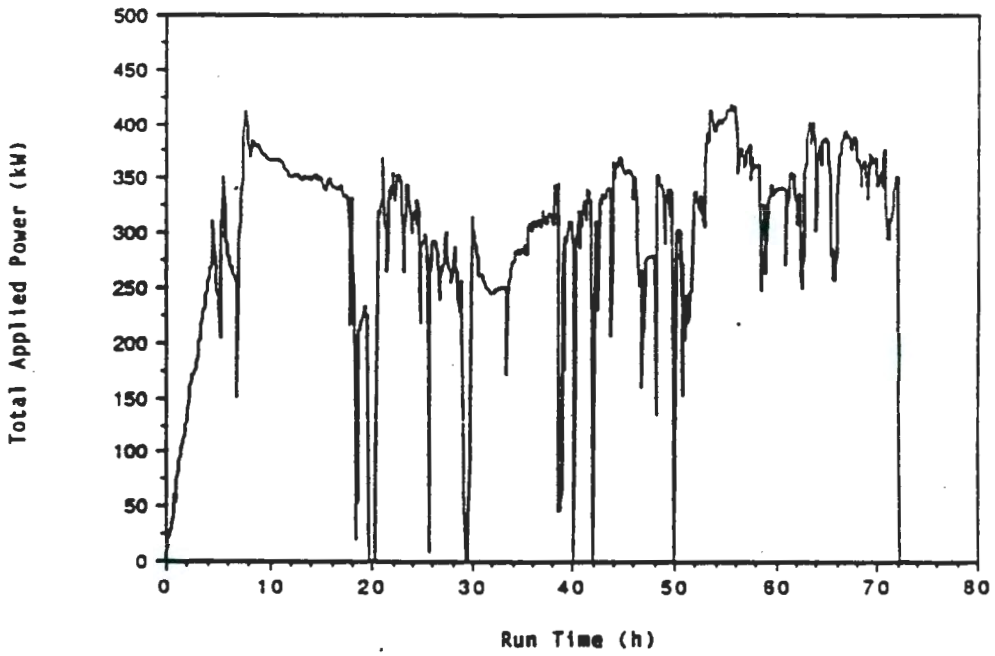

FIGURE 5.3. Total Power to Electrodes

metal pools at the bottom of the melt or partially melted metal objects. During the initial phase of the test, no evidence of electrical shorting from molten pools of metal was observed; however, in the second phase of the test, definite electrical shorting was observed when the electrodes were in contact with the bottom of the melt.

Power levels were increased to ~300 kW during the first 6 h, consistent with the graduated power build-up. Power levels averaged 300 kW for the duration of the test. A total of 4750 kWh was used during the initial 19-h period, and a total of 21,000 kWh was used for the second phase of the test for a total of approximately 26,000 kWh. The total kWh is high, since this included remelting the initial 1.06 m (42 in.) of glass.

A plot of electrical resistance for the molten soil is provided in Figure 5.4. The resistance plots follow an expected curve. Resistance typically decreases to between 1 to 2 ohms per phase when the starter path is fully molten. As the starter path is consumed by oxidation and the current is transferred to the surrounding molten soil, the resistance increases until the molten soil zone grows in size; resistance then begins to decline until a near steady-state value of between 1 and 2 ohms per phase is achieved.

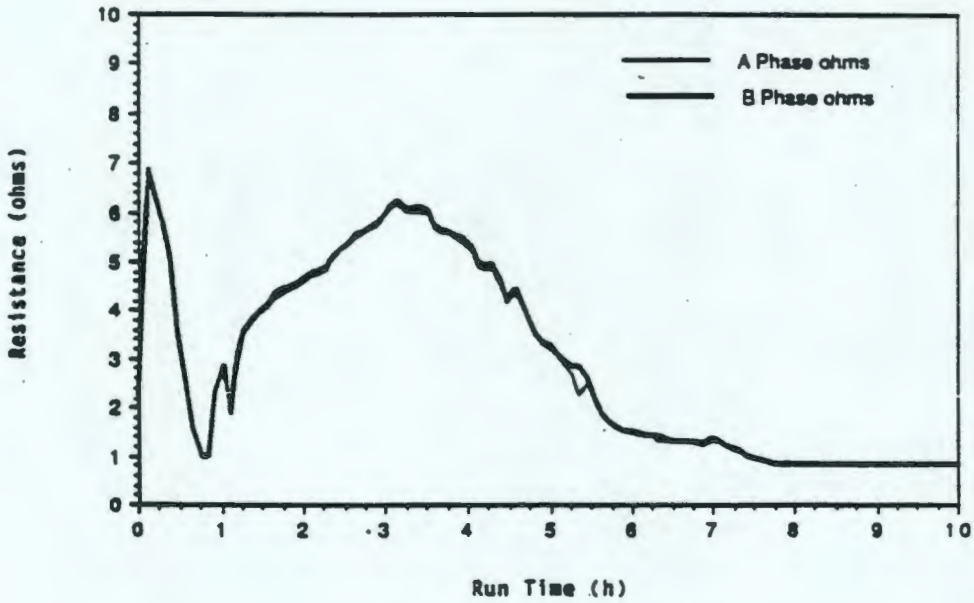

FIGURE 5.4. Resistance for the Initial Hours of the Restart (9/25/90)

During this test, gas releases from the melt caused a reduction of melt temperature due to increased heat transfer from the melt. This event resulted in a substantial reduction of the power to the melt due to a less electrically conductive melt. Approximately 30 min of powered operation was required to restore the melt to the previous power input level. This phenomenon is illustrated in Figures 5.5 though 5.7, which are plots of the hood vacuum, hood plenum temperature, and total electrode power. The plots show that the gas release from the tank resulted in the rapid heating of the plenum, and significant radiant heat losses from the molten glass increased the melt resistance and decreased the amount of power that could be applied. Operating staff observed an ~50-cm (20-in.)-diameter hole in the cold cap immediately after this event. The disrupted cold cap exposed the "white hot" molten pool resulting in the radiant heat losses. This gas release from the tank was relatively mild and occurred 17.65 h into the test.

The occasional periods of voltage imbalance between electrical phases occurred to a maximum of 100 A on the primary phase, but did not hamper operations. For large-scale applications, electrode feeding and independent control of the transformer's secondary power phases will result in controlled and balanced operations. The pilot-scale system transformer has only a single control on the primary side. Consequently, the only means to control an imbalance between phases is via electrode movement. Electrode feeding is essential because the electrodes that are inserted into the melt can be independently adjusted, for example, to retract them from a molten metal pool to prevent an electrical short circuit. However, PNL's reference large-scale design uses independent phase control to allow for a second mode of controlling electrical imbalances.

9613400.0921

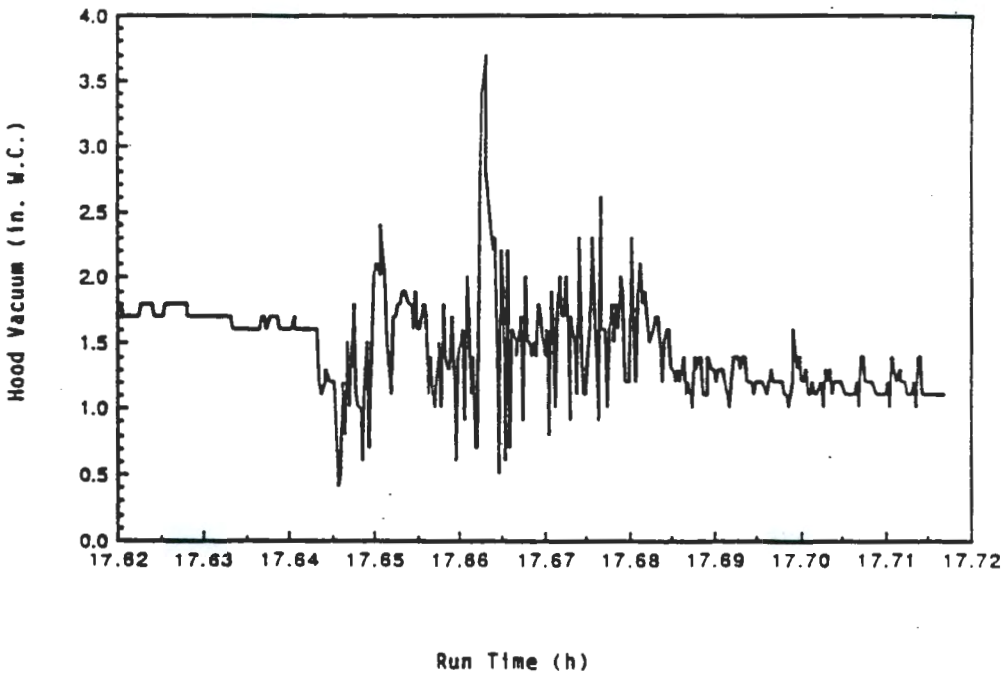

FIGURE 5.5. Hood Vacuum at 17.6 to 17.7 Test Hours (9/12/90)

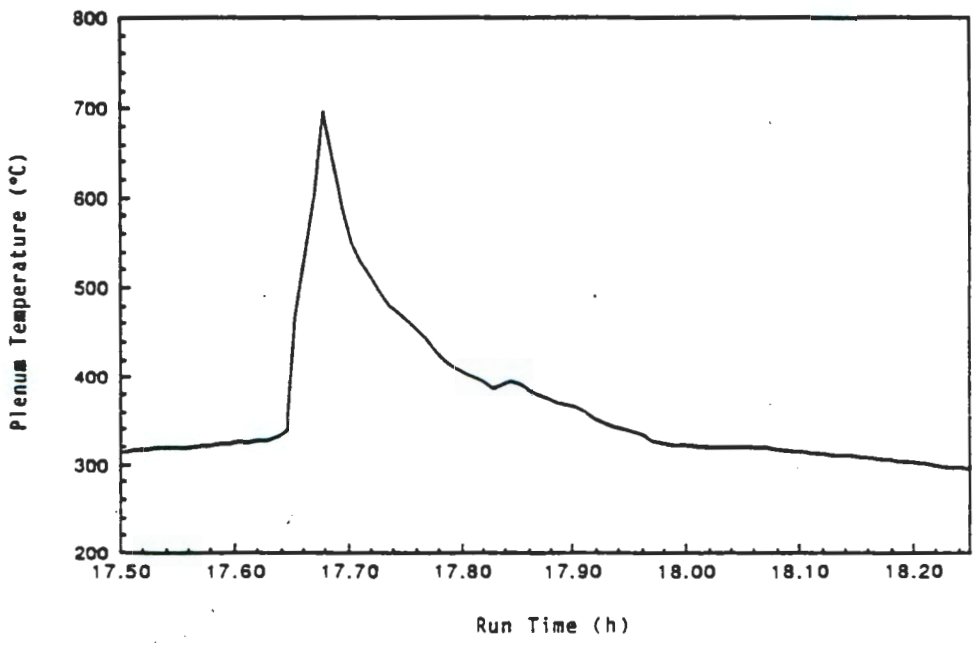

FIGURE 5.6. Plenum Temperature (DAS) at 17.5 to 18.2 Test Hours (9/12/90)

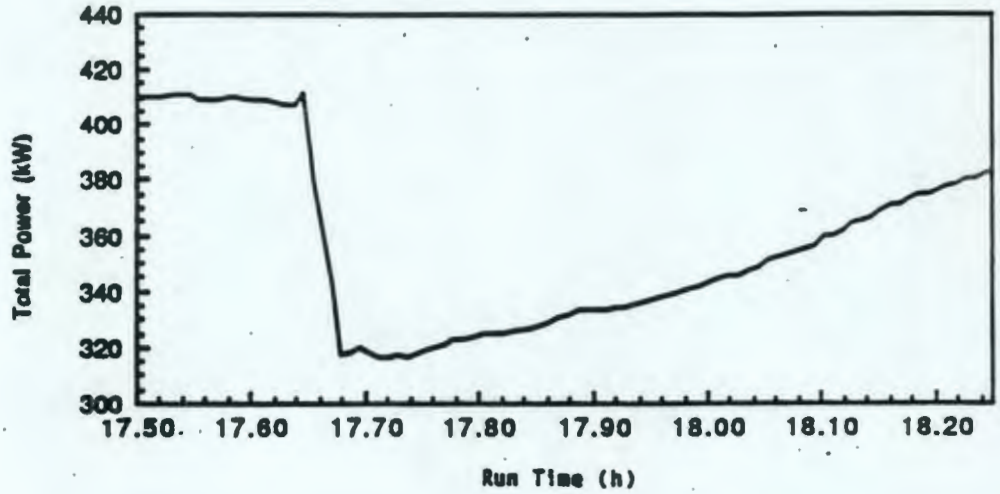

FIGURE 5.7. Total Power at 17.5 to 18.2 Test Hours (9/12/90)

5.3 ELECTRODE AND ELECTRODE FEED SYSTEM PERFORMANCE

The electrode feed system performed well throughout the test. The feed system was used to raise the electrodes a few centimeters from the bottom of the melt during the first phase of the test in an attempt to prevent the electrodes from contacting molten metal pools and to control the rate of downward melt growth. Normally, the feed system is not engaged unless partial retraction of one or more electrodes is desired. The electrodes are typically allowed to feed by gravity as they rest on the bottom of the molten pool and advance as the pool deepens. Holding the electrodes off the bottom of the melt did not appear to slow the rate of downward melt growth. It is suspected that only the amount of power delivered to the melt will control melt rate.

The electrodes used were uncoated 15-cm (6-in.)-diameter graphite rods consisting of either grade MH or grade MR graphite (from Superior Graphite Co.). Although quantitative data were not collected, posttest observations of the joint between grade MR and MH electrode sections revealed an approximate 1-cm (0.39-in.) step increase in the diameter of the MH section. Grade MH has an apparent density of 1.73 g/cm^3 and an apparent porosity of 22%; grade MR has an apparent density of 1.64 g/cm^3 with an apparent porosity of 23.2%. Additionally, grade MH has higher compressive, tensile, and flexural strength and slightly less electrical resistance. Both grades performed satisfactorily for this test; however, the higher density graphite grade appears more resistant to air oxidation and merits use in large-scale applications.

In general, electrodes become narrow and are prone to breakage due to air oxidation, primarily at the air/melt interface. Oxidation losses are most severe if the electrodes must be held in place for extended

periods of time, allowing the oxidation to continually occur at the same portion of the electrode at the air/melt interface. During this test, graphite loss due to air oxidation reduced the diameter of the uncoated electrodes only about 2.54 cm (1 in.) over the exposed length of the electrode during the test. This effect is typical and acceptable for the inexpensive graphite electrodes. However, after the test was restarted, one electrode failed due to air oxidation at the air/melt interface. The electrodes had frozen in place when the test was suspended at 19 h. Upon restart, the electrodes remained in place until the frozen layer of glass was remelted; this stationary period caused the failure. When the electrode failed, recovery merely involved adding a new section to the electrode and inserting it into the melt. This represents a near worst-case situation for graphite electrodes. In past ISV operations, especially using the fixed nonmovable electrode design, the electrodes were coated with a silica-based product designed to reduce oxidative losses. The coating can create a problem by causing the glass to adhere to the graphite, and consequently, the electrode may become bound to the frozen glass layer covering the melt, which renders the feed system useless, as demonstrated in a previous pilot-scale test (Callow et al. 1991).

5.4 OFF-GAS TREATMENT SYSTEM PERFORMANCE

Overall, the off-gas treatment system performed well during the operational phase of the test. Off-gas analytical data and scrubbing efficiencies are discussed in Section 8.0.

The Venturi-Ejector performance relative to heat removal is illustrated for the second test phase in Figure 5.8, which shows that the gas temperature entering the Venturi-Ejector typically ranged from 150° to 250°C. The exit temperature (Hydro-Sonic entrance) was usually less than 50°C. The differential pressure for the Venturi-Ejector, provided as Figure 5.9, shows a slight upward trend due to the deposit of solids. As a result of the major pressure spike at 19 h in phase 1, a significant amount of soil was entrained in the gas release and scrubbed out in the off-gas treatment system. As the scrub solution was recycled through the various scrubber spray nozzles, the particulate occasionally formed deposits, mainly at the entrance to the Venturi-Ejector. Some of the solids periodically dislodged and caused a lowered differential pressure. The presence of solids in the gas stream should be addressed in the design phase of any new machine, because hazardous and radioactive solids can potentially plug small-diameter tubing and result in a sludge buildup in the off-gas treatment system.

The Hydro-Sonic scrubber differential pressure was maintained well above 50-in. W.C. throughout the test, as shown in Figure 5.9. By design, this should have resulted in a particulate removal efficiency of >90% for particles sized >0.5 µm. The fluctuations of differential pressure, shown in Figure 5.9, were due to fluctuations in total off-gas flow created by intermittent off-gas releases from the melt and operational adjustments of hood vacuum.

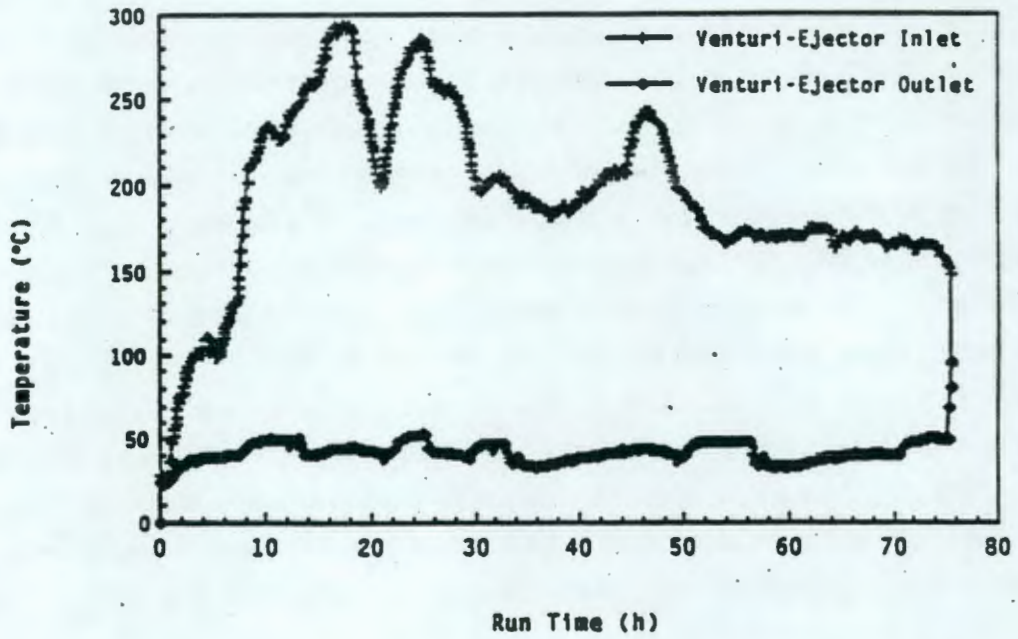

FIGURE 5.8. Average Venturi-Ejector Inlet and Outlet Temperatures

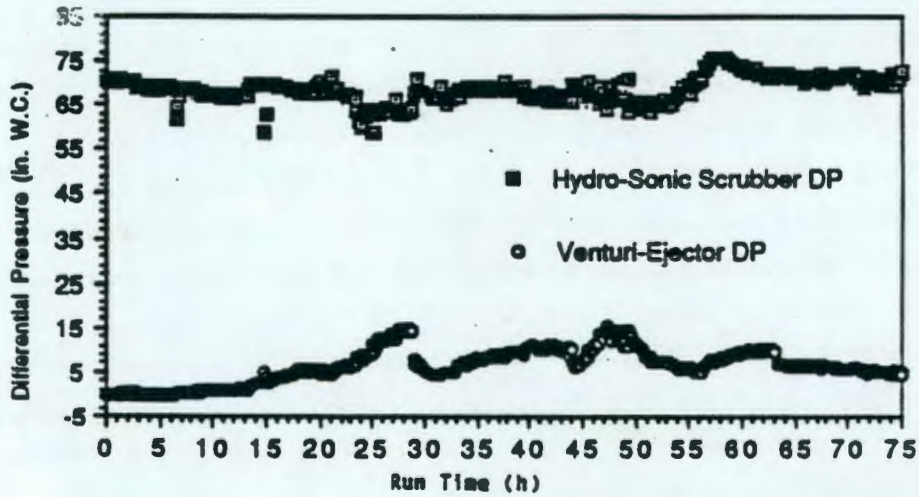

FIGURE 5.9. Average Differential Pressures for the Venturi-Ejector and the Hydro-Sonic Scrubbers

Differential pressure measured across the housing of the primary HEPA filter is shown in Figure 5.10. The differential pressure remained relatively constant throughout the test, indicating that the scrubbers effectively removed the vast majority of particulate, and the filters were not becoming loaded. These data demonstrate that a large-scale machine with a wet scrubbing system of comparable design could sufficiently remove particulate from the off-gas stream.

Total gas flow through the off-gas treatment system is shown in Figure 5.11. Total flow ranged from 12 to 17 m^3/min (400 to 600 cfm). Late in the test (at ~70 h) after power to the melt was terminated, off gassing from the melt decreased such that the total off-gas flow was approximately 12 m^3/min (400 cfm). This flow rate was largely representative of the controlled in-leakage of air into the hood, because off gassing from the melt at that point in time had significantly diminished.

Concentrations of oxygen and carbon monoxide were monitored at the off-gas stack throughout the test. The oxygen concentration averaged between 20% and 21%, with a decrease to 19.2% that occurred during the initial phase (at ~19 h) (Figure 5.12). As shown in Figure 5.13, carbon monoxide concentrations typically ranged from 0% to 0.1% with a maximum of 0.2% at start-up and during a period at ~53 h when processing the sludge layer. The greatest concentrations of carbon monoxide were expected shortly after start-up as the graphite portion of the starter path was consumed.

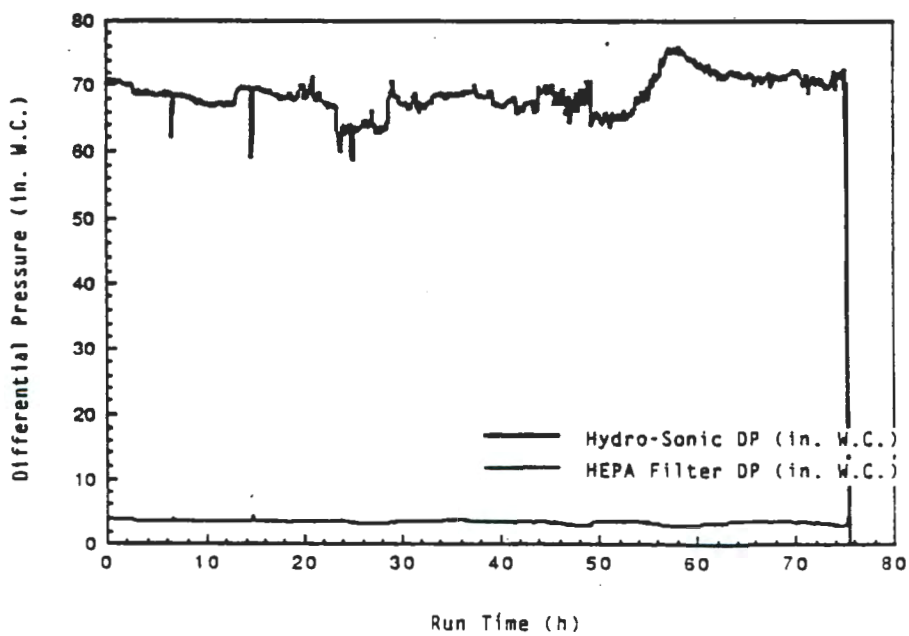

FIGURE 5.10. Hydro-Sonic Scrubber and Primary HEPA Filter Differential Pressure

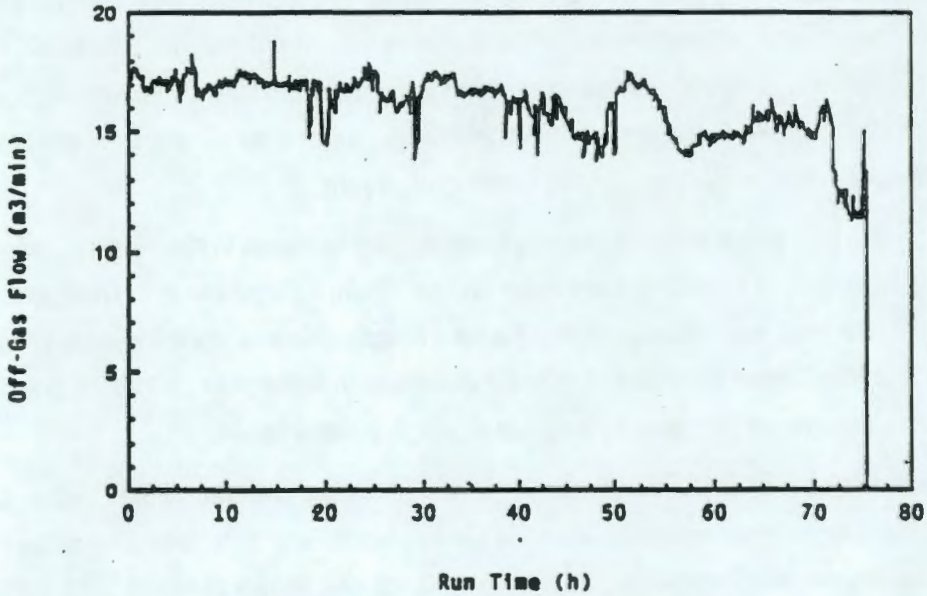

FIGURE 5.11. Average Stack Off-Gas Flow

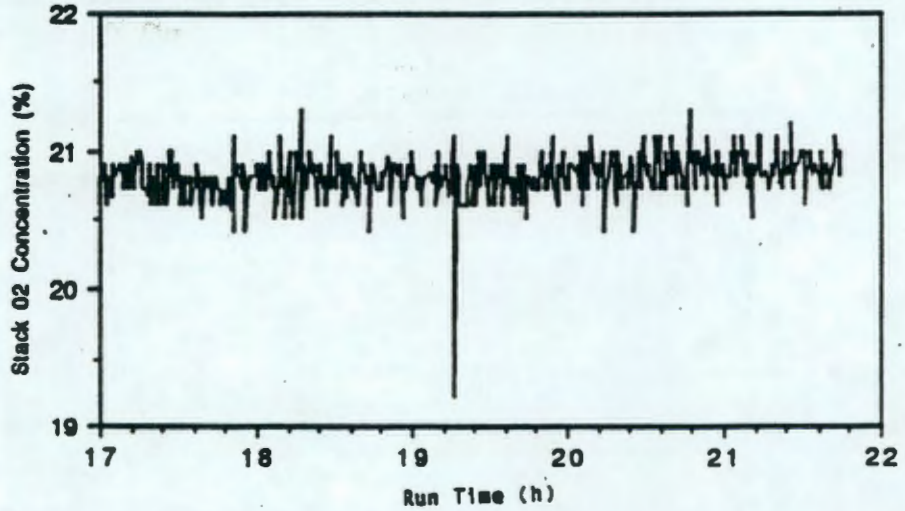

FIGURE 5.12. Stack Oxygen Concentrations During the Later Stages of Test Phase 1

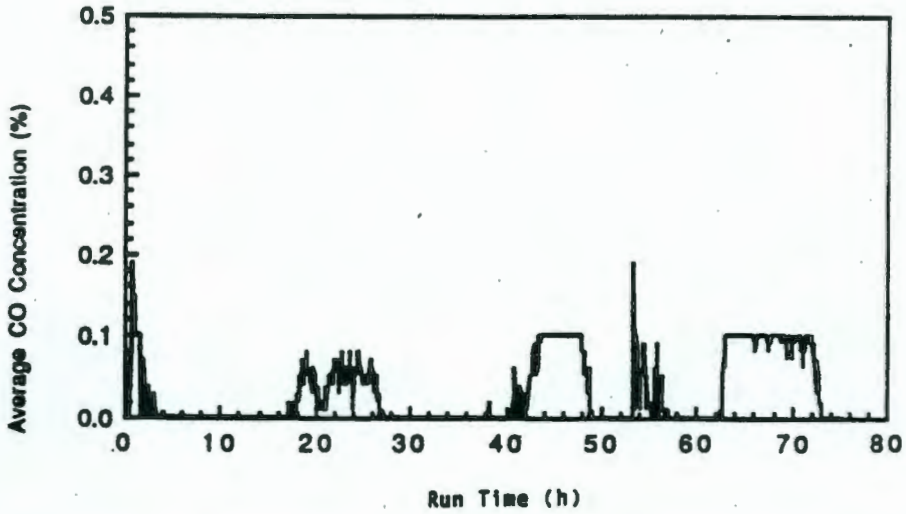

FIGURE 5.13. Average Carbon Monoxide Concentration During Test Phase 2

This test used a sludge layer that contained minimal water; consequently, the level of scrub solution in the process scrub tanks was easily maintained. When the test was near completion, the tanks were operated at a higher temperature to increase evaporation and reduce the generation of secondary waste. Note that large-scale operations on underground storage tanks having high water content will introduce large amounts of water vapor to the process off-gas system. Losses through evaporation are necessary to prevent the undesired accumulation of solution that would increase the secondary waste stream. To do so, large-scale machines designed to process underground tanks will require a significant evaporative capability.

5.5 OFF-GAS CONTAINMENT SYSTEM PERFORMANCE

Gas releases from the melt were relatively steady except for three separate events in test phase 1. The off-gas containment hood vacuum (Figure 5.14) averaged greater than 2-in. W.C. vacuum for the second phase. Differences in the steady-state values are due to operational adjustments.

The temperatures recorded by the thermocouple in the plenum are generally the highest in the hood, since this thermocouple is in the center of the hood cavity and is nearer to the molten glass than other thermocouples. The hood plenum temperature averaged 250°C (Figure 5.14). The plenum temperatures were approximately 50°C cooler than predicted due to the use of the radiant heat shield. During a 3-h period in test phase 1 (shown in Figure 5.15), the cooler hood roof and wall temperatures paralleled the plenum temperature.

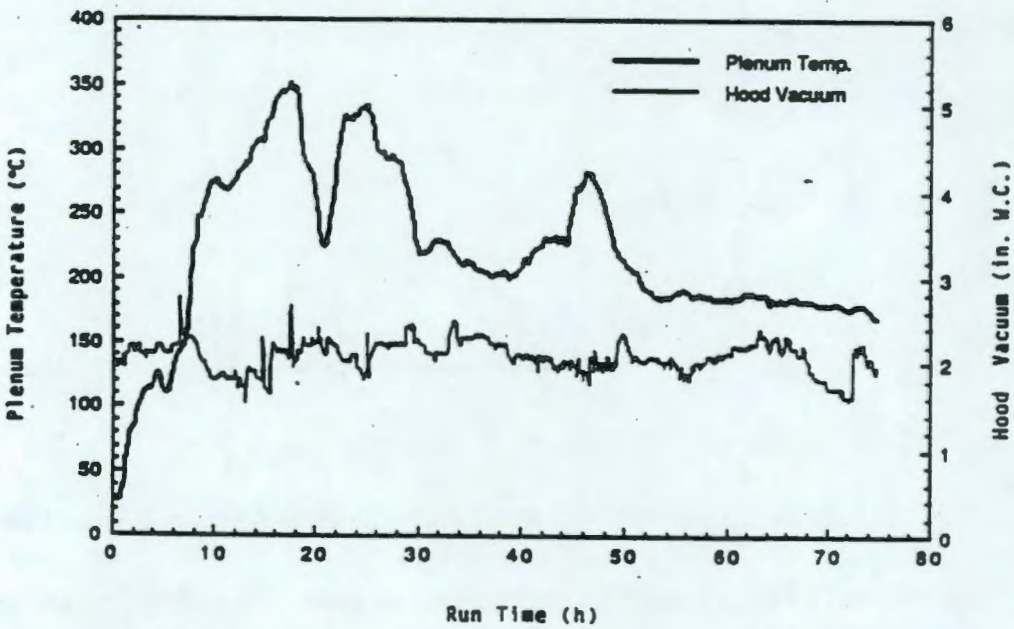

FIGURE 5.14. Hood Vacuum for Test Phase 2 and Average Plenum Temperature

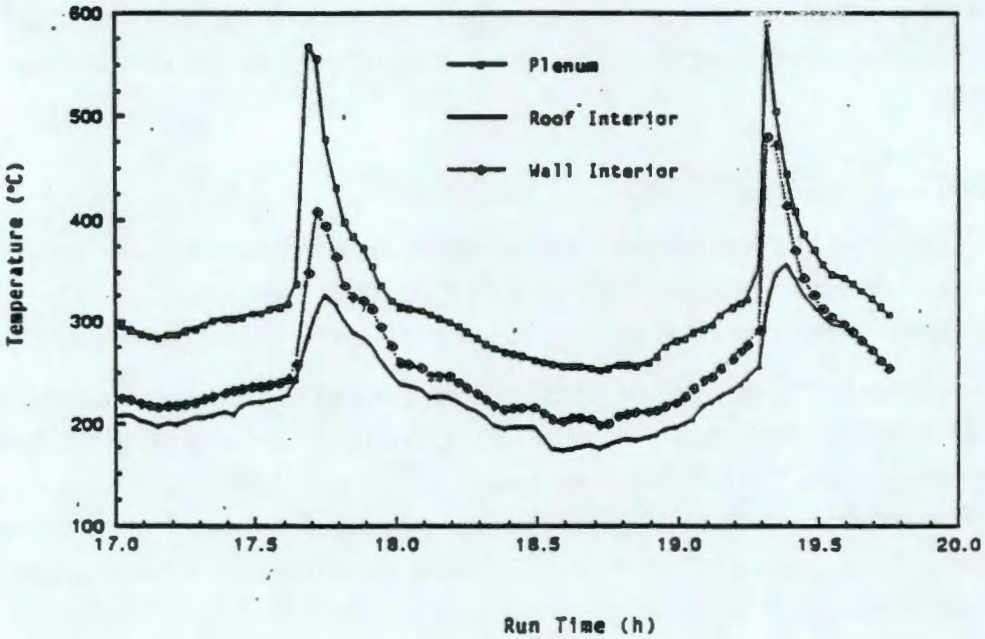

FIGURE 5.15. Plenum, Roof, and Wall Interior Temperature (9/12/90)

Relative to the overall processing temperature and temperature spikes, no significant thermally induced structural degradations of the hood were observed during extensive posttest examinations of the hood. The gas release at 19 h during test phase 1 caused molten glass to splatter from the melt and contact the high-temperature fabric used for the electrode seals. This contact did not noticeably affect the fabric. A high-temperature sealant (RTV-106) was used to seal the inner and outer seams at the joints of the metal panels that form the containment shell. Careful examinations following the test revealed no thermal degradation of the sealant on the external seams. Examinations of the internal seams revealed inconsequential surface degradation to less than 1 mm of the sealant that was directly exposed to the extreme temperatures. The balance of the sealant used on the inner seams remained pliant and showed no evidence of thermally induced degradation.

9613400.0926

6.0 MAJOR PRESSURE EVENT

6.1 EVENT DESCRIPTION

A major off-gas containment hood pressurization unexpectedly occurred at 14:43 h on September 12, 1990, approximately 19 h after test initiation. At the time of the event, the process had melted roughly one-third of the tank to a melt depth of ~1 m (42 in.) based on thermocouple data from the tank. Power to the melt was immediately terminated. An initial evaluation of the data revealed that within a span of 4 s the hood vacuum sharply decreased from 1.8-in. W.C. vacuum to a positive pressure in excess of 5-in. W.C. pressure. Concurrently, the off-gas exit temperature in the hood spiked from approximately 330°C to over 600°C (as shown in Figure 6.1). The maximum value of the hood pressurization was not obtained, because the pressure transducers were limited to a span of 5-in. W.C. vacuum to 5-in. W. C. pressure. Pressure data from the tank indicated that over a period of less than 1 min the pressure sharply increased from approximately 2.8 psig to a maximum of 3.3 psig and then dropped back down to 2.8 psig after the gas was released from the tank (Figure 6.2). This pressure at 3.3 psig approximately corresponds to the head pressure of the molten soil and an additional 0.5 psig, which was likely the pressure required to breach the soil/melt interface, which consisted of a layer of sintered soil beginning to melt. Before the event, the tank had been releasing gas at a relatively constant rate, as shown in Figure 6.2. The average

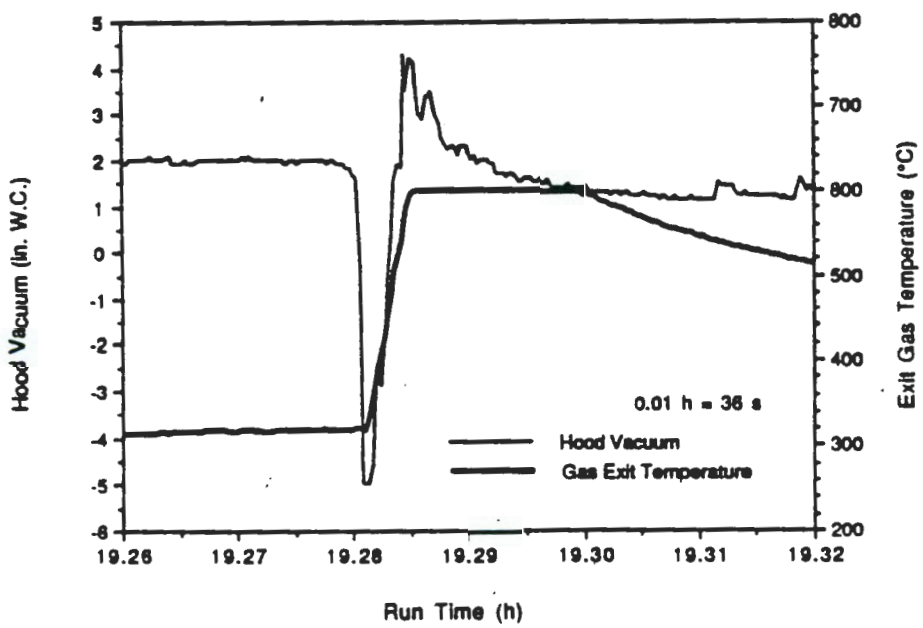

FIGURE 6.1. Hood Pressurization Event at 19.28 Test Hours on 9/12/90

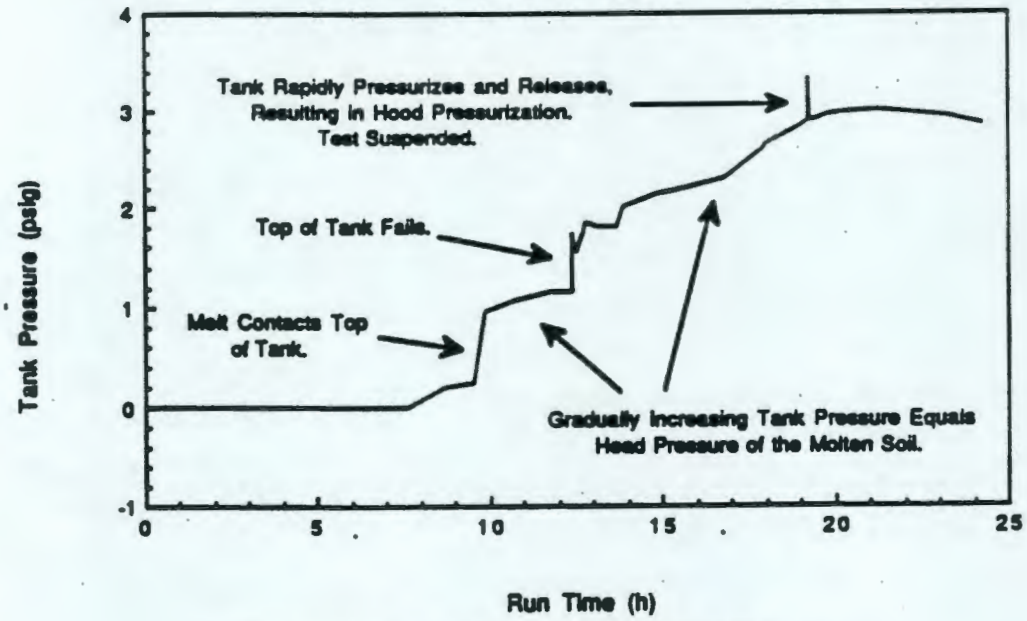

FIGURE 6.2. Tank Pressure During Test Phase 1

temperature in the tank cavity at the time of the event was approximately 50°C, and the effective remaining volume of the tank was estimated to be 480 L (125 gal), based on thermocouple data and melt depth.

6.2 ANALYSES OF MECHANISM

The reason the tank suddenly ceased to release gas and began to rapidly buildup pressure is uncertain. The tank pressurization probably resulted from the melt shifting downward over and past an area adjacent to a side wall that previously acted as a vent. As the glass contacted the relatively cooler region of the metal tank wall, the contact may have resulted in the wetting or sticking of glass to form a bond sufficient to contain a moderate overpressure in the tank cavity. Since the soil sintering and melting process occurs at temperatures less than the melting point of stainless steel, the metal side wall of the tank protruded up into the sintered layer and into the initial portion of the cooler molten glass. This condition would appear to effectively impede vapor/gas transport of gas leaving the tank since the gas permeability per unit volume of the sintered layer would be far less than that of dry soil, which surrounded the melt. It is suspected that before the event, the gas was released up along the inside of the side wall and down the outside of the side wall to the surrounding dry zone. The tank pressure was probably not being effectively relieved through the melt/soil interface directly above the tank because the characteristics of this low-permeable interface would be a sintered particle layer below a relatively cool viscous glass. Additionally, if the tank had been continually releasing its pressure up through the sintered layer and glass, regular bubbling in

9613460.0927

the melt would have been observed and the release would have continued regardless of the initiating mechanism that apparently caused the tank to rapidly pressurize.

Calculations using the Ideal Gas Law revealed that a volume of gas (primarily steam) released from the tank was approximately 0.7 moles of gas based on conditions in the tank both before and after the event. When the gas was released from the tank, it entrained a significant volume of the finely ground ORNL soil that had been used to backfill the tank and dispersed the soil as an airborne particulate into the hood. Once the bubble broke through or disrupted the cold cap and was released into the hood, the hood immediately began to pressurize and within 4 s exceeded the measuring limit of the pressure transducers for hood pressure to 5-in. W.C. pressure. Two to three seconds after the pressurization began, thermocouples in the hood showed the hood temperature rising sharply, with the off-gas exit temperature reaching over 700°C approximately 30 s later. After the test was suspended, observations within the hood revealed that the soil dispersed throughout the hood had coated essentially all the inner surfaces. Observations of the finely ground, reddish ORNL soil revealed that the soil was not at all discolored, which would have indicated thermal decomposition of some of the carbonates or oxides. This thermally induced discoloration is observed in the soil surrounding the melt if those soils have been heated in excess of 300° to 400°C. Consequently, the temperatures of the soil and the gas that were dispersed into the hood are suspected to have been insufficient to cause the thermal decomposition and discoloration of the soil. The data indicated that the gas release from the tank was nearly instantaneous and coincided with the hood pressurization.

Bounding calculations indicated that the approximate 0.7 moles of heated gas released from the tank were insufficient to cause a hood pressurization of the observed magnitude or account for a bulk gas temperature of 700°C that was measured exiting the hood. The 0.7 moles of superheated gas should only result in a maximum hood pressure of between 0 and 1.9-in. W.C. pressure. The fact that the plenum pressure exceeded 5-in. W.C. for 3 s indicated that a different mechanism was occurring.

The conclusion, which is strongly supported by calculations and analyses, is that the superheated gas bubble was partially responsible for the hood pressurization. The bubble broke through or disrupted the cold cap and started a mild pressurization. However, the key factor appears to be the disruption of the cold cap. Within 0.5 and 1.5 s after the bubble was released into the hood, the underlying molten pool of white-hot glass was exposed and immediately began to heat the entire hood volume of suspended particulate via radiant heat transfer. The particulate matter rapidly transferred its heat to the gas throughout the hood volume. The essential ingredient was the suspended particulate, which acted as radiant heat receptor. In previous ISV tests, reports of visual observations of the melt (via the viewing window) coincidental to such pressurization events noted that the amount of suspended particulate reduced visibility to zero. Likewise, in this test, the amount of soil dispersed into the hood that coated all inner surfaces

suggests the particulate concentration was extremely high. These types of conditions would result in 100% effective radiant heat transfer to the airborne particulate. (The discussion in Section 5.2 and supporting figures provides evidence of radiant heat losses from the melt.) Note that some of the most significant hood pressurizations in past pilot-scale tests have been observed to be accompanied by significant quantities of soil or dust being expelled into the hood plenum (Oma, Timmerman, and Buelt 1989).

Radiant heat transfer calculations performed using the Stephan-Boltzman law revealed that the rapid formation of a 50-cm (20-in.) hole in the cold cap could result in 137 kW of radiating energy assuming a melt temperature of 1600°C and a plenum temperature of 300°C. If this were the case, this significant energy source could instantaneously heat the suspended particulate and hood surfaces. As a result, the gas in the hood would attempt to expand to several times the volume based on the amount of energy radiating from the melt. This expansion would create significant overpressures in the hood that could reach several psig if the hood was a completely sealed container without release pathways. Since the expansion occurred very rapidly (less than 4 s) during the test, the surge protection system and the primary off-gas blower were unable to accommodate this sudden and significant change.

The nearly instantaneous heating of the hood is revealed by the recorded response time (time constant) of the 1/8-in.-sheathed thermocouples used in the hood (Figure 6.3). According to Figure 6.3,

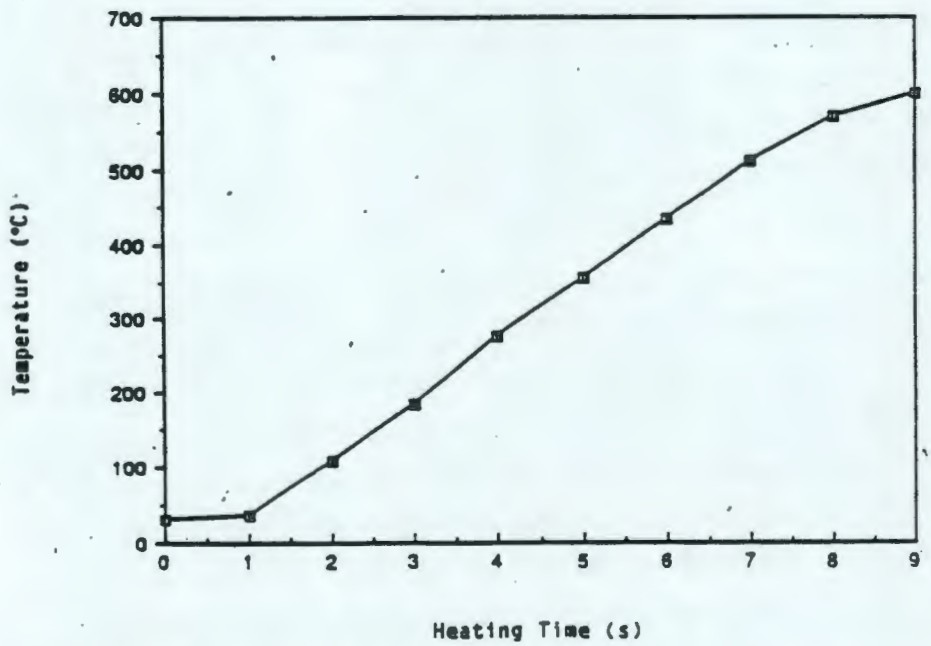

FIGURE 6.3. Response of a 1/8-in. Sheathed Type K Thermocouple Exposed to a 950°C Flame at T = 0

the 1/8-in. sheathed thermocouple responded 1 s after exposure to a 950°C flame at time zero. Then the thermocouple temperature tracked upward, taking in excess of 10 s to reach 62.3% of its maximum. This response indicates the likelihood that the temperature in the hood reached approximately 600°C 1 or 2 s after the initiation of the event.

6.3 RADIANT HEAT TRANSFER MODELING

In an attempt to fully analyze the event and to understand the actual maximum conditions in the hood, a simple computational model was constructed. The model, P3-ISV, is a set of computer-based algorithms for estimating the pressure and temperature transients in the containment hood resulting from a sudden expulsion of vapor, soil, and molten soil from the melt. The model accurately predicts the measured temperature within a few degrees and effectively mimics the pressure response for the first half of the event. P3-ISV calculated that the maximum temperature achieved in the hood as a result of the event was 640°C at 8 s and a maximum overpressure of 82-in. W.C. The model and the resulting outputs are discussed in more detail in Appendix A. The actual pressure achieved in the hood is thought to be lower than the predicted value due to several conservative assumptions, which are discussed in Appendix A. However, for the purpose of initially bounding the event, the model appears to accurately reflect the measured behavior for at least the first half of the event.

6.4 EVENT RECOVERY AND CORRECTIVE ACTIONS

The recovery involved a two-fold solution. First, a radiant heat shield was suspended above the melt surface to reduce the amount of gas that could be exposed to the melt's thermal radiation. Then, a graphite pipe was installed to the bottom of the tank to act as a passive vent.

The heat shield was constructed of a high-temperature, noncoated silica fabric (melting temperature >1650°C) supported by a carbon steel framework. The fabric was installed on the inside of the steel framework to minimize the framework's exposure to excessive temperatures. The passive vent consisted of a single 15-cm (6-in.)-diameter graphite pipe installed through the previously vitrified soil to the bottom of the tank. The vent pipe had an ID of 5-cm (2-in.), extended above grade, and was supported in position by the heat shield structure.

The solution of the vent and heat shield was successful in that there were no additional transient gas releases from the tank during the second test phase. The only pressures noted in the tank were minimal and were likely due to the pressure generated by the resistance to gas movement through the finely ground soil in the tank. Since the evaluation of the event and installation of the heat shield and vent required approximately 3 weeks, the heat from the initial melt effectively dried the tank and sludge, which

may have contributed to the success of the solution. However, it was evident that gas was being generated in the tank during the balance of the tank vitrification since a gentle 15-cm (6-in.)- high flame was observed throughout the test at the top exit of the vent pipe.

7.0 POSTTEST MONITORING, EXCAVATION, AND SAMPLING

The vitrified block was left undisturbed for several weeks following the test; the block was allowed to cool to near ambient conditions, which produced a representative waste form. During the cool down period, the thermal profiles around the block were monitored, and the off-gas containment hood and off-gas line were sampled, decontaminated, and disassembled. Excavation commenced approximately 6 weeks after termination of the powered phase of the test.

7.1 MONITORING OF THERMAL GRADIENTS

The vertical and horizontal thermocouple arrays allowed for monitoring of the thermal profiles (or isothermal bands) around the block during and after processing. The primary purposes of these thermocouples were to track melt growth and to determine appropriate isothermally based sampling locations in the surrounding soil. The insulative characteristics of soil resulted in relatively steep thermal gradients around the advancing melt front. During the powered test operations, the 100°C isothermal band was typically 45 to 60 cm (18 to 24 in.) away from the edge of the molten block; this is illustrated in Figure 7.1 at a point where the melt depth was approximately 2.1 m (7 ft) deep. After power to the melt was terminated, the thermal gradients continued to move outward away from the melt until the heat flux from the block declined and the surrounding soil began to cool. At this point, the thermal gradients around the block began to recede back toward the block. During this test, the 100°C isotherm reached a maximum distance of 0.9 m (3 ft) from the edge of the block approximately three weeks (21 days) after powered operations ceased.

The temperature profiles behind the castable wall and the rock zone were monitored following the test to help determine whether the wall effectively interrupted heat transfer away from the block. The position of the 100°C isothermal band was monitored over time, as illustrated in Figure 7.2. The temperature data behind the wall shown in the figure illustrate that the maximum distance of the 100°C thermal gradient occurred at approximately 19 days, which is relatively consistent with the gradients in the unconfined soil on the opposite side of the block (21 days) discussed above. Note that the thermal gradients behind the wall moved further away from the melt face behind the wall as opposed to the unconfined soils. Since the melt was asymmetric, the 100°C gradient behind the wall was actually closer to the center of the melt. Additionally, the heat flux that emanated from the uniform wall face was greater than the heat flux from the outer edge of the block.

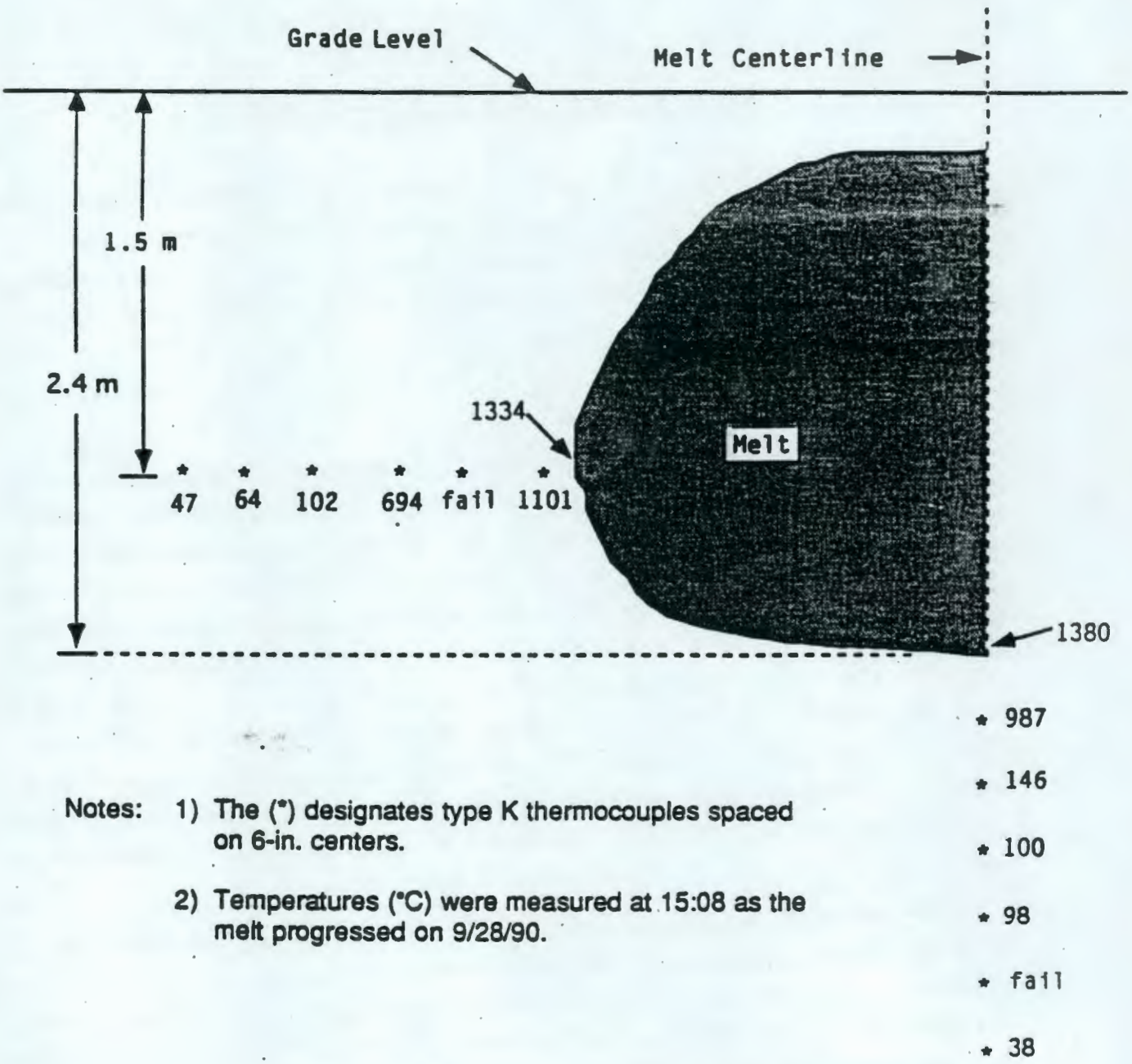

Notes: 1) The (*) designates type K thermocouples spaced on 6-in. centers.

2) Temperatures (°C) were measured at 15:08 as the melt progressed on 9/28/90.

FIGURE 7.1. Surrounding Soil Temperatures During Late Stages of Powered Operations (values in °C)

7.2 EVALUATION OF CASTABLE WALL

For actual remedial operations in a tank farm, nearby tanks or pipelines may require thermal protection from the destructive forces of the ISV process; such protection may be afforded by a castable barrier wall. To enhance the performance of the barrier wall, passive air vents could be installed behind the wall to remove heat transferred through the wall. Also, a powered blower system could be employed to increase the effectiveness and reliability of the thermal barrier. However, assuming the cooling air is potentially

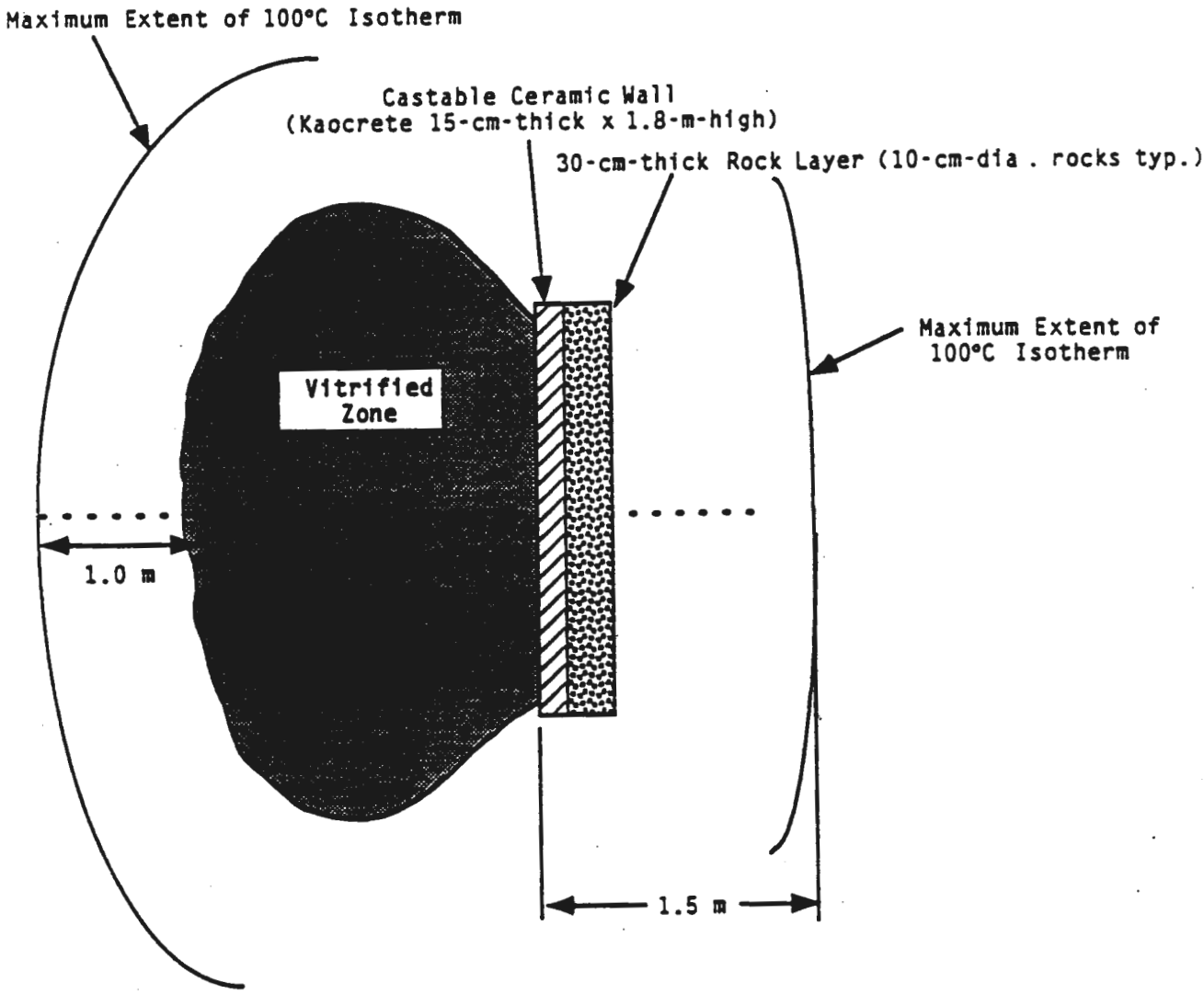

FIGURE 7.2. Posttest Location of the 100°C Isotherm Versus Time

contaminated and thus returned to the containment hood for off-gas treatment, the design capacity of the off-gas processing system would need to be increased to account for this additional volume of air.

In this pilot-scale test, the castable barrier wall performed extremely well by effectively deflecting the melt. The wall was within 6 cm (2.5 in.) of the west electrode and directly contacted the melt for the duration of the test, including the initial 19-h test phase and the subsequent 72-h period following restart. The precast wall showed no evidence of thermal degradation or corrosion from the molten glass contact. The composition of the castable material included organic-based fibers that decompose as the wall temperature increases, resulting in pathways for waters of hydration to escape from or through the matrix without

cracking the wall. The heat transfer through the block was sufficient to partially melt adjacent sand and rock to the back side of the wall as shown in Figure 7.3. Upon excavation and fracturing of the block, the wall was pried off the side of the vitrified block in a single piece (using a back hoe), which attests to the structural strength and condition of the wall following the test. No degradation at the glass/wall interface was observed.

7.3 POSTTEST SAMPLING

7.3.1 Internal Hood Samples

Approximately one week after powered operations were completed, the following samples were collected from the hood: undisturbed particulate deposited on the hood surface and solids deposited on the fabric used to cover the soil surfaces inside the hood surrounding the vitrified zone. Samples were also collected from the fabric of the heat shield. Using cloth wetted with water, hood samples were collected from target surfaces and then sealed in 250-mL plastic sample containers. Solids were either scraped off the fabric surface, or actual portions of the fabric were collected and placed into 250-mL plastic sample containers. The head space within these containers was excessive due to the type of samples being collected (fabric or small quantities of solids).

7.3.2 Near-Surface Soil Samples

After the ground cover inside the hood was removed, two initial soil samples (grab samples) were collected, primarily to determine if the control zone could be released for excavation work. The first sample was a surface-soil sample 0.76 m (30 in.) west of the western electrode, and the second sample was from a depth of 30 cm (1 ft), 0.76 m (30 m) south of the southern electrode. Both samples were collected from soils within 15 to 30 cm (6 to 12 in.) of the vitrified block. The samples were collected using clean stainless steel sampling tools, and the samples were placed into 250-mL plastic wide-mouth bottles leaving no head space.

7.3.3 Surrounding Soil Samples

The soil surrounding the vitrified block was removed with the back hoe to an approximate depth of 1.5 m (5 ft) from grade. Soil samples were collected in the ORNL soil zone to the east of the block by digging with hand tools an additional 15 to 30 cm (6 to 12 in.) into undisturbed soil to the specified target level of approximately 1.7 m (5.5 ft), which was at the same elevation as the original sludge layer. Excavation with the back hoe then continued until the block was removed and the undisturbed soil below the block could be sampled. The soil samples were collected both from the side of the block and directly below the block on the vertical centerline as shown in Figure 7.4. The samples consisted of composite

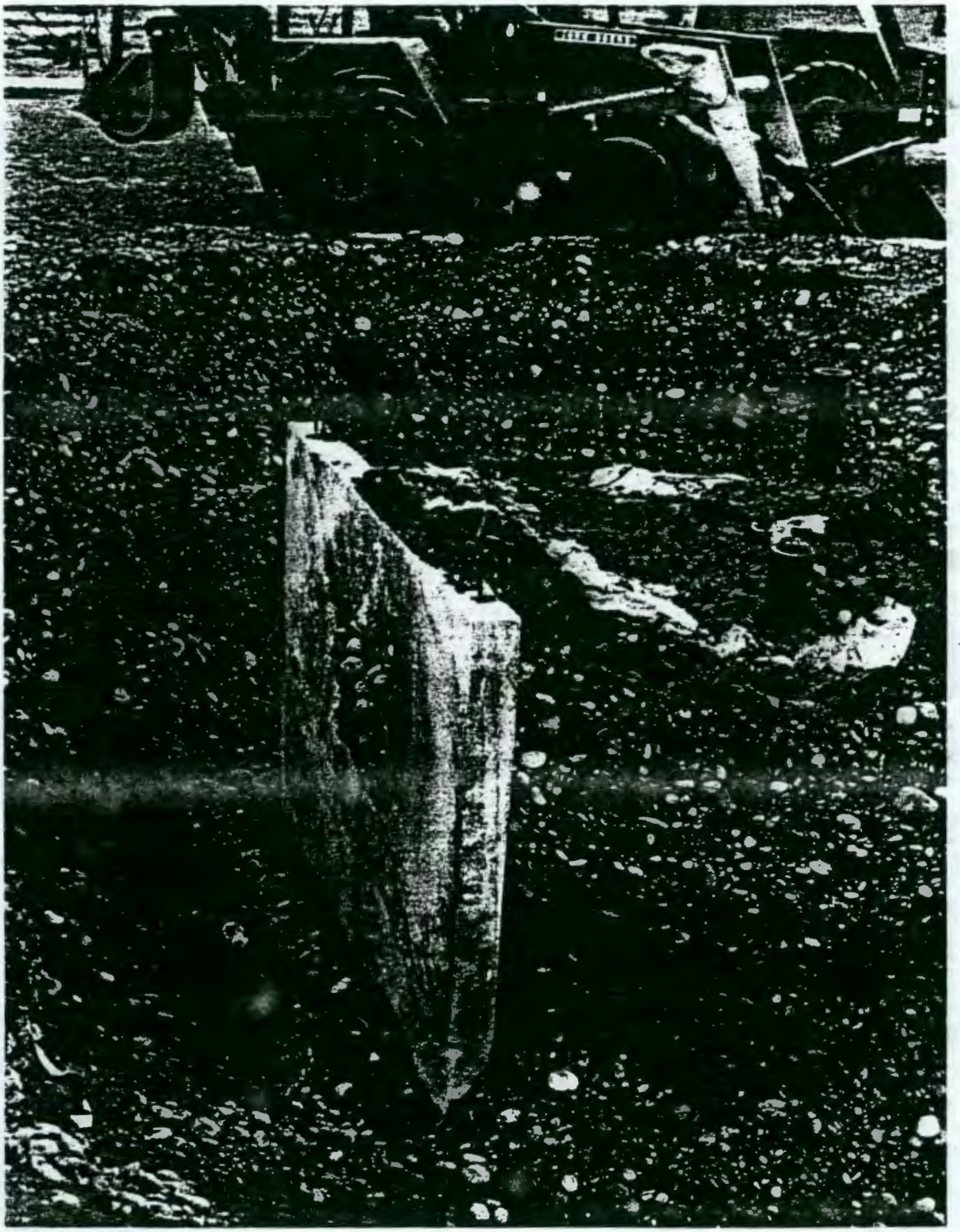

FIGURE 7.3. Castable Barrier Wall Abutted Against the Vitrified Block

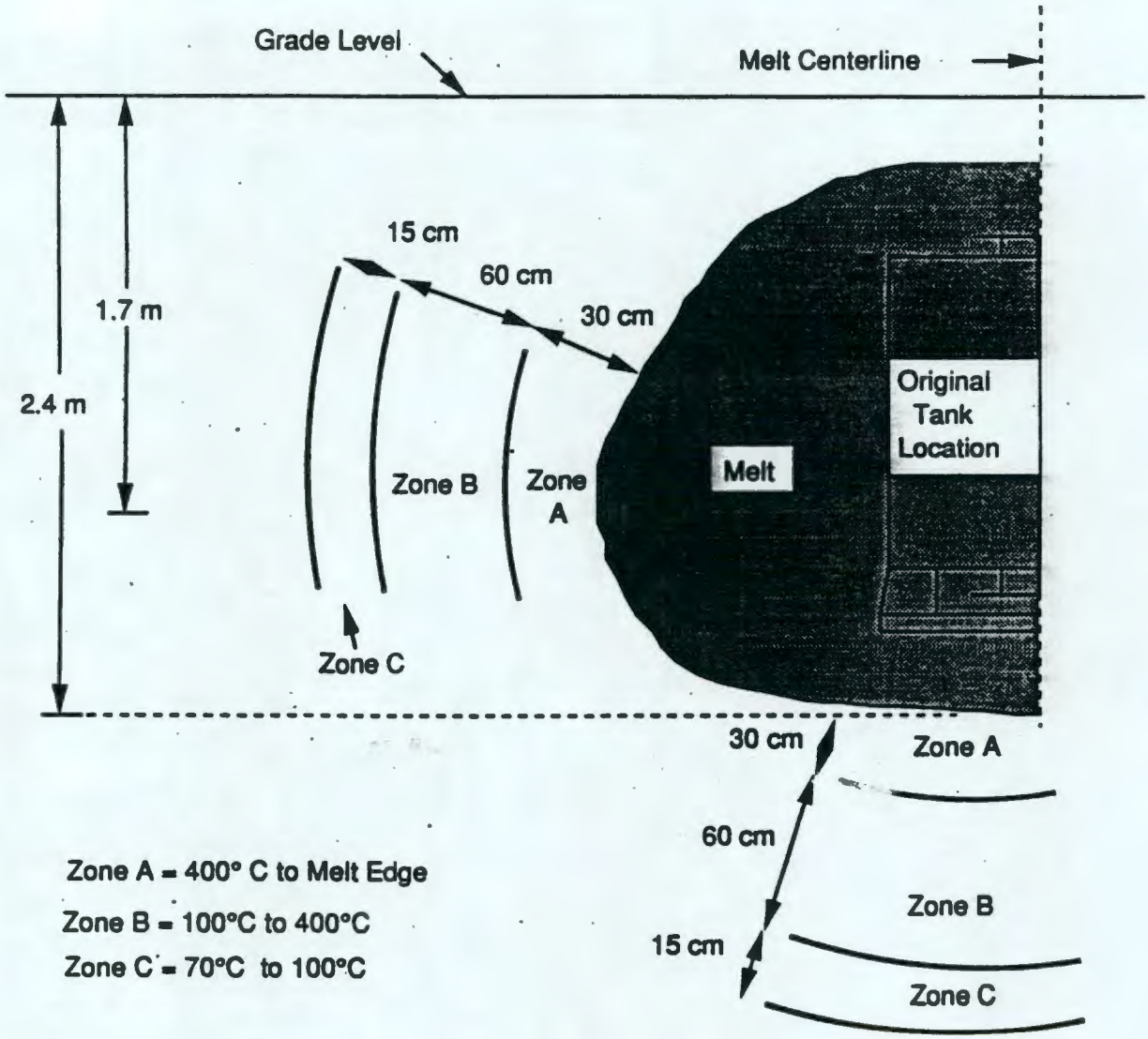

Composite samples from each zone were collected directly below the block and at the 1.7 m level on the side of the block in ORNL soil.

FIGURE 7.4. Soil Sampling Locations

samples within each of the sampling zones. The samples were collected along the entire length of each zone, and each zone sample was directly adjacent to the next zone's sample, thereby leaving no unsampled area and no overlap of samples. The samples were collected with clean stainless steel sampling instruments and placed in 250-mL plastic bottles leaving no head space. Additional samples of the partially fused soil zone directly adjacent to the vitrified block were also collected.

9615906.0952

The width dimensions of the soil sampling zones shown in Figure 7.4 were determined after the test by monitoring the movement of the thermal gradients around the melt as described in Section 7.1. Approximately three weeks following the completion of powered operations, the maximum distance of the 100°C and the 400°C isothermal band was established. After this point, the declining heat flux from the block resulted in the net inward movement of these isotherms back toward the block. The sampling locations were selected based on the thermal profiles. At the 100°C boundary, water vapor condensed in the soil and formed a wet layer surrounding the melt. If any contaminants migrated into the surrounding soil, water-soluble contaminants would be expected to deposit in the wet zone farthest from the block, volatile metals such as mercury or cadmium would condense in the 100° to 400°C zone, and the semi or nonvolatile components would be found closer to the block in the higher temperature zone.

7.4 VITRIFIED PRODUCT

7.4.1 Vitrified Product Sampling

The block was completely excavated on all sides following soil sampling (soil sampling below the block commenced once the block was removed). The shape of the block was influenced by the castable refractory wall and by the two soil types, since the north and south quadrants of the block extended beyond the ORNL soil zone and melted into the surrounding Hanford soil zone. Hanford soil has a higher alkali concentration, which makes it easier to melt relative to ORNL soil. Consequently, the block's shape was asymmetrical and wider in the north-south direction [approximately 4.1 m (13.4 ft) wider] than in the east-west direction [2.2 m (7.2 ft)]. Based on the dimensions of the block, the mass was calculated to slightly greater than 24,000 kg.

Melt depth averaged just over 2.4 m (8 ft), although an unusual 46-cm (18-in.) appendage of the vitrified product formed below the west electrode. This unusual feature or leg, depicted in Figure 7.5, was likely due to the difference in soil density adjacent to the wall (the soil was not compacted between the wall and the tank). Additionally, the wall created a preferential melting of the soil due to a net reduction of heat transfer away from the adjacent soil and melt. Increased electrical conduction to metallic pools at the bottom of the melt is not suspected to be the sole cause of this leg formation since other metal pools were found in other areas of the melt at the 2.4-m (8-ft) depth. The largest metal pool was predictably located in the center of the melt at the 2.4-m (8-ft) depth with smaller pools under 3 of the 4 electrodes. In all cases, the heat transfer through the molten metal was sufficient to at least fuse, and in most cases vitrify, the soil below the metal to a depth of approximately 1 cm (0.39 in.).

To obtain product samples and to aid in the removal of the vitrified block, a back hoe was used to fracture the block (Figure 7.6). The castable wall was pried off the block, and the block was broken into

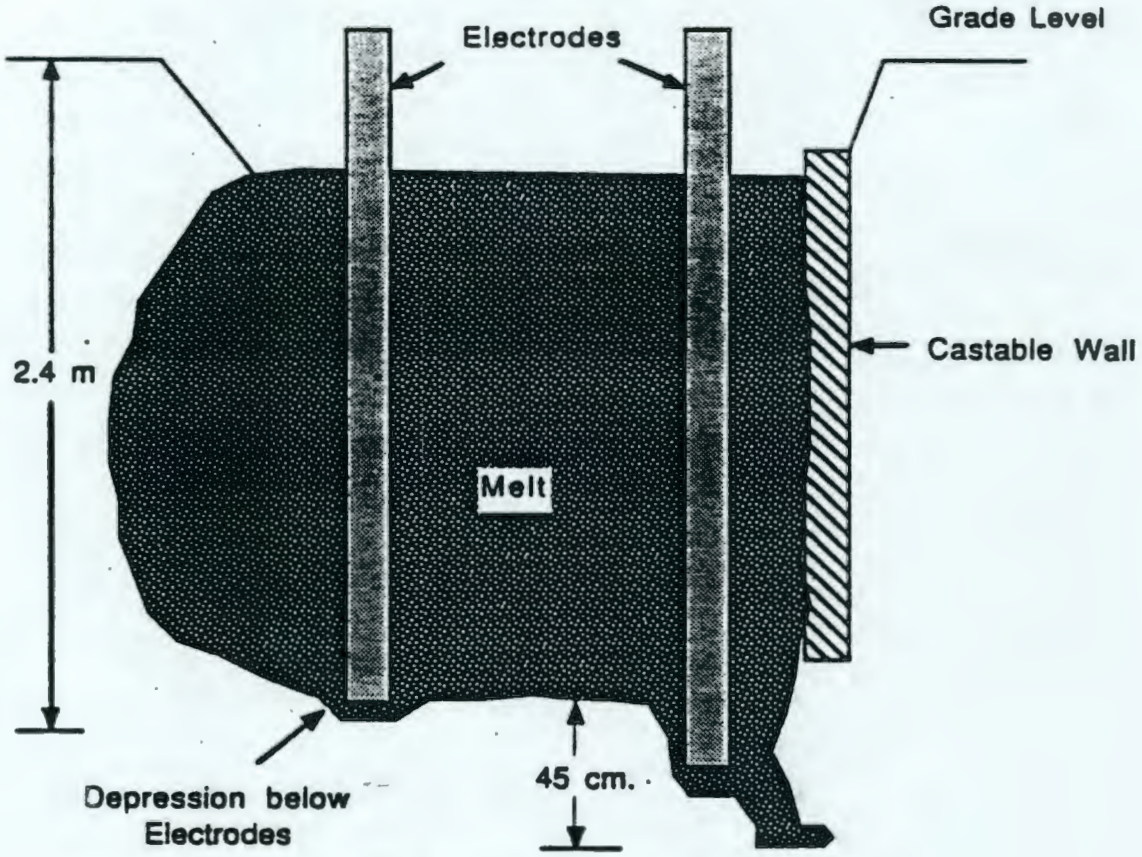

FIGURE 7.5. Vitrified Block Shape

large boulder-sized pieces. Vitrified product samples were collected by chipping pieces off the boulders from known locations. Most vitrified product samples were collected from the bottom third of the block within a 0.5-m (1.6-ft) horizontal radius of the block center; one sample was collected from an outer region of the block, again in the lower third.

7.4.2 Geologic Description of the Block

The block was a mixture of varying proportions of glass and fine crystals. As a whole, the block may be described as chemically similar to andesitic volcanic rock, although the composition of the crystals was unknown. The crystalline texture varied slightly with the location from which the samples were taken; this variation within the block was presumably a result of cooling history. Samples from the block's edge were assumed to be composed of a very fine intermixture of crystals and glass. Because the crystals were too small to be visible to the naked eye, their presence was assumed based on the cloudy appearance of the material. This extremely fine grain size may be a result of rapid quenching during the early stages of crystalline growth. Within the center of the block, the crystals were slightly better developed and were

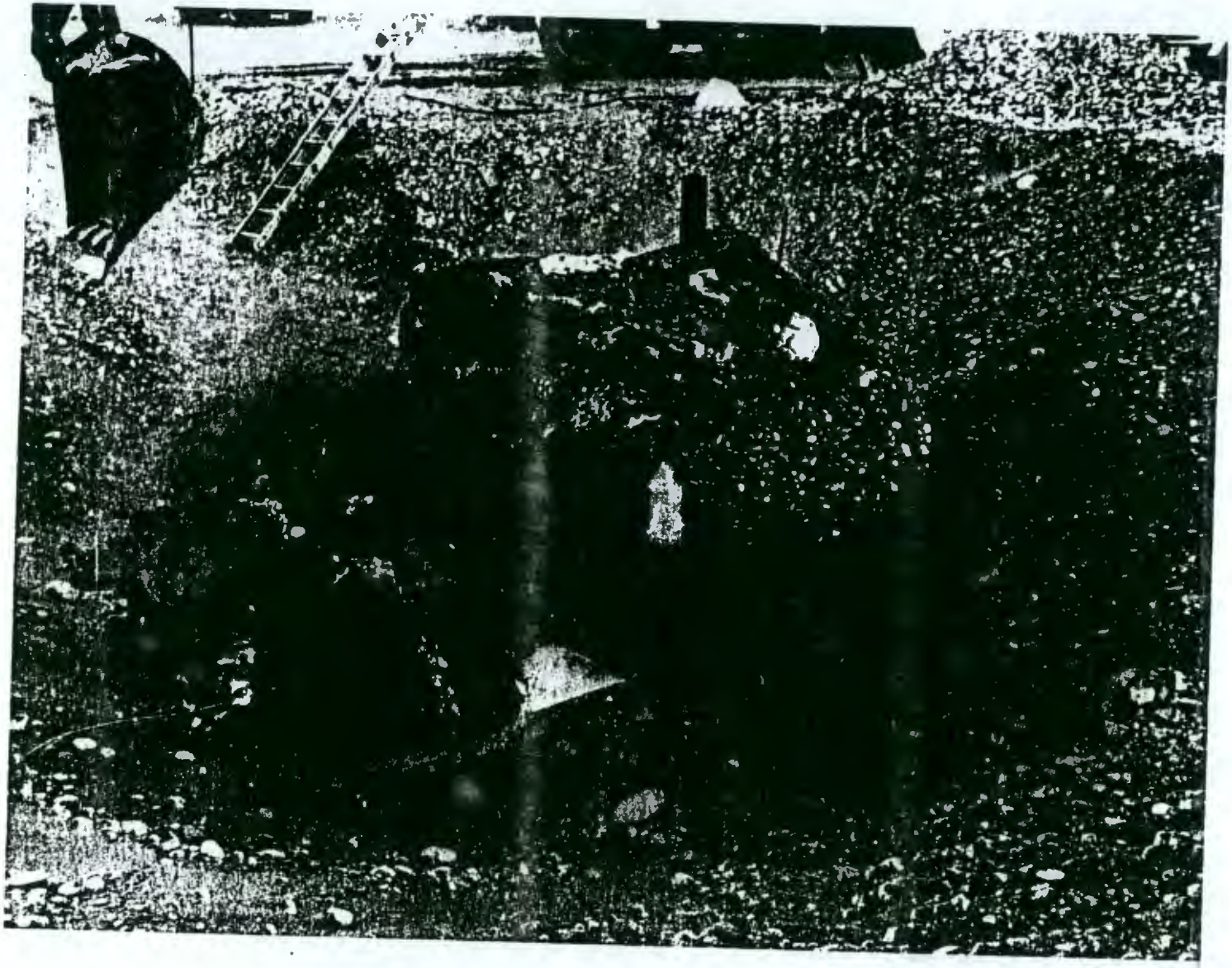

FIGURE 7.6. Vitrified Block Demolition by Use of a Back Hoe

9613400.0933

characterized by feathery and spherulitic textures, with crystalline clusters approximately 2 mm in diameter. This latter texture also indicated rapid crystal growth due to rapid cooling (Swanson 1977), but the better developed crystalline textures suggested slower cooling than at the melt's edge. The ratio of crystal to glass in this edge region was estimated at 60%. This estimate could be improved by petrographic observation of a sample.

Various metallic ingots were collected and visually examined. Except for some glass phases mixed with the metal, visual observations did not reveal any obvious heterogeneities within the metal phase. Sampling was structured to quantify the uniformity of the metal-phase composition. The metal phase was extremely hard and brittle, and individual samples were collected by fracturing the metal with a hammer; the metal was highly crystallized.

8.0 ANALYTICAL RESULTS AND INTERPRETATION

The sampling and analyses efforts were designed to quantify the overall process performance related to several areas including the following:

- product quality and composition of the resulting glass and metal waste forms
- contaminant migration into surrounding clean soils
- off-gas characteristics relative to selected gaseous and particulate components released from the melt
- removal efficiency of the off-gas treatment system
- an overall water balance accounting for the water originally present in the site.

In analyzing the vitrified product and surrounding soil samples, multiple analytical techniques were employed to assess the accuracy of laboratory analysis and to provide additional assurance of each sample's composition. In many instances, individual samples were split after preparation so each portion could be analyzed to assess the precision of the analytical technique. One of the goals for the pilot-scale test was to produce a mass balance for the key hazardous components. This information would permit an assessment of the destruction removal efficiency of the ISV process, including the melt and the off-gas treatment system. Most vitrified soil and surrounding soil analyses were specifically targeted for cesium, strontium, mercury, cadmium, and lead. These five species were of particular interest since cesium and strontium are the predominant radionuclides in the inactive tanks at ORNL. Mercury, cadmium, and lead represent a greater challenge to the integrity of the metallic waste form and are species that may possibly migrate into clean surrounding soils due to their relatively high volatilities. Analytical data for other species in the simulated sludge are presented where available; however, the behaviors of other species were considered to be more predictable and less significant to the process and waste form integrity.

8.1 GLASS WASTE FORM CHARACTERISTICS

Analytical results of vitrified product samples are provided in Table 8.1. The analytical methods used consisted of x-ray fluorescence (XRF), SW-846 methods involving a hydrofluoric (HF) acid/microwave sample digestion, and inductively coupled plasma (ICP) emission spectrophotometer analyses following sodium fusion sample preparation. For approximately half of the samples where the HF acid/microwave sample digestion preparation method was used, the digestion vial was cooled before opening to reduce volatile losses (noted in the table as appropriate). Minimal amounts of mercury were detected in four of six of the vitrified soil samples. Three different analytical laboratories were involved with the mercury analyses

TABLE 8.1. Vitrified Product Composition for Target Simulated-Waste Components

Sample Number[a]	Component (µg/g)				
	Sr	Cs	Pb	Cd	Hg
X-Ray Fluorescence					
10S1	275 ± 19	<13	187.1 ± 9.8	<5.9	<2.9
10S2	273 ± 19	<13	189.9 ± 9.9	<6.1	<3.0
11S1	278 ± 20	21.6 ± 7.3	189.4 ± 9.9	<6.3	<2.9
11S2	271 ± 19	21.6 ± 7.3	189.4 ± 9.9	<6.3	<2.9
SW-846 Method[b]					
9	–[c]	15.4	–	–	<0.0
1A	–	23 ± 10	179	–	0.18
2A	–	14.3	180	–	0.42
3A	–	15.3	241	–	0.72
Na Fusion/ICP Scan					
7	296	–	–	13.5	–
7A	306	–	–	12 ± 7	–
8	307 ± 25	–	–	7.6 ± 1.3	–
8A	295	–	–	6.9 ± 0.7	–
Method[d]					
PTRA-12	277 ± 27	9.5 ± 1.1	184	0.31 ± 0.04	1.9 ± 0.8
PTRA-13[e]	124 ± 13	7.88	180	<1	<1

(a) Samples 10S1, 11S1, 7, and 8 were split to produce additional samples 10S2, 11S2, 7A, and 7B.
(b) SW-846 method includes methods 303A for Cs, 7421 for Pb, and 7471 for Hg.
(c) (–) indicates that the method was not applicable and/or the sample was not analyzed.
(d) Sample preparation involved an HF acid/microwave digestion. Vial was cooled before opening to limit volatile losses. Analytical methods included ICP scan for Sr and Cd, and SW-846 type methods for Hg, Cs, and Pb.
(e) Sample PTRA-13 was collected from the outer edge of the vitrified block.

these six samples, which provides some degree of confidence that some mercury was retained in the glass. According to Table 8.1, the results are consistent, particularly regarding strontium and lead, which indicates that the sludge components were evenly distributed at least throughout the lower third of the vitrified mass where most samples were collected.

Three vitrified product samples were submitted for Toxicity Characteristic Leach Procedure (TCLP) analyses, and the results are presented in Table 8.2. Consistent with previous ISV testing, the

TABLE 8.2. TCLP Results for the Vitrified Product

Species	Vitrified Product Leachate (ppm)	Regulatory Limit (ppm)
As	0.012	5
Ba	<0.05	100
Cd	0.27	1
Cr	0.28	5
Pb	0.07	5
Hg	<0.0004	0.2
Se	<0.01	1
Ag	<0.05	5

concentrations of hazardous metals in the leach extract were well below regulatory limits for the vitrified product. The bulk composition of the vitrified product is given in Table 8.3. The data reveal a high concentration of CaO from the 1400 kg (3080 lb) of concrete and 1300 kg (2860 lb) of limestone gravel that surrounded the tank. Additionally, the north and south quadrants of the block melted into the surrounding Hanford soil. Consequently, the bulk composition of the glass reflects the mixture of these various

TABLE 8.3. Bulk Elemental Composition of the Vitrified Product

	XRF Method (wt%)			SW-846 Method (wt%)	
Species	10S1	11S1	Species	1A	2A
Al_2O_3	13.43	13.19	Al_2O_3	13.09	11.62
SiO_2	60.55	60.12	SiO_2	47.50	45.00
CaO	9.89	9.89	CaO	18.33	11.47
K_2O	2.52	2.54	K_2O	1.24	2.44
Fe_2O_3	6.60	6.53	Fe_2O_3	5.86	6.90
Cr_2O_3	0.39	0.39	Cr_2O_3	0.29	0.47
TiO_2	0.97	0.95	TiO_2	1.03	0.93
MnO	0.22	0.20	MnO	0.11	0.20
Na_2O	NA(a)	NA	Na_2O	1.67	1.90
Total	94.57	93.81		89.12	80.93

(a) Na_2O data unavailable for XRF method.

components. The XRF method produced significantly better results than the SW-846 method (6010) in this case. The XRF data for each of the two samples are relatively similar and the values are consistent with expectations based on soil composition and the composition of other items (e.g., concrete, tank sludge, limestone gravel). The expected degree of homogeneity of the vitrified mass, illustrated in Table 8.1, is evident from the two samples analyzed by the XRF technique. However, the data from the two samples analyzed via the SW-846 method do not indicate the expected degree of homogeneity, particularly for CaO and K_2O. In addition, it is apparent that all of the silicates in the product were not dissolved into solution during the sample preparation phase for the SW-846 method because the values for SiO_2 are much lower than expected.

8.2 METAL PHASE

Three samples of the metal phase found at the bottom of the solidified melt were submitted for compositional analyses by SW-846 methods, including methods 7471 for mercury and 7421 for lead. Additionally, method 6010 involving an ICP scan was performed. The analytical results are presented in Table 8.4. The particular laboratory analyzing these samples encountered extreme difficulties with the cesium analyses and, consequently, produced useless data (the reported detection limit exceeded expected cesium concentrations). Note that many of the metal samples had glass phases intermixed with the metal. Therefore, acid digestion sample preparation methods did not result in total dissolution of the entire sample including the glass phase. However, the ratio of the metal species in the sample is thought to be representative. Eight additional metal samples were analyzed via XRF, and the results are presented in Table 8.5 along with the XRF results of a 304 series stainless steel. The only significant difference between the results in Tables 8.4 and 8.5 is the cadmium concentrations; those values reported for the SW-846 methods are much higher than the XRF values. The commercial laboratory that performed these SW-846 analyses had difficulty in obtaining consistent values for lead, mercury, and cadmium, even with blank pretest samples. Based on the thermal history of the metal phase, it is suspected that most of the cadmium would have been volatilized rather than pooled at the base of the melt since cadmium is a vapor at 765°C, well below the melting point of stainless steel (1427°C), and cadmium oxide has a vapor pressure approximately 400 mm of mercury at 1484°C (Lide 1990). Considering mass balance information discussed later in this section and the laboratory's difficulty in obtaining consistent and reasonable values for the metals of interest, it is suspected that the XRF data for cadmium in the metal phase are more accurate.

Three samples of the metal were submitted for TCLP analyses, and the results are presented in Table 8.6. The leachate extract from the metal waste form was below regulatory limits for all metals. Only

TABLE 8.4. Composition of Metallic Phase via SW-846 Methods[a,b]

	Metal Composition (ppm)			
Species	Sample M4	Sample M5	Sample M6	Average Composition
Ag	22.55	27.20	18.30	22.68
Ba	2.70	13.66	8.54	8.30
Cd	856.53	1,183.95	628.97	889.82
Co	1,959.51	373.03	1,654.70	1,329.08
Cr	20,798.30	6,239.10	23,344.90	16,794.10
Cu	2,230.50	923.05	1,474.40	1,542.65
Fe	721,599.60	1,065,905.40	568,806.80	785,437.27
Hg	6.8	8.7	4.7	6.7
Mn	225.86	5,510.40	172.01	1,969.42
Ni	63,511.20	10,232.70	53,524.90	42,422.93
Pb	171.70	267.60	156.55	198.62
Va	628.90	719.88	585.74	644.84
Zn	442.12	426.67	802.24	557.01

(a) SW-846 methods 7471 and 7421 used for mercury and lead, respectively, following acid digestion. Balance of components measured via ICP scan.
(b) Metallic samples had undissolved glass phases.

cadmium concentrations in the leach extract approached the regulatory limit. Several observations can be made from the compositional data. Considering that the vast majority of the metal is from the tank (304L stainless), it is apparent that the chromium from the stainless steel was oxidized and dissolving into the glass phase while iron from the soil was reduced to its metallic state. As expected, the chromium oxide from the original sludge layer remained in its oxide form and was dissolved into the glass matrix. This is not surprising based on the more negative reduction potentials of these metals relative to others, such as iron and lead (Lide 1990). Additionally, no cesium and minimal amounts of strontium (10 to 250 µg/g) were found in the metal phase samples. Relative to the toxic metals, mercury, and cadmium were not found as expected based on their relative volatility. Barium remained an oxide and was largely dissolved in the vitrified product, as was lead.

TABLE 8.5. Metal Phase Composition via X-Ray Fluorescence

Species	Sample Number[a]									
	M8-S	M8-S2	M10-S1	M10-S2	M9-S1	M9 Nodules	M7-S1	M7-S2	Average	304 Series SS
Values in %										
As	0.019	0.058	0.032	0.014	0.111	0.11	0.037	0.038	0.052	0. 01
Co	ND[b]	0.113	ND	ND	0.145	0.078	0.023	ND	0.045	ND
Cr	3.03	3.3	15.43	4.92	4.48	0.268	4.44	9.51	5.674	18. 08
Cu	0.393	0.544	0.368	0.493	0.86	0.768	0.4	0.337	0.521	0.156
Fe	88.3	86.3	72.4	82.1	83.8	85.1	84.9	81.1	83.000	69.5
Ga	0.02	0.026	0.007	0.018	0.016	0.021	0.013	0.03	0.019	ND
Hg	ND	ND	ND	ND	ND	ND	ND	ND	ND	ND
Mn	ND	ND	1.115	0.169	0.07	ND	ND	ND	0.169	1.726
Mo	0.53	0.707	0.541	0.622	0.273	0.514	0.314	0.409	0.489	0.123
Nd	ND	0.001	0.044	0.027	0.002	0.001	0	0.007	0.010	0.104
Ni	7.7	8.76	9.69	11.31	9.84	12.82	9.72	8.34	9.798	10.17
Pb	0.004	0.122	ND	ND	0.215	0.099	ND	0.002	0.055	ND
Se	0.007	0.003	ND	ND	ND	ND	0.004	0.003	0.002	0.004
Ti	ND	ND	0.118	0.198	ND	0.201	ND	0.072	0.074	0.043
Va	ND	0.061	0.096	0.032	0.027	0.01	0.079	0.17	0.059	0.055
Zn	0.01	0.039	0.046	0.044	0.141	0.062	0.076	0.048	0.058	0.047
Rb	ND	ND	0.005	0.021	0.003	0	0	0.003	0.004	0.004
Sr	ND	ND	0.004	0.025	0.004	0.001	0.011	0.01	0.007	0.002
Yt	ND	0.001	ND	0.005	0.008	0.001	0	0.007	0.003	0.004
Zr	0.002	0.001	0.008	0.035	0.002	0.006	0.021	0.008	0.010	ND
Values in ppm										
Ag	ND	26	ND	ND	ND	ND	ND	ND	3.250	ND
Ba	ND	ND	155	727	ND	ND	ND	210	136.500	ND
Cd	ND	ND	41	ND	ND	102	ND	ND	17.875	ND
Cs	ND	ND	ND	ND	ND	ND	ND	ND	ND	ND
Sn	300	298	419	448	251	219	72	106	264.125	71

(a) Samples included glass phases. Also, samples M8-S, M10-S, and M7-S were split to obtain samples M8-S1, M10-S2, and M7-S2.
(b) ND = not detected.

TABLE 8.6. TCLP Results of Metal Phase Samples[a]

Species	Sample M1	Sample M2	Sample M3	Average	Limit
As	0.01	0.01	0.01	0.01	5.00
Ba	0.07	0.05	0.12	0.08	100.00
Cd	0.83	0.43	0.89	0.72	1.00
Cr	0.32	0.65	0.22	0.40	5.00
Pb	0.19	0.13	0.11	0.14	5.00
Hg	<0.00040	<0.00040	<0.00040	<0.00040	0.20
Se	0.01	0.01	0.01	0.01	1.00
Ag	0.05	0.05	0.05	0.05	5.00

(a) Values in ppm.

8.3 SURROUNDING SOIL ANALYSES

Most surrounding soil samples were analyzed primarily using SW-846 methods with one blank and one posttest sample analyzed by XRF. Results are provided in Table 8.7.

8.3.1 Strontium

Surrounding soil analyses were relatively consistent for strontium with the exception of samples X-2, BC-A, BC-B, 100-D, and 70-F. Sample X-2 was collected at a 30-cm (1-ft) depth in Hanford soil adjacent to the south side of the block in the 100° to 400°C isoband. Sample 70-F was collected approximately 1-m directly below the block in Hanford soil in the 70° to 100°C isoband. Hanford soil has a higher concentration of naturally occurring strontium; consequently, the higher value of strontium in these two samples is not surprising. Samples BC-A and BC-B were collected from the soil/melt interface (crust) at the bottom of the block. In this narrow interfacial region, the temperatures ranged from the melting temperature of ORNL soil (approximately 1550°C) to just below the fusion temperature. Both samples show about twice the background levels of strontium. However, samples SC-A and SC-B, which are side crust samples at a 5-ft depth at the original level of the tank sludge, do not indicate any significant increase in strontium concentrations above background levels. Based on results from numerous ISV tests that show extremely high retentions of strontium in the vitrified product (Buelt et al. 1987), it is suspected that no consistent or significant quantities of strontium evolved from the melt to the surrounding soils. This conclusion is further substantiated by the mass balance information discussed in Section 8.6.

8.3.2 Cesium

The data in Table 8.7 reveal that the levels of cesium in all of the surrounding soil samples are consistent with the range expected for background levels. It is concluded that no migration of cesium from the melt to surrounding soil occurred.

8.3.3 Mercury

The three samples analyzed for mercury showed no evidence of mercury contamination in the surrounding soils. Additional samples were submitted for analyses to an offsite laboratory; however, the samples were contaminated during the analyses of a 1000 µg/g spike sample and were determined to be useless for reporting purposes. To confirm the samples were indeed contaminated and the values useless for reporting purposes, the mercury concentrations measured in the contaminated samples were used to calculate the equivalent quantity of mercury in the total volume of soil around the vitrified block. The results of the calculation indicate that the amount of mercury reported in the samples corresponded to a total of 15 kg (33 lb) of mercury (assuming even distribution in the soils surrounding the block that were represented by the samples), which is roughly two orders of magnitude more mercury than was available in the tank sludge.

8.3.4 Cadmium

Analytical results for cadmium (presented in Table 8.7) ranged from less than 1 to 6.8 µg/g. Data do not indicate a pattern to suggest transport of cadmium is occurring. Cadmium has a negligible vapor pressure below 500°C; therefore, it is expected that any cadmium found in surrounding soils would be found in the soils directly adjacent to the block (crust samples) or in 400-series samples (below block). No cadmium contamination would be expected in the 100° to 400°C or the 70° to 100°C isobands (100- series and 70-series samples). However, samples 100-D and 70-F showed cadmium concentrations consistent with crust samples SC-A and SC-B at concentrations similar to background levels.

8.4 OFF GAS

The off-gas sampling results are summarized in Table 8.8. The data indicate that roughly 54% of the cadmium, 23% of the mercury, and only 10% of the lead were released from the melt. As expected, only 0.05% of the nonvolatile strontium was released from the melt. The laboratory that analyzed these samples encountered extreme difficulty with the cesium analyses (the reported detection limit exceeded the expected concentrations); consequently, the cesium data were useless for reporting purposes. The distribution of these four species in the hood and off gas are shown in Table 8.9 and reveals that the bulk of

TABLE 8.7. Surrounding Soil Analytical Results for Target Simulated-Waste Components

	XRF		Microwave/HF Digestion Plus SW-846 Methods										
	Pretest ONRL	Posttest, 1-ft Depth	Pretest	Side Crust 5-ft Depth		Bottom Crust		Below Block Soil Samples					
Component	X-1	X-2	D-2	SC-A	SC-B	BC-A	BC-B	400-B	400-A	100-D	100-C	70-F	70-E
Sr	134	398 ± 20	105	125	120	250	254	153	98.7	246	57.8	432	44.8
Cs	<13	<12	4.11	4.1	4.5	4.7	3.8	7.5	6	5.9	4.82	2.6	5
Hg	<3.0	<3.0	0.53 ± 0.1	NA	NA	NA	NA	NA	0.6	NA	0.6	NA	<1.0
Cd	<6.9	<6.1	0.37 ± 0.13	6.8 ± 1	5.38	<5	<5	<5	0.17 ± 0.04	5.0 ± 2	0.40 ± 0.1	6.7	<1.0
Pb	39.7	9.9	11.6	<1	3.3	<1	<1	50/7.2	15.3	<1	13.9	<1	11.6

Notes:
1. All values are in µg/g.
2. NA indicates sample not analyzed for the component.
3. Crust samples were collected from the partially fused soil zone immediately adjacent to the vitrified block.
4. After microwave digestion, vials were cooled before opening to reduce volatile losses.
5. Samples X-2 and 70-F contained Hanford soil, which has a significantly higher concentration of naturally occurring strontium.

TABLE 8.8. Hood and Off-Gas Sample Composition Summary for Target Simulated-Waste Components[a]

Element	Pretest Elemental Concentration (g)[b]	Total in Hood and Off-Gas Samples (g)[c]	Percentage Released from the Melt (%)
Cd	70.21	38.21	54.43
Hg	259.56	59.90	23.08
Pb	4784.18	482.58	10.09
Sr	2104.07	0.99	0.05

(a) Cs data unavailable (see discussion in Section 8.4).
(b) The pretest elemental concentration includes the quantity from the sludge, tank structure, limestone, and soil consumed by the melt.
(c) The total in hood and off-gas is a calculated value representing the total mass of each element released from the melt based on representative smear samples of the hood and off-gas line, ground cover and heat shield samples, and MM5 filters and impinger solutions samples.

TABLE 8.9. Elemental Distribution of Target Simulated-Sludge Components in the Off Gas[a]

Element	Ground Cover	Heat Shield	Hood Wall	Hood Roof	Off-Gas Line	Total Entering Scrub System: MM5 Filters	Total Entering Scrub System: MM5 Impingers	Total Released from Melt
Cd	0.16	0.09	0.34	0.05	0.04	37.46	0.07	38.21
Hg	0.06	0.01	0.07	0.01	0.30	0.18	56.26	56.90
Pb	1.15	0.50	16.38	2.59	2.21	459.41	0.34	482.58
Sr	0.59	0.01	0.25	0.02	0.03	0[b]	0.09	0.98

(a) All values are in grams.
(b) No analysis.

the more volatile contaminants released to the off gas were captured either on the EPA Modified Method 5 (MM5) filter or in the MM5 impinger solutions in the case of mercury. Strontium tended to stay in the hood rather than be carried out in the off-gas stream as indicated by the strontium values on the ground cover (0.59 g) and on the hood walls (0.25 g).

Off-gas analyses following off-gas treatment for the stack MM% sampler are provided in Table 8.10. No strontium or cadmium were detected on the stack MM5 filters or impinger solution samples. A total of 0.61 g of mercury and 0.58 g of lead was exhausted out the stack after off-gas treatment during the 65-h

TABLE 8.10. Stack Off-Gas Composition for Target Simulated-Sludge Components[a]

Element	MM5 Filter Totals (µg/g)	Impinger Solution Totals (mg/L)	Total Exhausted Out the Stack (g)
Cd	0	0	0
Hg	258	0.31	0.61
Pb	116	0.32	0.58
Sr	0	0	0

(a) Data unavailable for Cs.

sampling period. Assuming all the lead and mercury in the sludge layer was released from the melt over a 13-h period (the time required to melt through the sludge layer), concentrations in the off gas would be 52 and 49 µg/m^3 for mercury and lead, respectively, at an off-gas flow rate of 10 m^3/min.

Note that the presence of the hollow vent pipe may have decreased the melt retention of the volatile and semivolatile metals. The vent was essentially an open pathway to the off-gas hood.

Detailed worksheets tabularizing all analytical results and calculations for the hood and off-gas line smear samples, ground cover and heat shield fabric samples from the hood, and the MM5 filter and impinger solution analyses from the off-gas line and stack are included in Appendix B.

8.5 WATER BALANCE

An attempt was made to account for all water originally present in the pretest soils, concrete, limestone, sludge, and for air in the form of humidity drawn into the off-gas hood to determine if there was a net movement of water vapor away from the melt. This is a significant issue relative to the potential migration of water-soluble contaminants or other species with appreciable vapor pressure. Previous test data tend to support the theory that there is actually a net movement of water toward the melt; this has been described in several reports (e.g., Timmerman and Peterson 1990).

The two separate phases of this test caused difficulty in measuring the water balance since the initial test phase was halted after 19 h at a 1.06-m melt depth. The thermal flux from this melt continued to drive downward for the next three weeks, which dried out the surrounding soils until the restart at grade level. However, the method of accounting for water using the MM5 samplers is straightforward. An isokinetic off-gas sample is drawn through the impingers that are housed in an ice bath to condense water vapor in the

sample. Any remaining water vapor in the off-gas stream is removed by a column of silica gel. The total volume of water that passed through the off-gas line during the sampling period is determined on a gravimetric basis using the ratio of off-gas volume-to-sample volume.

The entire pretest region had a mass of 4186 kg (9209 lb) of water, including the water in the soil consumed by the melt, the surrounding soil volume, the concrete components, the limestone, and the sludge and soil in the tank. The first phase of the test, including the three-week restart or test recovery period, removed a total of 1712 kg (3766 lb) of water either in the soil and tank region that was melted or in the surrounding soil thermally influenced by the process. The second phase of the test removed the remaining 2477 kg (5449 lb) of water in the test site. The MM5 sampling occurred over a 57.1-h period and was initiated in the second test phase only after the majority of the initial melt was remelted and the lower regions of the tank were beginning to heat. Assuming that the 57.1-h MM5 sampling period occurred when the majority of water from the second test phase was evaporating, the 2477 kg (5499 lb) of water would have evaporated during this 57.1-h sampling period (the upper regions that had to be remelted were already dry as a result of the initial test phase). A total of 2536 kg (5579 lb) of water was collected during the 57.1-h sampling period. Using these assumptions and the actual value of water recovered in the second phase, a total of 102% of the water originally present in the test site is accounted for. This value is remarkably close to a 100% accountability of the water and undoubtedly has some error associated with the assumptions. These results should be considered qualitative but they generally support the theory and observations that there was no net movement of water away from the vitrified zone. (The worksheets and data regarding the MM5 samplers are included in Appendix B.)

8.6 TOTAL MASS BALANCE

A mass balance for the target simulated-waste species was performed to assess the overall performance of the ISV process including the melt and the off-gas treatment. The mass balance is summarized in Table 8.11. The tabulated data reveal that the mass balance is difficult to verify because the quantities of strontium, cadmium, cesium, and lead accounted for in the samples are greater than the maximum possible quantities by factors of 1.3 to 3.9. The amount of mercury accounted for in the system is only 32% of the total in the system. The mass balance calculations assume a homogenous distribution of each species in each of the product phases based on the average analytical value. It is suspected that the wide standard deviation in the metal phase samples contributes to the error. Additionally, most of the glass samples were collected from the center core of the bottom third of the vitrified mass, and the assumed homogenous distribution throughout the entire mass is likely incorrect. For example, glass sample PTRA-13 was the only sample collected near the outer edge of the block and has a strontium value approximately 50% less than the samples taken from the core of the block, consistent with background soil concentrations. While it is generally true that the convective currents in the melt uniformly mix the inorganic

9615401.0940

TABLE 8.11. Mass Balance Distribution of Elemental Target Simulated-Sludge Components[a]

Element	Pretest Totals (g) [b]	Melt (g)	Soil (g)	Metal (g)	Hood (g)	Off-Gas Stack (g)
Cd	70.21	159.9	0	60.4	41.23	0
Cs	283.74	375.2	0	0	unknown	unknown
Hg	259.56	17.2	0	0	65.28	0.84
Pb	4784.18	4636.9	0	1857.9	519.80	0.79
Sr	2104.07	6556.9	0	23.65	0.98	0

(a) Cs data for hood and off gas are unavailable.
(b) Pretest totals include the sum of each element in the pretest soils, metal, sludge, concrete, and limestone in grams.

species throughout the entire waste form, previous studies have shown that this mixing does not result in an absolutely uniform distribution (Timmerman and Oma 1984). It is suspected that the contaminants were distributed only throughout the center core of the vitrified block.

The samples that best reflect the reliability of analyses involve the impinger solutions and glass fiber filters of the MM5 samplers. Consequently, the values for the amount of each species released to the off gas are judged relatively accurate. Considering the amount of each species released from the melt, the quantity of strontium retained in the melt and in the metal phase represents 99.96% of the total inventory. Using this same approach, 89.91% of the lead was retained in the melt or metal phase. The quantity of cadmium released to the off gas amounted to 54.43% of the original inventory. The total quantity of the mercury could not be accounted for using either the soil or off-gas analytical approach; 23.08% of the total mercury inventory was accounted for in off-gas releases from the melt. However, only an additional 6.6% of the mercury could be accounted for in the vitrified product, the metal phases, and the surrounding soils. Therefore, the overall distribution of mercury cannot be conclusively established. A summary distribution of the target sludge species based on the off-gas and surrounding soil analyses is provided as Table 8.12.

TABLE 8.12. Summary Distribution of Target Sludge Species Based on Off Gas and Surrounding Soil Data[a]

Species	Melt/Metal (%)	Soil (%)	Hood/Off Gas (%)
Cd	45.57	0	54.43
Hg	76.92[b]	0	23.08
Pb	89.91	0	10.09
Sr	99.96	0	0.04

(a) Cs data unavailable from off-gas analyses; soil results indicated no surrounding soil contamination.
(b) A Hg retention value of 76.92% is indicated but suspect.

9.0. REFERENCES

Autrey, J. W., D. A. Costanzo, W. H. Griest, L. L. Kaiser, J. M. Keller, C. E. Nix, and B. A. Tomkins. 1990. Sampling and Analysis of the Inactive Waste Storage Tank Contents at ORNL. ORNL/ER-13, Oak Ridge National Laboratory, Oak Ridge, Tennessee.

Brouns, R. A., J. L. Buelt, and W. F. Bonner. 1983. "In Situ Vitrification." U.S. Patent 4,376,598.

Buelt, J. L., C. L. Timmerman, K. H. Oma, V. F. FitzPatrick, and J. G. Carter. 1987. In Situ Vitrification of Transuranic Wastes: An Updated Systems Evaluation and Applications Assessment. PNL-4800, Suppl. 1, Pacific Northwest Laboratory, Richland, Washington.

Callow, R. A., L. E. Thompson, and J. R. Weidner. 1991. In Situ Vitrification Application to Buried Waste: Interim Report of Intermediate Field Tests at Idaho National Engineering Laboratory. EGG-WTD-9422, Rev. 1, Idaho National Engineering Laboratory, Idaho Falls, Idaho.

Campbell, B. E., C. L. Timmerman, and W. F. Bonner. 1990. Underground Tank Vitrification: Engineering-Scale Test Results. PNL-7295, Pacific Northwest Laboratory, Richland, Washington.

DeFigh-Price, C. 1990. Hanford Cleanup Overview. Presented at the Society of American Military Engineers Northwest Regional Conference, Walla Walla, Washington. WHC-SA-0991, Westinghouse Hanford Company, Richland, Washington.

Lide, D. R., editor-in-chief. 1990. CRC Handbook of Chemistry and Physics, 71st Ed. CRC Press, Boston.

Oma, K. H., C. L. Timmerman, and J. L. Buelt. 1989. Test Report on Pilot-Scale In Situ Vitrification of PCB-Contaminated Soil. PNL-6788, Pacific Northwest Laboratory, Richland, Washington.

Swanson, S. E. 1977. "Relation of Nucleation and Crystal Growth to the Development of Granitic Textures." The American Mineralogist. 62:966-978.

Timmerman, C. L., and K. H. Oma. 1984. An In Situ Vitrification Pilot-Scale Radioactive Test. PNL-5240, Pacific Northwest Laboratory, Richland, Washington.

Timmerman, C. L., and M. E. Peterson. 1990. Pilot-Scale Testing of In Situ Vitrification of Arnold Engineering Development Center Site 10 Contaminated Soils. PNL-7211, Pacific Northwest Laboratory, Richland, Washington.

Waite, J. L. 1991. Tank Wastes Discharged Directly to the Soil at the Hanford Site. WHC-MR-0227, Westinghouse Hanford Company, Richland, Washington.

9613400.0942

APPENDIX A

MODELING PRESSURE PULSES DURING IN SITU VITRIFICATION

9613400.0945

APPENDIX A

MODELING PRESSURE PULSES DURING IN SITU VITRIFICATION

A.1 INTRODUCTION

This appendix describes the technical bases of computer code P3-ISV (Pressure Pulse Predictor - In Situ Vitrification) and its use in interpreting a particular pressurization event. P3-ISV is a set of computer-based algorithms for estimating pressure and temperature transients in the containment hood during a vitrification process that is interrupted by an eruption of gas, soil, and lava in the hood followed by the exposure of the melt surface. The code describes the dynamic heat transfer and flow processes that occur during such an event.

A.2 TRANSIENT RESPONSE OF THE MODEL

The following descriptions of the eruption and melt exposure phases of the pressurization event are only qualitative. A detailed technical basis showing equations and numerical methods is beyond the scope of this appendix.

The two principal parts of P3-ISV are numerical solutions of unsteady-state difference equations for the coupled mass and energy balances of the hood gas space. These balances and their important components are described here. The mass balance (gas space mole balance) is the simpler of the two balances. A vacuum exhaust system is assumed to provide a constant outflow from the hood. The inflow resistance is calculated from this outflow at normal vacuum (1.8-in. W.C.). During a pressurization event, the hood can exhaust through two other paths. The first path is the normal inflow path when hood vacuum becomes negative. A second path is opened up when hood vacuum exceeds -1-in. W.C. and remains open. This path has a flow resistance assumed equal to the normal inflow resistance. The gas volume is assumed to be well-mixed and to obey the ideal gas law. The temperature of the gas is obtained from the energy balance.

Airborne dust from the eruption is allowed to reach a maximum concentration of 10 g/m^3 (a stable aerosol for short-term events). The aerosol is depleted by inflow and outflow following the eruption. No gravitational settling of particles is presently modeled mechanistically for the short duration event. This airborne dust is critical for absorbing melt and lava radiation and reradiation to the hood surfaces.

The gas space energy balance has input/output flow enthalpy rates from gas inflow and outflow, radiative transfer as mentioned above, and convective transfer from cooling lava and melt surfaces. For

the short duration of the modeled event, no net convective transfer of heat is modeled from the gas to the hood walls. A net enthalpy term exists for convection to the gas space equal to the amount required to heat gas leaking into the hood during preevent conditions.

The eruption phase of the pressurization event is characterized by an initial slow eruption (corresponding to the initial gas release) that rapidly accelerates, resulting in the exposure of the melt surface. P3-ISV approximates this eruption with the ejection of gases, particles, and molten lava at an accelerating rate. The particles are allowed to transfer excess enthalpy into the gas upon becoming airborne. The lava ejected from the melt is assumed to puddle and commence the release of both convective and radiative heat to the hood gas space. At the end of the short eruption phase, the melt surface exposure phase begins.

The melt exposure phase is characterized by radiation and free convective heat transfer to the hood gas (suspended particulate) from the melt and lava surfaces. The temperature difference between the melt and gas drives the free convection. With 10 g/m^3 of suspended particles in the hood, almost no radiation initially penetrates directly to the hood walls. Penetration can occur once the aerosol is sufficiently diluted.

A.3 SIMULATION OF P3-ISV TO PILOT-SCALE TANK TEST

A pilot-scale tank test pressurization event produced temperature and pressure data that served as bases of comparison for adjustment of model parameters and for quantitatively interpreting the event-controlling parameters. A suitable set of parameters was obtained for the event.

Figure A.1 contains the actual temperature and pressure data as recorded during the initial 10 s of the pressurization event. The pressure sensor has a cutoff response at -5-in. W.C. vacuum, and the thermocouple has an inherent time response constant of approximately 10 s. Figure A.2 contains the calculated traces of the same instruments as simulated by P3-ISV. The temperature match is very close. The pressure match reveals a discrepancy after 5 s. Figure A.3 is a plot of the actual hood pressure and temperature as calculated by P3-ISV. The hood reached a maximum overpressure of 82-in. W.C. at 5 s and a maximum temperature of 640°C at 8 s. With data from Figures A.1 and A.2 in mind, it is probably safe to conclude that the maximum overpressure was probably too high.

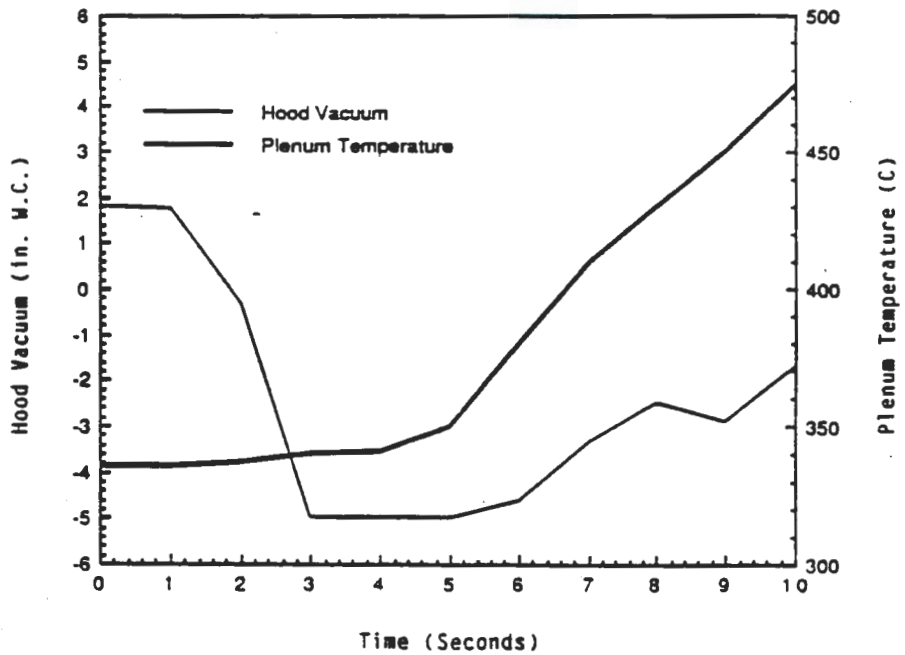

FIGURE A.1. Measured Pressure and Temperature Data from the Pilot-Scale UTV Pressurization Event

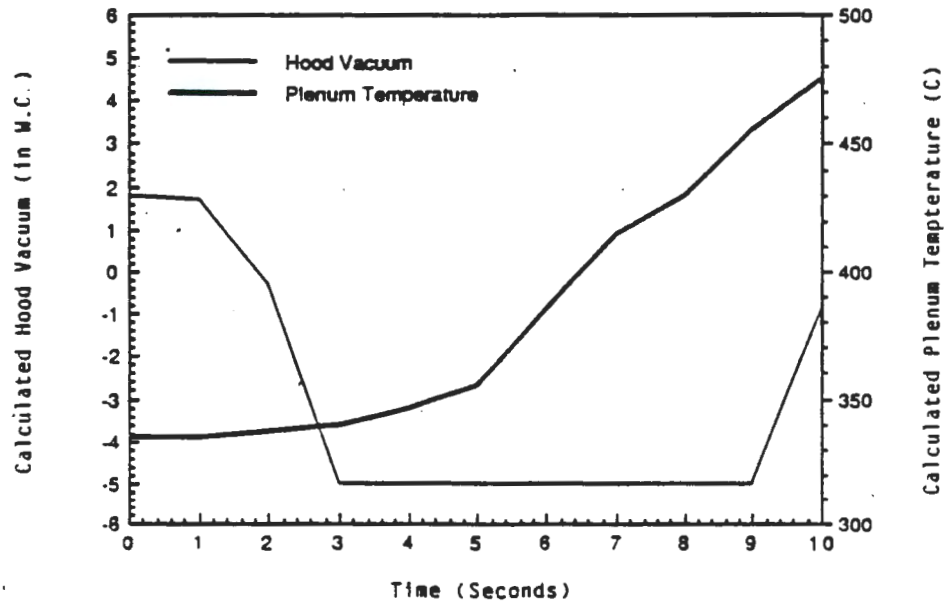

FIGURE A.2. P3-ISV Calculated Plenum Temperature and Hood Pressure Instrumentation Response for Pressurization Event

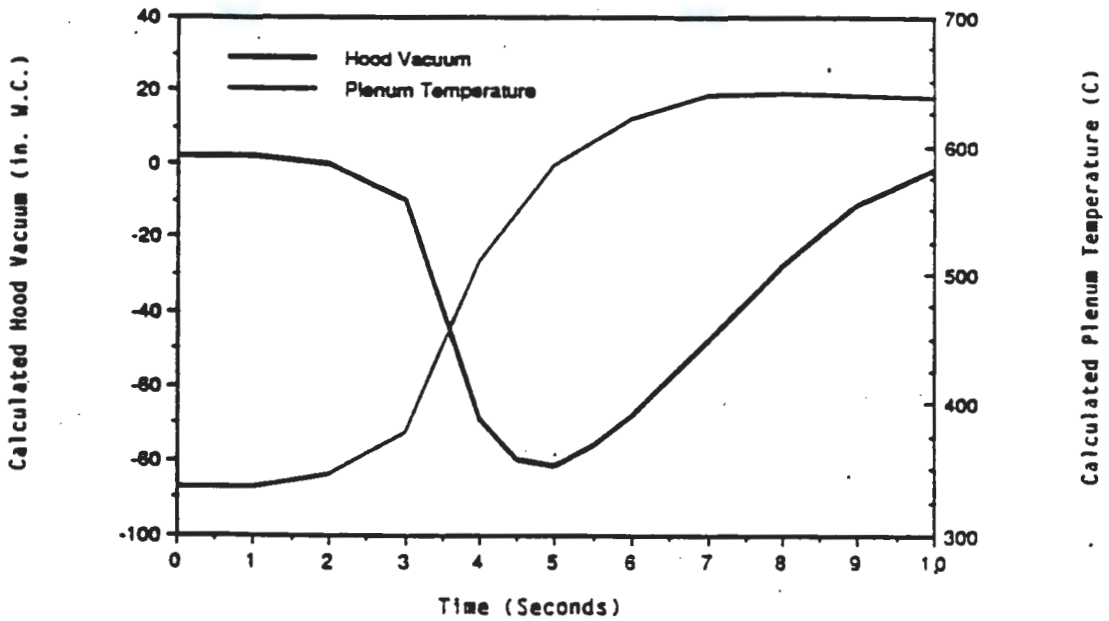

FIGURE A.3. P3-ISV Calculated Plenum Temperature and Hood Pressure for the Pilot-Scale UTV Pressurization Event

The following P3-ISV input parameters were initially fixed, and were not adjusted to minimize experimental data/calculated data differences.

initial hood gas temperature, 335°C

initial hood vacuum, 1.8-in. W.C.

melt surface diameter, 61 m (2-ft-diameter hole in cold cap responsible for thermal radiation)

melt and lava emissivity, 0.8

radiation attenuation coefficient for airborne particles, 1 μm

volume of soil particles erupted, 0.1 m^3 (3.53 ft^3)

gas erupted, 0.72 gmoles

bulk density of soil erupted, 1500 kg/m^3

porosity of soil erupted, 0.5

mass of lava erupted, 20 kg (44 lb)

duration of eruption, 3 s

normal gas flow out of hood, 15 m^3/min

temperature of inleakage gas, 25°C.

The following P3-ISV input parameters were obtained by adjusting calculated output to match experimental data:

initial lava temperature, 1650°C

initial melt temperature, 1700°C

temperature of gas and soil erupted, 375°C.

The pressure response curves generated by P3-ISV could be produced more realistically by improving the outflow resistance of the pressure relief system and by including a gas generation term for the soil that is pressure sensitive. The longer (>10 s) response time of the temperature curve could be suspect if analyzed. Therefore, a more complete heat transfer model might be indicated. Additional features that would likely improve the predictive capability of the model include the following:

- a model of the pressure relief system as a HEPA filter
- a model of gas outflow from the soil
- a model of the soil as a gas storage reservoir that could store hood gases during rising hood pressure and could release the stored gases during falling hood pressure
- a model of appropriate flow resistances for the soil reservoir
- a model of the hood dome and any interior equipment for appropriate heat transfer.

9613400.0946

APPENDIX B

OFF-GAS DATA FROM METHOD 5 SAMPLERS

9615400.0947

Percent Retention

	Total Consumed by melt grams (1)	Total in Off-gas and hood grams (2)	Percentage in off-gas % (3)
Sr	2104.07	0.9842	0.05%
Hg	259.56	65.2832	25.15%
Cd	70.21	41.2356	58.73%
Pb	4784.18	519.8096	10.87%

Notes:
(1) soil, limestone, metal(tank), sludge consumed in a volume of 356.8 cu.ft.
(2) mass of Sr, Hg, Cd, Pb as found via smear samples and MM5 data
(3) =(col.d/col.b)*100

	GROUND COVER FABRIC GRAMS	HEAT SHIELD FABRIC GRAMS	SMEAR TOTALS GRAMS	MM5 FILTERS OG LINE GRAMS	MM5 OG LINE IMPINGERS GRAMS	OFF-GAS STREAM GRAMS	TOTAL OFFGAS GRAMS
Ba	1.0036	0.0043	0.1447	0.0675	0.2126	0.2801	1.4327
Mg	20.1596	0.1667	4.4513	4.2531	0.2338	4.4869	29.2645
Sn	0.0405	0.0021	0.0874	0.4301	0	0.4301	0.5601
Tl	0.0297	0.0111	0.0356	0.3082	0.0259	0.3341	0.4105
V	0.2588	0.0061	0.0624	0.0720	0	0.072	0.3993
Na	6.3648	0.2598	3.4995	20.4081	5.1879	25.596	35.7201
Mo	0.1056	0.0188	0.2217	0.3001	0.0439	0.344	0.6901
Al	75.0041	0.276	18.7564	10.8056	0.9278	11.7334	105.7699
Sb	0.0554	0	0.0469	0.0776	0.0334	0.111	0.2133
Be	0	0	0	0.0000	0	0	0
Ca	69.5461	0.1774	16.2331	6.1592	3.4719	9.6311	95.5877
Zn	0.625	0.065	3.318	289.3188	0.0848	289.4036	293.4116
Cu	0.1303	0.0314	0.5811	0.7549	0	0.7549	1.4977
Ag	0.0139	0.0008	0	0.0286	0	0.0286	0.0433
Pb	1.1532	0.4982	21.1903	496.7584	0.2095	496.9679	519.8096
Tl	0.8979	0.0413	0.1612	0.4069	0	0.4069	1.5073
Cd	0.1593	0.0852	0.4414	40.5048	0.0449	40.5497	41.2356
Co	0.0701	0.0137	0.1001	0.2560	0.0249	0.2809	0.4648
Ni	0.2386	0.4399	4.4871	46.9773	0.0499	47.0272	52.1928
K	23.2407	0.2079	4.938	34.2428	0.8081	35.0509	63.4375
Mn	1.3029	0.0145	2.1734	0.5439	0.5587	1.1026	4.5934
Fe	67.1692	5.7075	101.9531	540.1503	0.1097	540.26	715.0898
Cr	0.4789	0.0142	2.6433	21.1083	0	21.1083	24.2447
Hg	0.0643	0.0096	0.3839	0.1948	64.6306	64.8254	65.2832
Sr	0.5898	0.0066	0.3	0	0.0878	0.0878	0.9842

Off-Gas Totals

Total Smears

	HOOD ROOF GRAMS	HOOD WALLS GRAMS	OG LINE GRAMS	TOTAL GRAMS
Ba	0.0112	0.0709	0.0626	0.1447
Mg	0.3738	2.3599	1.7176	4.4513
Sn	0.0091	0.0572	0.0211	0.0874
Tl	0.0027	0.0169	0.016	0.0356
V	0.0061	0.0388	0.0175	0.0624
Na	0.2866	1.8092	1.4037	3.4995
Mo	0.0253	0.1599	0.0365	0.2217
Al	1.7216	10.8685	6.1663	18.7564
Sb	0.0048	0.0305	0.0116	0.0469
Be	0	0.0000	0	0
Ca	1.4869	9.3871	5.3591	16.2331
Zn	0.405	2.5565	0.3565	3.318
Cu	0.0729	0.4602	0.048	0.5811
Ag	0	0.0000	0	0
Pb	2.5959	16.3880	2.2064	21.1903
Ti	0.0133	0.0842	0.0637	0.1612
Cd	0.0544	0.3435	0.0435	0.4414
Co	0.0119	0.0749	0.0133	0.1001
Ni	0.5836	3.6840	0.2195	4.4871
K	0.4278	2.7007	1.8095	4.938
Mn	0.2866	1.8092	0.0776	2.1734
Fe	12.9171	81.5468	7.4892	101.9531
Cr	0.3032	1.9141	0.426	2.6433
Hg	0.0091	0.0721	0.3027	0.3839
Sr	0.0204	0.2478	0.0318	0.3

Hood Roof Smears

	SAMPLE # HSPT ug/g	SAMPLE WT. GRAMS	SAMPLE AREA FT.2	AREA OF ROOF FT2	TOTAL MASS GRAMS
Ba	5.41	5.1	0.1056	43	0.0112
Mg	180	5.1	0.1056	43	0.3738
Sn	4.36	5.1	0.1056	43	0.0091
Tl	1.29	5.1	0.1056	43	0.0027
V	2.96	5.1	0.1056	43	0.0061
Na	138	5.1	0.1056	43	0.2866
Mo	12.2	5.1	0.1056	43	0.0253
Al	829	5.1	0.1056	43	1.7216
Sb	2.33	5.1	0.1056	43	0.0048
Be	0	5.1	0.1056	43	0.0000
Ca	716	5.1	0.1056	43	1.4869
Zn	195	5.1	0.1056	43	0.4050
Cu	35.1	5.1	0.1056	43	0.0729
Ag	0	5.1	0.1056	43	0.0000
Pb	1250	5.1	0.1056	43	2.5959
Tl	6.42	5.1	0.1056	43	0.0133
Cd	26.2	5.1	0.1056	43	0.0544
Co	5.71	5.1	0.1056	43	0.0119
Ni	281	5.1	0.1056	43	0.5836
K	206	5.1	0.1056	43	0.4278
Mn	138	5.1	0.1056	43	0.2866
Fe	6220	5.1	0.1056	43	12.9171
Cr	146	5.1	0.1056	43	0.3032
Hg	4.38	5.1	0.1056	43	0.0091
Sr	9.82	5.1	0.1056	43	0.0204

Hood Wall Smear

	SAMPLE # PTDS ug/g	SAMPLE WT. GRAMS	SAMPLE AREA FT 2	AREA OF WALLS FT2	TOTAL MASS GRAMS
Ba	5.41	4.06	0.1056	341	0.0709
Mg	180	4.06	0.1056	341	2.3599
Sn	4.36	4.06	0.1056	341	0.0572
Tl	1.29	4.06	0.1056	341	0.0169
V	2.96	4.06	0.1056	341	0.0388
Na	138	4.06	0.1056	341	1.8092
Mo	12.2	4.06	0.1056	341	0.1599
Al	829	4.06	0.1056	341	10.8685
Sb	2.33	4.06	0.1056	341	0.0305
Be	0	4.06	0.1056	341	0.0000
Ca	716	4.06	0.1056	341	9.3871
Zn	195	4.06	0.1056	341	2.5565
Cu	35.1	4.06	0.1056	341	0.4602
Ag	0	4.06	0.1056	341	0.0000
Pb	1250	4.06	0.1056	341	16.3880
Ti	6.42	4.06	0.1056	341	0.0842
Cd	26.2	4.06	0.1056	341	0.3435
Co	5.71	4.06	0.1056	341	0.0749
Ni	281	4.06	0.1056	341	3.6840
K	206	4.06	0.1056	341	2.7007
Mn	138	4.06	0.1056	341	1.8092
Fe	6220	4.06	0.1056	341	81.5468
Cr	146	4.06	0.1056	341	1.9141
Hg	5.5	4.06	0.1056	341	0.0721
Sr	18.9	4.06	0.1056	341	0.2478

Off-Gas Line Smear

	SAMPLE # OGL 2 ug/g	SAMPLE WT. GRAMS	SAMPLE AREA FT.2	AREA OF LINE FT2	TOTAL MASS GRAMS
Ba	27.9	5.76	0.1736	67.58	0.0626
Mg	766	5.76	0.1736	67.58	1.7176
Sn	9.4	5.76	0.1736	67.58	0.0211
Tl	7.12	5.76	0.1736	67.58	0.0160
V	7.79	5.76	0.1736	67.58	0.0175
Na	626	5.76	0.1736	67.58	1.4037
Mo	16.3	5.76	0.1736	67.58	0.0365
Al	2750	5.76	0.1736	67.58	6.1663
Sb	5.16	5.76	0.1736	67.58	0.0116
Be	0	5.76	0.1736	67.58	0.0000
Ca	2390	5.76	0.1736	67.58	5.3591
Zn	159	5.76	0.1736	67.58	0.3565
Cu	21.4	5.76	0.1736	67.58	0.0480
Ag	0	5.76	0.1736	67.58	0.0000
Pb	984	5.76	0.1736	67.58	2.2064
Tl	28.4	5.76	0.1736	67.58	0.0637
Cd	19.4	5.76	0.1736	67.58	0.0435
Co	5.91	5.76	0.1736	67.58	0.0133
Ni	97.9	5.76	0.1736	67.58	0.2195
K	807	5.76	0.1736	67.58	1.8095
Mn	34.6	5.76	0.1736	67.58	0.0776
Fe	3340	5.76	0.1736	67.58	7.4892
Cr	190	5.76	0.1736	67.58	0.4260
Hg	135	5.76	0.1736	67.58	0.3027
Sr	14.18	5.76	0.1736	67.58	0.0318

Heat Shield Ground Cover Totals

	GROUND COVEF GRAMS	HEAT SHIELD GRAMS	TOTAL GRAMS
Ba	1.0036	0.0043	1.0079
Mg	20.1596	0.1667	20.3263
Sn	0.0405	0.0021	0.0426
Tl	0.0297	0.0111	0.0408
V	0.2588	0.0061	0.2649
Na	6.3648	0.2598	6.6246
Mo	0.1056	0.0188	0.1244
Al	75.0041	0.276	75.2801
Sb	0.0554	0	0.0554
Be	0	0	0
Ca	69.5461	0.1774	69.7235
Zn	0.625	0.065	0.69
Cu	0.1303	0.0314	0.1617
Ag	0.0139	0.0008	0.0147
Pb	1.1532	0.4982	1.6514
Tl	0.8979	0.0413	0.9392
Cd	0.1593	0.0852	0.2445
Co	0.0701	0.0137	0.0838
Ni	0.2386	0.4399	0.6785
K	23.2407	0.2079	23.4486
Mn	1.3029	0.0145	1.3174
Fe	67.1692	5.7075	72.8767
Cr	0.4789	0.0142	0.4931
Hg	0.0643	0.0096	0.0739
Sr	0.5898	0.0066	0.5964

Ground Cloth Analysis

	SAMPLE # K A2	SAMPLE WT. GRAMS	GROUND COVER FABRIC WT. G.	TOTAL MASS GRAMS
Ba	114	8.54	8803.3	1.0036
Mg	2290	8.54	8803.3	20.1596
Sn	4.6	8.54	8803.3	0.0405
Tl	3.37	8.54	8803.3	0.0297
V	29.4	8.54	8803.3	0.2588
Na	723	8.54	8803.3	6.3648
Mo	12	8.54	8803.3	0.1056
Al	8520	8.54	8803.3	75.0041
Sb	6.29	8.54	8803.3	0.0554
Be	0	8.54	8803.3	0.0000
Ca	7900	8.54	8803.3	69.5461
Zn	71	8.54	8803.3	0.6250
Cu	14.8	8.54	8803.3	0.1303
Ag	1.58	8.54	8803.3	0.0139
Pb	131	8.54	8803.3	1.1532
Ti	102	8.54	8803.3	0.8979
Cd	18.1	8.54	8803.3	0.1593
Co	7.96	8.54	8803.3	0.0701
Ni	27.1	8.54	8803.3	0.2386
K	2640	8.54	8803.3	23.2407
Mn	148	8.54	8803.3	1.3029
Fe	7630	8.54	8803.3	67.1692
Cr	54.4	8.54	8803.3	0.4789
Hg	7.3	8.54	8803.3	0.0643
Sr	67	8.54	8803.3	0.5898

9615430.3951

Heat Shield Fabric Analysis

	SAMPLE # HS A2	SAMPLE WT. GRAMS	HEAT SHIELD FABRIC WT.	TOTAL MASS GRAMS
Ba	4.78	6.76	896	0.0043
Mg	186	6.76	896	0.1667
Sn	2.33	6.76	896	0.0021
Tl	12.4	6.76	896	0.0111
V	6.84	6.76	896	0.0061
Na	290	6.76	896	0.2598
Mo	21	6.76	896	0.0188
Al	308	6.76	896	0.2760
Sb	0	6.76	896	0.0000
Be	0	6.76	896	0.0000
Ca	198	6.76	896	0.1774
Zn	72.6	6.76	896	0.0650
Cu	35.1	6.76	896	0.0314
Ag	0.882	6.76	896	0.0008
Pb	556	6.76	896	0.4982
Ti	46.1	6.76	896	0.0413
Cd	95.1	6.76	896	0.0852
Co	15.3	6.76	896	0.0137
Ni	491	6.76	896	0.4399
K	232	6.76	896	0.2079
Mn	16.2	6.76	896	0.0145
Fe	6370	6.76	896	5.7075
Cr	15.9	6.76	896	0.0142
Hg	10.7	6.76	896	0.0096
Sr	7.35	6.76	896	0.0066

Restart MM5 Calculations, Off-Gas Line

	DATA
Area of stack ft. squared	0.35
temperature off-gas degrees R	810
pressure at sample point in. Hg	30
barometric pressure in. Hg	30
Δpressure pitot tube	0.05
ΔH across flow orifice	0.81
Average temp meter degrees R	580
dry gas meter factor	1
sample volume cf	1803
sample time	3428
water gain impingers ml	1712
water gain silica gel grams	189
dia. nozzle in.	0.375
pitot tube coefficient	0.84
Particulate collected grams	2.68
degrees F to degrees R= F+460	

total off-gas flow (cfm)
323.25

CALCULATIONS

standard sample volume metered
1649.008

water gained in impingers std. cu. ft.
80.584

water gained in silica gel std. cu. ft.
8.911

moisture in off-gas
0.051

mole weight of off-gas lb./lb*mole
30.000

wet mole weight of off-gas lb./lb.*mole
29.382

off-gas velocity ft./sec.
15.393

off-gas flowrate dscf/hr.
12023.898

sample flowrate cu.ft./min.
0.511

9613400.0952

Phase 1 MM5 Calculations, Off-Gas Line

	DATA
Area of stack ft. squared	0.35
temperature off-gas degrees R	847.75
pressure at sample point in. Hg	29
barometric pressure in. Hg	29
Δpressure pitot tube	0.05
ΔH across flow orifice	1.3
Average temp meter degrees R	580.3
dry gas meter factor	1
sample volume cf	259
sample time min.	330
water gain impingers ml	272
water gain silica gel grams	0
dia. nozzle in.	0.375
pitot tube coefficient	0.84
Particulate collected grams	2.079
degrees F to degrees R= F+460	

Total off-gas flow (cfm)
336.45

CALCULATIONS

standard sample volume metered
229.164

water gained in impingers std. cu. ft.
12.803

water gained in silica gel std. cu. ft.
0.000

moisture in off-gas
0.0529

mole weight of off-gas lb./lb*mole
30.000

wet mole weight of off-gas lb./lb.*mole
29.365

off-gas velocity ft./sec.
16.021

off-gas flowrate dscf/hr.
11541.504

sample flowrate cu.ft./min.
0.509

Off-Gas Line MM5 Filter Totals

Element	Concentration ug/g filter #1	Filter Wt. #1 gr.	Concentration ug/g Filter #2	Filter Wt. gr. Filter #2	OG flowrate DSCF/min	Sample Vol. DSCF	Sample Time min.	Total in offgas grams
Ba	5.44	2.682	72.77	1.077	349.53	1649	3428	0.0675
Mg	1560	2.682	1550	1.077	349.53	1649	3428	4.2531
Sn	181	2.682	98.9	1.077	349.53	1649	3428	0.4301
Ti	116	2.682	105	1.077	349.53	1649	3428	0.3082
V	36.06	2.682	2.17	1.077	349.53	1649	3428	0.0720
Na	10100	2.682	927	1.077	349.53	1649	3428	20.4081
Mo	147	2.682	17.4	1.077	349.53	1649	3428	0.3001
Al	4320	2.682	3050	1.077	349.53	1649	3428	10.8056
Sb	39.8	2.682	0	1.077	349.53	1649	3428	0.0776
Be	0	2.682	0	1.077	349.53	1649	3428	0.0000
Ca	2000	2.682	2890	1.077	349.53	1649	3428	6.1592
Zn	145656.3	2.682	6985.2	1.077	349.53	1649	3428	289.3188
Cu	365.02	2.682	55.67	1.077	349.53	1649	3428	0.7549
Ag	14.67	2.682	0.05	1.077	349.53	1649	3428	0.0286
Pb	200156.0000	2.682	136343.8	1.077	349.53	1649	3428	496.7584
Tl	80.3	2.682	320	1.077	349.53	1649	3428	0.4069
Cd	19571	2.682	3022.38	1.077	349.53	1649	3428	40.5048
Co	128.73	2.682	6.62	1.077	349.53	1649	3428	0.2560
Ni	24066.8	2.682	97.52	1.077	349.53	1649	3428	46.9773
K	16700	2.682	2170	1.077	349.53	1649	3428	34.2428
Mn	190.45	2.682	220.8	1.077	349.53	1649	3428	0.5439
Fe	273655.5	2.682	8760	1.077	349.53	1649	3428	540.1503
Cr	10820.7	2.682	26.91	1.077	349.53	1649	3428	21.1083
Hg	58.96	2.682	102.14	1.077	349.53	1649	3428	0.1948

9619400.0953

Off-Gas Line Impinger Totals

	CONCENTRATION mg/l	OG LINE MM5 SOLUTION VOLUME LITERS	SOLUTION TOTAL GRAMS	TOTAL OG LINE GRAMS
Ba	0.23	1.272	0.0003	0.2126
Mg	0.253	1.272	0.0003	0.2338
Sn	0	1.272	0.0000	0.0000
Tl	0.052	1.272	0.0001	0.0481
V	0	1.272	0.0000	0.0000
Na	10.4	1.272	0.0132	9.6120
Mo	0.088	1.272	0.0001	0.0813
Al	1.86	1.272	0.0024	1.7191
Sb	0.067	1.272	0.0001	0.0619
Be	0	1.272	0.0000	0.0000
Ca	6.96	1.272	0.0089	6.4327
Zn	0.17	1.272	0.0002	0.1571
Cu	0	1.272	0.0000	0.0000
Ag	0	1.272	0.0000	0.0000
Pb	0.42	1.272	0.0005	0.3882
Ti	0	1.272	0.0000	0.0000
Cd	0.09	1.272	0.0001	0.0832
Co	0.05	1.272	0.0001	0.0462
Ni	0.1	1.272	0.0001	0.0924
K	1.62	1.272	0.0021	1.4973
Mn	1.12	1.272	0.0014	1.0351
Fe	0.22	1.272	0.0003	0.2033
Cr	0	1.272	0.0000	0.0000
Hg	2.13	1.272	0.0027	1.9686
Sr	0.176	1.272	0.0002	0.1627
Hg	224	0.385	0.0862	62.6620

Phase 1 MM5 Calculations, Stack

	DATA	CALCULATIONS
		standard sample volume metered
Area of stack ft. squared	0.2006	822.616
temperature off-gas degrees R	655.5	
pressure at sample point in. Hg	29.01	water gained in impingers std. cu. ft.
barometric pressure in. Hg	29	42.457
Δpressure pitot tube	0.45	
ΔH across flow orifice	1.4	water gained in silica gel std. cu. ft.
Average temp meter degrees R	580	3.536
dry gas meter factor	1	
sample volume cf	929	moisture in off-gas
sample time min.	1375	0.053
water gain impingers ml	902	
water gain silica gel grams	75	mole weight of off-gas lb./lb*mole
dia. nozzle in.	0.25	30.000
pitot tube coefficient	0.84	
Particulate collected grams	0	wet mole weight of off-gas lb./lb.*mole
degrees F to degrees R= F+460		29.365
		off-gas velocity ft./sec.
stack flowrate (cfm)		42.257
508.61		
		off-gas flowrate dscf/hr.
		22571.206
		sample flowrate cu.ft./min.
		0.771

Restart MM5 Calculations, Stack

	DATA
Area of stack ft. squared	0.2006
temperature off-gas degrees R	668.4
pressure at sample point in. Hg	30
barometric pressure in. Hg	30
Δpressure pitot tube	0.4
ΔH across flow orifice	1.27
Average temp meter degrees R	578.2
dry gas meter factor	0.9425
sample volume cf	2565
sample time min.	3889
water gain impingers ml	3435
water gain silica gel grams	795.5
dia. nozzle in.	0.25
pitot tube coefficient	0.84
particulate collected grams	0.11
degrees F to degrees R= F+460	

CALCULATIONS

standard sample volume metered
2220.414

water gained in impingers std. cu. ft.
161.685

water gained in silica gel std. cu. ft.
37.508

moisture in off-gas
0.082

mole weight of off-gas lb./lb*mole
30.000

wet mole weight of off-gas lb./lb.*mole
29.012

off-gas velocity ft./sec.
39.801

off-gas flowrate dscf/hr.
20891.625

sample flowrate cu.ft./min.
0.710

Stack Flowrate (CFM)
479.04

MM5 Stack Impinger Totals

	CONCENTRATION mg/l	OG LINE MM5 SOLUTION VOLUME LITERS	SOLUTION TOTAL GRAMS	TOTAL STACK GRAMS
Ba	0	3.435	0.0000	0.0000
Mg	0	3.435	0.0000	0.0000
Sn	0	3.435	0.0000	0.0000
Tl	0	3.435	0.0000	0.0000
V	0	3.435	0.0000	0.0000
Na	0.528	3.435	0.0018	0.8887
Mo	0	3.435	0.0000	0.0000
Al	0	3.435	0.0000	0.0000
Sb	0	3.435	0.0000	0.0000
Be	0	3.435	0.0000	0.0000
Ca	0.657	3.435	0.0023	1.1058
Zn	0	3.435	0.0000	0.0000
Cu	0	3.435	0.0000	0.0000
Ag	0	3.435	0.0000	0.0000
Pb	0.32	3.435	0.0011	0.5386
Ti	0	3.435	0.0000	0.0000
Cd	0	3.435	0.0000	0.0000
Co	0	3.435	0.0000	0.0000
Ni	0	3.435	0.0000	0.0000
K	0.268	3.435	0.0009	0.4511
Mn	0.75	3.435	0.0026	1.2624
Fe	0	3.435	0.0000	0.0000
Cr	0	3.435	0.0000	0.0000
Hg	0.31	3.435	0.0011	0.5218
Sr	0	3.435	0.0000	0.0000

Stack MM5 Filter Totals

Element	Concentration ug/g	Filter Wt. grams	OG flowrate DSCF/min.	Sample Vol. DSCF	Sample Time min.	Total in offgas grams
Ba	0	0.62	349.5	2355.9	3889	0.0000
Mg	96.7	0.62	349.5	2355.9	3889	0.0346
Sn	85.1	0.62	349.5	2355.9	3889	0.0304
Tl	0	0.62	349.5	2355.9	3889	0.0000
V	0	0.62	349.5	2355.9	3889	0.0000
Na	418	0.62	349.5	2355.9	3889	0.1495
Mo	0	0.62	349.5	2355.9	3889	0.0000
Al	392	0.62	349.5	2355.9	3889	0.1402
Sb	0	0.62	349.5	2355.9	3889	0.0000
Be	0	0.62	349.5	2355.9	3889	0.0000
Ca	1590	0.62	349.5	2355.9	3889	0.5687
Zn	57	0.62	349.5	2355.9	3889	0.0204
Cu	0	0.62	349.5	2355.9	3889	0.0000
Ag	0	0.62	349.5	2355.9	3889	0.0000
Pb	116	0.62	349.5	2355.9	3889	0.0415
Tl	63.3	0.62	349.5	2355.9	3889	0.0226
Cd	0	0.62	349.5	2355.9	3889	0.0000
Co	0	0.62	349.5	2355.9	3889	0.0000
Ni	0	0.62	349.5	2355.9	3889	0.0000
K	51	0.62	349.5	2355.9	3889	0.0182
Mn	0	0.62	349.5	2355.9	3889	0.0000
Fe	128	0.62	349.5	2355.9	3889	0.0458
Cr	0	0.62	349.5	2355.9	3889	0.0000
Hg	258	0.62	349.5	2355.9	3889	0.0923
Sr	0	0.62	349.5	2355.9	3889	0.0000

9615410.0956

DISTRIBUTION

No. of Copies

OFFSITE

12 DOE/Office of Scientific and Technical Information

4 DOE Office of Technology Development
Trevion II Building
12800 Middlebrook Road
Germantown, MD 20874
ATTN: D. L. Biancosino, EM-551
J. S. Walker, EM-541 (3)

J. E. Lytle, EM-30
DOE Office of Waste Operations
Forrestal Building
U.S. Department of Energy
1000 Independence Ave. S.W.
Washington, DC 20585

C. W. Frank, EM-50
DOE Office of Technology Development
Forrestal Building
U.S. Department of Energy
1000 Independence Ave. S.W.
Washington, DC 20585

R. P. Whitfield, EM-40
DOE Office of Environmental Restoration
Forrestal Building
U.S. Department of Energy
1000 Independence Ave. S.W.
Washington, DC 20585

2 DOE Oak Ridge Office
P.O. Box 2001
Oak Ridge, TN 37831
ATTN: J. Moore
J. Sweeney

No. of Copies

3 Battelle Columbus
505 King Ave nue
Columbus, OH 43201-2693
ATTN: W. J. Madia
B. G. Maiden
R. Nathan

J. Koger
Martin Marietta Energy Systems
P.O. Box 2009
Oak Ridge, TN 37831-8097

P. T. Owen
Martin Marietta Energy Systems
P.O. Box 2003
Oak Ridge, TN 37831-7256

2 Oak Ridge National Laboratory
P.O. Box 2008
Oak Ridge, TN 37831-6330
ATTN: J. B. Berry
A. P. Malinauskas, MS 7122

W. Bliss
Environmental Managment Division
Reynolds Electrical and Engineering Co., Inc.
2501 Wyandotte
P.O. Box 98521
Las Vegas, NW 89193-8521

B. Craig
HAZWRAP
P.O. Box 2003, MS 7606
Oak Ridge, TN 37831-7606

No. of
Copies

6 Oak Ridge National Laboratory
P.O. Box Y
Oak Ridge, TN 37830
ATTN: G. K. Jacobs
M. Naney
B. P. Spalding (4)

7 Geosafe Corporation
2950 George Washington Way
Richland, WA 99352
ATTN: B. E. Campbell
J. E. Hansen (2)
J. L. McElroy
C. L. Timmerman
L. E. Thompson (2)

ONSITE

DOE Richland Operations Office

D. E. Trader, A5-90

4 Westinghouse Hanford Company

J. D. Berger, L0-18
K. D. Boomer, H5-49
J. J. Garfield, H5-49
R. M. Marusich, H5-32

No. of
Copies

33 Pacific Northwest Laboratory

L. Ballou, P7-18
K. A. Blanchard, P7-18
J. L. Buelt, P7-41
H. C. Burkholder, P7-41
C. C. Chapman, P7-41
D. K. Kreid, K1-22
N. J. Lombardo, K7-02
P. S. Lowery, K7-34
J. Luey, P7-34
M. C. Miller, P7-41
T. L. Page, B1-40
M. E. Peterson, P7-41
T. D. Powell, P7-39
D. K. Seiler, P7-34
S. C. Slate, K1-19
S. L. Stein, BSRS
J. S. Tixier, P7-34 (10)
C. L. Widrig, K1-21
Publishing Coordination
Technical Report Files (5)